ALDH1A enzymes regulate retinoic acid homeostasis in a tissue specific manner: A model of how novel methods can unravel old unanswered questions

Samuel La Montagne Arnold

A dissertation

submitted in partial fulfillment of the

requirements for the degree of

Doctor of Philosophy

University of Washington

2015

Reading Committee:

Nina Isoherranen, Chair

Ronald Stenkamp

Abhinav Nath

Program Authorized to Offer Degree:
Pharmaceutics

University of Washington

Abstract

ALDH1A enzymes regulate retinoic acid homeostasis in a tissue specific manner: A model of how novel methods can unravel old unanswered questions

Samuel La Montagne Arnold

Chair of the Supervisory Committee:
Professor Nina Isoherranen
Department of Pharmaceutics

Retinoic acid (RA), the active form of vitamin A, is an essential signaling molecule in many tissues and the concentrations of RA are spatiotemporally controlled in target tissues. However, the source of RA in each tissue is not clear and the role of specific enzymes in RA synthesis and metabolism has not been described. While the enzymes of the aldehyde dehydrogenase 1A family (ALDH1A) are believed to control the synthesis of RA, general knowledge on the expression pattern and relative contribution of these enzymes to tissue RA formation is unknown. In addition, a direct relationship between altered ALDH1A activity and tissue RA concentrations has never been shown. To characterize the importance of each ALDH1A isoform to RA formation, novel methods were developed to measure tissue RA, ALDH1A protein tissue expression levels, and intrinsic RA formation. These methods were applied to the human testis to demonstrate that the intratesticular concentration of RA is positively associated with RA formation by ALDH1A in the testis. In addition, a distinct localization of ALDH1A was identified in the testis suggesting a specific role for each enzyme in controlling RA formation. To directly test whether inhibition of ALDH1A enzymes decreases RA concentrations in vivo, the potent ALDH1A inhibitor WIN 18,446 was used to inhibit ALDH1A activity in mice. ALDH1A expression levels, RA formation

kinetics by ALDH1A, kinetics of ALDH1A inhibition by WIN 18,446, and WIN 18,446 disposition were used to predict the time course and extent of inhibition of RA formation in the mouse testis and liver. While ALDH1A1 and ALDH1A2 were responsible for the majority of RA formation in the mouse testis, ALDH1A1 and aldehyde oxidase contributed to RA formation in the liver. Due to the different complement of enzymes contributing to RA formation in each tissue and the distinct inhibition kinetics of WIN 18,446, WIN 18,446 administration was predicted to generate a tissue specific reduction in *at*RA concentrations. As predicted, WIN 18,446 decreased liver RA only 50% but testicular RA was decreased over 95%. These data demonstrate that inhibition of ALDH1A enzymes will decrease RA concentrations in a tissue specific manner and selective ALDH1A inhibition could be used to alter RA concentrations in select target tissues. Taken together, the comprehensive novel methodology developed to evaluate RA homeostasis in individual tissues provides insight to how the individual ALDH1A enzymes mediate RA concentrations in tissue and specific cell types.

Table of Contents

List of Figures

List of Tables

List of Abbreviations

RA: retinoic acid

*at*RA: all-*trans* retinoic acid

9-*cis*RA: 9-*cis* retinoic acid

13-*cis*RA: 13-*cis* retinoic acid

9,13-*cis*RA: 9,13-*dicis* retinoic acid

11-*cis*RA: 11-*cis* retinoic acid

ADH: alcohol dehydrogenase

RDH: retinol dehydrogenase

SDR: short chain reductase

RALDH: retinal dehydrogenase

NAD: nicotinamide adenine dinucleotide

RAR: retinoic acid receptor

PPAR – Peroxisome Proliferator-Activated Receptor

RXR: retinoid X receptor

CRABP: cellular retinoic acid binding protein

CRBP: cellular retinol binding protein

CYP or P450: cytochrome P450

mRNA: messenger ribonucleic acid

RT-PCR: reverse-transcriptase polymerase chain reaction

UHPLC: ultra high performance liquid chromatograph

MS: mass spectrometry

UPLC: ultra performance liquid chromatography

Cl_{int}: intrinsic clearance

Vmax: maximal velocity

AUC: area under the curve

CL_f: intrinsic clearance

ER: endoplasmic reticulum

f_u: fraction unbound

$t_{½}$: half life

Cmax: maximum concentration achieved

Tmax: time at which maximum concentration was achieved

F: bioavailability

APL: acute promyelocytic leukemia

IC_{50}: concentration at which 50% of the enzyme activity is inhibited

HLM: human liver microsomes

HLC: human liver cytosol

ACN – Acetonitrile

APCI – Atmospheric Pressure Corona Ionization

CE – Collision energy

CV – Coefficient of Variation

CXP - Collision cell exit potential

DP - Declustering potential

EP - Entrance potential

UHPLC – Ultra high performance liquid chromatography

LXR – Liver X Receptor

LLOQ – Lower limit of quantification

LLOD- Lower limit of detection

MS – Mass spectrometry

MS/MS- Tandem mass spectrometry

RAR – Retinoic Acid Receptor

RXR – Retinoid X Receptor

MRM – Multiple reaction monitoring

QC – quality control

Acknowledgements

First, I would like to thank my advisor, Professor Nina Isoherranen, for her thoughtful guidance and support throughout my graduate school career. As a student, I was continuously encouraged to explore my ideas and the only limitations placed on my development as an independent researcher were those that I created for myself.

In addition, I would like to thank my fellow members of the Isoherannen lab. It is very clear that the camaraderie we feel in the lab is something many groups strive to attain and we are fortunate to be able to effortlessly transition from conversations about work to those about life either in the lab or over beer at the pub.

I would also like to thank all members of the Departments of Pharmaceutics and Medicinal Chemistry for their support and guidance over the years. My genuine appreciation goes to Professors Abhinav Nath, Ronald Stenkamp, John Amory, Kent Kunze, and Danny Shen, the members of my committee, for contributing their knowledge and time to my thesis.

Finally, I would like to thank my friends and family for their encouragement and support.

Dedication

This dissertation is dedicated to my friend, Michael W. Mann, for his unwavering friendship throughout the years.

Chapter 1
Introduction

1.1. Vitamin A and retinoic acid history, chemistry, analysis, and pharmacology

Historical references of vitamin A date back to at least the ancient Greeks who detailed the symptoms of night blindness and its contemporary treatment with raw beef liver (Wolf, 1996). Not long after, historic texts written by cultures throughout the world reveal the use of livers from a variety of animals such as goat, ox, pig, and shark to cure the ailment that descended upon the eyes of the patient along with the sun (Lee, 1967; Wolf, 1996). We now know that the liver provides a reliable, robust source of vitamin A and this essential nutritional factor was the foundation of the cure. In addition to night blindness, the manifestation of vitamin A deficiency extended to disruption of epithelial integrity. In the early 19th century, dogs were reported to develop cornea ulcerations (keratomalacia) when they were fed a diet based purely on sugar water (Lanska, 2010). However, an association between night blindness and keratomalacia was not acknowledged until historical analysis revealed the prevalence of both conditions in human populations who were predicted to have decreased vitamin A intake due to war and/or famine (Wolf, 1996). As time went on, the scientific community began to recognize that specific nutritional factors were required for normal health and development, but the identification and sources of these nutrients remained a mystery.

At the start of the 20th century, the research community initiated a series of studies designed to identify essential nutrients in our diet (Lanska, 2010). McCollum unknowingly commenced his research on vitamin A by investigating the effect of diet on cows (Lanska, 2010). The livestock were fed a diet that consisted entirely of wheat, oats, or yellow maize. While cows fed wheat or oats succumbed to poor health and gave birth to premature dead calves, cows fed yellow maize displayed normal health and reproduction. However, McCollum was unable to determine the essential factor(s) missing from the wheat and oats that were responsible for

maintaining the health of the cows. To accelerate his research, McCollum began to use rats as his animal model and quickly discovered as essential nutrient in butter fat and egg yolk. Young rats fed a diet consisting of olive oil, sugar, and protein failed to grow without the addition of the butter fat or egg yolk to their diets. Future work demonstrated that ether extract of liver, kidney, or butter fat contained the nutrient that was supporting the growth of the rats which he later designated as "fat-soluble factor A". However, it would take another 20 years to isolate "vitamin A" and determine its chemical structure.

Vitamin A, otherwise known as retinol, belongs to a structurally diverse class of compounds collectively known as "retinoids" that contains over 4,000 natural and synthetic molecules based on the structure of retinol and the function of its active metabolites (Bushue and Wan, 2010) (Figure 1.1). The in vivo regulation of retinoids is a complex process comprising multiple metabolic enzymes, transporters, and binding proteins in tissues throughout the body. Retinol does not have any inherent biological activity and enzyme dependent steps are required to synthesize the active metabolites known as retinal and retinoic acid (RA) (Berggren Soderlund et al., 2003; Eckhoff et al., 1991). The concentrations of the active vitamin A metabolites are continuously controlled in an orchestrated manner that commences with retinoid intake through the diet. Retinoids are acquired from the diet either as a proretinoid carotenoid or as retinol and retinyl esters (D'Ambrosio et al., 2011) (Figure 1.2). Proretinoid carotenoids, such as β-carotene, are converted to retinal by β-carotene monooxygenase (BCMO) enzymes in the intestine and subsequently reduced to retinol. Next, retinol is esterified by lecithin: retinol acetyl transferase (LRAT) (Figure 1.2). The retinyl esters are packaged into chylomicrons by microsomal triglyceride transfer protein (MTP) and distributed throughout the body by the lymphatic system (D'Ambrosio et al., 2011). Approximately 70% of the retinyl esters from chylomicron remnants

are taken up by the liver, processed by hepatocytes, and stored in the hepatic stellate cells (Goodman et al., 1965). The remaining 30% are taken up by peripheral tissues and stored in lipid droplets as retinyl esters. While retinol uptake and esterification are believed to occur in each retinoid dependent tissue, a majority of research on the storage of vitamin A has focused on the liver since it contains approximately 70% of the body's retinol stores (Blomhoff, 1987).

In the liver, multiple enzymes and binding proteins expressed across several cell types are responsible for the complex regulation of vitamin A homeostasis. In the hepatocytes of the liver, retinyl ester hydolases (REH) are believed to hydrolyze dietary retinyl esters derived from chylomicron remnants to form retinol (Figure 1.3). In times of sufficient dietary intake, retinol bound to cellular retinol binding protein 1 (CRBP1) is transferred to the stellate cells where it is reesterified by LRAT and stored in lipid droplets (D'Ambrosio et al., 2011). When the vitamin A stores need to be appropriated, retinyl esters are hydrolyzed by REH enzymes in the stellate cells to form retinol (Figure 1.3). The retinol is further metabolized to form RA, which has an important role in the activation of hepatic stellate cells and in controlling hepatic lipid metabolism (Berry and Noy, 2009; Bonet et al., 2012; Hellemans et al., 2004; Wolf, 2010), or is transferred to hepatocytes and binds retinol binding protein 4 (RBP4) and transthyretin (TTR) and released into circulation (Quadro et al., 2004). Retinol is the main circulating retinoid and is found at concentrations of 1-3 μM in serum as the ternary complex of RBP4-retinol-TTR (Berggren Soderlund et al., 2003; Eckhoff et al., 1991). Extrahepatic tissue uptake of circulating retinol bound to RBP4:TTR is mediated by an uptake transporter known as stimulated by retinoic acid protein 6 (STRA6). Depending on the vitamin A status of the tissue, the retinol acquired from circulation can either be stored after esterification by LRAT or can be further metabolized to form RA in the target tissue.

The range of biologically observed RA isomers complicates understanding of its physiological role. At least 5 geometric isomers of RA have been reported including all-*trans* RA (*at*RA), 9-*cis*RA, 13-*cis*RA, 9,13-*dicis*RA and 11-*cis*RA (Kunchala et al., 2000). Of the five geometric isomers, we have identified *at*RA (3.1 ± 0.2 nM), 9-*cis*RA (0.1 ± 0.02 nM), 9,13-*dicis*RA (0.4 ± 0.4 nM), and 13-*cis*RA (5.3 ± 1.3 nM) in human serum using LC-MS/MS (Arnold et al., 2012) (Figure 1.4). The central role of the *at*RA as a signaling molecule is well established in many post natal biological processes including spermatogenesis (Chung et al., 2009; Raverdeau et al., 2012), the gut-homing specificity of both T cells and B cells (Iwata et al., 2004; Mucida et al., 2007), regulation of apoptosis (Noy, 2010a), energy homeostasis (Kiefer et al., 2012), and stem cell differentiation (Gudas and Wagner, 2011). In addition, *at*RA has been shown to induce remission in patients with acute promyelocytic leukemia (APL) (Veal et al., 2007). The biological role of the other RA isomers is not fully understood and they continue to be an area of active research. 9-*cis*RA is involved in regulating insulin stimulated glucose secretion (Chung and Wolgemuth, 2004; Kane et al., 2010; Kane et al., 2008) and has been used to treat severe chronic hand eczema (Schmitt-Hoffmann et al., 2011). In contrast to *at*RA and 9-*cis*RA, an in vivo role for 13-*cis*RA and 9,13-*dicis*RA has not been established. 13-*cis*RA was used for the treatment of acne and in children with high risk neuroblastoma (Veal et al., 2007), but the pharmacological effects may have been due to 13-*cis*RA isomerization in vivo to *at*RA.

The biological activity of the active RA isomers is mediated predominantly by their association with nuclear receptors, mainly the retinoic acid receptors (RARα, RARβ, and RARγ) (Petkovich et al., 1987). However, in addition to RARs, binding of RA to retinoid X receptors (RXRα, RXRβ, and RXRγ) and peroxisome proliferator-activated receptor (PPAR) (β/δ) has also been shown (Schug et al., 2007). The specific binding of nuclear receptors by the RA isomers is

believed to contribute to their distinct activity. While *at*RA acts as a signaling molecule by activating the RARs (Idres et al., 2002) and PPAR β/δ (Mark et al., 2006; Schug et al., 2007), 9-*cis*RA binds to either RARs or RXRs (Idres et al., 2002; Mangelsdorf and Evans, 1995). A powerful tool to study the role of RA signaling during development and in adults has been the use of RAR knockout models. When RARα or RARγ is knocked out, the mice display a phenotype similar to that seen in a dietary induced vitamin A deficient (VAD) animal model with symptoms that include early postnatal lethality (Lufkin et al., 1993). The global knockouts of the individual RARs have demonstrated the importance of RA signaling in individual tissues. RARα and RARγ signaling are critical for spermatogenesis (Raverdeau et al., 2012), but *Rarβ*$^{-/-}$ mice have normal fertility (Luo et al., 1995). While retinoid dependent tissues can theoretically modulate RA signaling by controlling the expression of nuclear receptors and/or adjusting the concentration of the individual RA isomers, the mechanism behind the regulation of RA signaling is not known.

The analysis of RA isomers has been difficult due to their similar structures and low concentrations in human and mouse tissues. As a result, a lack of data on the tissue concentrations of the individual RA isomers has been one of the major limitations in understanding the roles and importance of the specific RA isomers in vivo (Napoli, 1996). In the last 10 years, advances in mass spectrometry and liquid chromatography have made it possible to measure endogenous RA concentrations in mouse tissues (Kane et al., 2008), but data from humans tissues is lacking. The work in mouse tissue has made it clear that *at*RA concentrations differ in each tissue (liver ≈ testis > kidney > white adipose tissue ≈ serum) and that circulating retinol and RA concentrations can not be used to predict tissue RA concentrations (Obrochta et al., 2014). The different tissue concentrations suggest that RA homeostasis is independently

regulated in each tissue, but the mechanism of the tissue specific regulation is unclear. Based on evidence RA signalizing is required in the testis and liver, a majority of research on postnatal RA signaling has focused on these tissues.

Although the precise roles for RA in spermatogenesis have not been elucidated, it is clear that RA signaling via various receptors is critical at different stages of spermatogenesis for healthy sperm maturation and production. The requirement of vitamin A for spermatogenesis was first described in 1925, and has remained an area of active research (Wolbach and Howe, 1925). In VAD mice and rats, spermatogenesis is suspended at the first differentiation step ($A \rightarrow A_1$ transition) (Mitranond et al., 1979; Unni et al., 1983; van Pelt and de Rooij, 1990). However, it was not until the *Rarα*$^{-/-}$ mouse model was generated that a direct role for RA in spermatogenesis was demonstrated. The loss of RARα results in spermatogenesis arrested at the $A \rightarrow A_1$ transition (Lohnes et al., 1993) demonstrating that RA is the vitamin A metabolite required for spermatogenesis. The localization of the RARα signaling responsible for the $A \rightarrow A_1$ transition was investigated with a germ cell specific RARα knockout model and the testicular phenotype of these mice was similar to the *Rarα*$^{-/-}$ mouse model (Chung et al., 2009). These results were further validated by the administration of an oral RAR antagonist which reversibly inhibited spermatogenesis and generated a testicular phenotype similar to the *Rarα*$^{-/-}$ mice (Chung et al., 2011). In addition to RARα, knockout models of RARβ and RARγ have shown that *Rarβ*$^{-/-}$ mice have normal fertility (Luo et al., 1995) and *Rarγ*$^{-/-}$ mice are infertile due to squamous metaplasia of the seminal vesicles (Lohnes et al., 1993). The distinct phenotypes of the *Rarα*$^{-/-}$ and *Rarγ*$^{-/-}$ mouse models suggest RA may have multiple roles in spermatogenesis. The role of the RXR receptors is still not clear and deletion of *Rxrγ* in mice has no effect on spermatogenesis within the seminiferous tubules. *Rxrβ*$^{-/-}$ mice are still able to produce sperm, but

the spermatids are unable to release within the seminiferous epithelium (Kastner et al., 1996).

In the liver, RA signaling is believed to play an important role in controlling lipid metabolism (Berry and Noy, 2009; Wolf, 2010) and studies using mouse models of obesity and diabetes have demonstrated RA protects these animals against obesity (Berry et al., 2012; Tsuchiya et al., 2012). In healthy and obese mice, activation of RARβ and PPARβ/δ in the liver by RA induces the hepatic expression of carnitine palmitoyltransferase 1 (CPT1) and uncoupling protein 1 (UCP1) (Amengual et al., 2012; Bonet et al., 2012; Li et al., 2013) which causes a reduction in fatty acid and triacylglycerol synthesis and an increase in fatty acid oxidation. Consistent with the upregulation CPT1 and UCP1, healthy and obese mice administered RA display a reduction in the hepatic liver triacylglycerol content (Amengual et al., 2010). In contrast, when RA signaling is reduced in the liver, mice suffer from steatosis and have an increased risk of liver cancer (Shiota, 2005). While we are gaining a better understanding of RA signaling in the testis and liver, the source of RA in each of these tissues is not clear. However, past results suggest the primary source of *at*RA in most tissues is synthesis within the target tissue (Kurlandsky et al., 1995).

1.2. Retinoic acid formation and homeostasis

In most organs, the primary source of *at*RA is in situ synthesis which is mediated by a complex set of interacting enzymes, transporters, and binding proteins (Kurlandsky et al., 1995). As a result, concentrations of *at*RA are tissue specific and do not correlate with circulating *at*RA levels (Obrochta et al., 2014). The biosynthesis of *at*RA in each tissue can be supported through two pathways, and each route requires the formation of the *at*RA precursor *all-trans* retinal (*at*-retinal). The first pathway involves reversible catalysis of retinol to/from retinal by the cytosolic alcohol dehydrogenases (ADH) and microsomal short-chain dehydrogenase/reductase (SDR)

enzyme families (Figure 1.3) (Kavanagh et al., 2008). Of the two enzyme families, the SDR enzymes, including retinol dehydrogenases RDH10 and RDH11, are believed to be the predominant enzymes responsible for maintaining the postnatal supply of retinol and retinal with the ADH enzymes serving as a backup (Kedishvili, 2013). While a number of the SDR enzymes recognize and metabolize retinol in vitro, their individual contributions to vitamin A metabolism in vivo are not clear (Kavanagh et al., 2008). Based on the fact that *Rdh10*$^{-/-}$ mice die during prenatal development due to reduced RA biosynthesis and signaling, RDH10 is believed to contribute to retinal formation from retinol during embryonic development (Ashique et al., 2012; Sandell et al., 2007). In order to study the postnatal role of RDH10 in the testis, RDH10 was selectively deleted from germ cells and/or Sertoli cells (Tong et al., 2013). The testis specific knockouts demonstrated RDH10 expression in Sertoli cells is essential for spermatogenesis in juvenile mice, but the mice gained fertility and recovered at 9 weeks of age (Tong et al., 2013). While the reason for the delayed fertility is unclear, reduced testicular RDH10 may cause an alteration in the expression of other RA related enzyme pathways resulting in RA concentrations reaching sufficient testicular concentrations to initiate spermatogenesis. However, methods to quantify the expression of the enzymes responsible for RA formation were not available at the time. RDH11 has been extensively studied due to its perceived role in forming retinol from retinal, which likely makes it an important enzyme in the storage of retinol and in the processing of carotenoids. However, unlike the *Rdh10*$^{-/-}$ mouse model, *Rdh11*$^{-/-}$ mice are healthy and fertile (Kim et al., 2005b). An alternate pathway to retinal is the cleavage of β-carotene by BCMO to form two molecules of retinal. However, the role of this pathway in forming retinal is unclear and based on the data with the individual *Rdh*$^{-/-}$ mouse models, β-carotene does not appear to be a predominant source of retinal in the testis. The distinct roles for each of these enzymes is still a

topic of further investigation, and the ambiguity is only increased by the lack of quantitative protein expression data for each of the enzymes.

The final irreversible step in RA synthesis is the oxidation of retinal to RA, and multiple enzymes of the aldehyde dehydrogenase (ALDH), aldehyde oxidase (AOX), xanthine oxidase (XOX), and cytochrome P450 (Gagnon et al., 2002, 2003; Graham et al., 2006; Huang et al., 1999; Raner et al., 1996; Roberts et al., 1992; Taibi et al., 2001; Watanabe et al., 1991) families have been demonstrated to catalyze the formation of RA from retinal in vitro. Of these enzymes, the ALDH1A enzymes (ALDH1A1, ALDH1A2, and ALDH1A3) are generally believed to be the most important. This is due to the fact that *Aldh1a2*$^{-/-}$ and *Aldh1a3*$^{-/-}$ mice die during embryonic development and have typical malformations relating to vitamin A deficiency (Dupe et al., 2003; Niederreither et al., 1999). *Aldh1a1*$^{-/-}$ mice are viable and fertile and have increased circulating concentrations of retinal, but whether tissue RA concentrations are decreased in *Aldh1a1*$^{-/-}$ mice is unclear (Molotkov and Duester, 2003). Despite the distinct phenotypes of the these mice, it is not known whether decreased activity of ALDH1A enzymes will alter tissue RA concentrations in adult animals or if other enzymes are important in RA formation in postnatal life.

Metabolic elimination of RA is predominantly mediated by the CYP26 family of enzymes (Thatcher and Isoherranen, 2009). There are three CYP26 isoforms (A1, B1, and C1) and knockout models of the individual isoforms have shown that only CYP26A1 (Abu-Abed et al., 2001) and CYP26B1 (Yashiro et al., 2004) are essential for embryonic development (Uehara et al., 2007). The distinct phenotypes generated by the CYP26A1 and CYP26B1 knockout models suggest that the individual isoforms have specific roles in controlling RA homoeostasis during development. The importance of CYP26 extends into adulthood, and mRNA was used to

identify a distinct tissue localization pattern for the CYP26 isoforms (Xi and Yang, 2008). CYP26A1 expression is highest in the liver and is expressed ubiquitously across the body with the exception of the brain. Whether CYP26B1 is expressed in the human liver is still unclear, but when compared to CYP26A1, robust expression was detected in the testis, ovary, placenta, and brain (Xi and Yang, 2008). In vivo, studies predicted to change in vivo RA concentrations have been shown to cause altered CYP26 expression. CYP26A1 mRNA in the liver was significantly decreased in the animals treated with an ALDH1A inhibitor suggesting the mice responded to RA deprivation by reducing the elimination of RA by CYP26A1 (Paik et al., 2014b). When mice or rats are on a low vitamin A diet and are switched to a vitamin A sufficient diet, the CYP26A1 mRNA in the liver increases up to 8-fold (Ross et al., 2011; Zhang et al., 2007). However, the quantitative contribution of liver CYP26A1 to the overall total body clearance of *at*RA is unclear and based on the broad tissue expression of CYP26 enzymes, it is likely that CYP26 expression in extrahepatic tissues contribute to RA elimination. The tissue specific role of CYP26 is supported by the expression of CYP26 in the peritubular myoid cells that line the outside of the seminiferous tubules in the testis (Vernet et al., 2006). The CYP26 expression is predicted to generate a metabolic barrier preventing RA in circulation from accessing the protected environment within the seminiferous tubule (Vernet et al., 2006).

RA signaling in the testis is required for spermatogenesis, but the source of RA is still unclear (Figure 1.5). When VAD mice are administered *at*RA, they are healthy but remain infertile suggesting that circulating RA is not able to cross into the seminiferous tubules of the testis (Wolbach and Howe, 1925) most likely due to the CYP26 expressed in the peritubular myoid cells. Therefore, the source of *at*RA in the testis is likely local synthesis of retinal derived from circulating retinol, β-carotene, and/or chylomicron remnants. The delayed fertility of Sertoli

cell specific *Rdh10*$^{-/-}$ mice suggests the initial source of *at*RA may be from retinal generated from retinol within the Sertoli cells by RDH10. After uptake into or formation within the Sertoli cells, retinol can either be stored in the form of retinyl esters or metabolized to form retinal. RA formed in the Sertoli cells from oxidation of retinal by ALDH1A enzymes can then diffuse into the spermatogonia and activate RARα. However, it is possible that retinol and retinal can diffuse into the spermatogonia and be subsequently metabolized to form RA within the germ cell. Whether RA diffuses within the testis between different cell types has not been well established and the role of ALDH1A enzymes in the different cell types to regulate RA concentrations has not been determined. During development, a RA gradient is generated by the spatiotemporal regulation of ALDH1A enzymes. It seems plausible that a similar RA gradient is generated in the testis between the different cell types within the seminiferous tubule.

1.3. Contribution of ALDH1A to RA formation

Cytosolic enzymes appear to be responsible for the overwhelming majority of *at*RA formation from *at*-retinal (Dockham et al., 1992; Lee et al., 1991; Napoli and Race, 1987, 1990). The ALDH enzymes along with AOX and XOX are cytosolic soluble enzymes that form *at*RA from *at*-retinal (Garattini et al., 2008; Yoshida et al., 1998). The $NAD(P)^+$ dependent ALDH superfamily of enzymes irreversibly catalyze many different endogenous and exogenous compounds and exist in vivo as either homotetramers or homodimers (Koppaka et al., 2012; Yoshida et al., 1998). In contrast to ALDH, AOX and XOX are cytosolic molybdenum containing enzymes that only form homodimers and do not require a pyridine nucleotide cofactor (Garattini et al., 2008; Taibi et al., 2001). Although it is unclear if AOX catalyzes formation of RA from multiple retinal isomers, the ALDH1A enzymes exhibit isomer specificity (Bhat and Samaha, 1999; Yoshida et al., 1992). The role of the ALDH and AOX enzymes in forming *at*RA

was investigated in mouse liver cytosolic protein. The necessity of $NAD(P)^+$ for the majority of *at*RA formation (Lee et al., 1991) in the mouse liver was used to show that ALDH enzymes contribute to the majority of *at*RA formation. The predominant contribution of ALDH to *at*RA formation was further supported by the fact an AOX inhibitor, pyridoxal, only inhibited approximately 5% of the *at*RA formation. Similarly, 80% of the *at*RA formation in human liver cytosol was NAD^+ dependent and the overall contribution of AOX was approximately 10% (Dockham et al., 1992). Whether microsomal NADPH dependent enzymes such as cytochrome P450s contribute to in vivo *at*RA synthesis is poorly studied. This is mainly because the K_m values for *at*-retinal with cytochrome P450 are nearly 70-fold higher than endogenous concentrations of *at*-retinal suggesting they most likely do not have a significant role in *at*RA biosynthesis (Obrochta et al., 2014; Raner et al., 1996). An in vivo role for the ALDH1A enzymes is further supported by the fact they catalyze the formation of *at*RA from *at*-retinal bound to cellular retinol binding protein 1 (CRBP1) which is expressed ubiquitously across the body (Kato et al., 1985a; Posch et al., 1992; Zhai et al., 2001).

The intrinsic capability of the human ALDH1A enzymes to form RA from retinal is unclear. There have been numerous studies on the in vitro formation of RA from retinal by the ALDH1A isoforms and this has resulted in the generation of a wide range of kinetic parameters (Bhat and Samaha, 1999; Brodeur et al., 2006; Gagnon et al., 2002, 2003; Graham et al., 2006; Lin et al., 2003; Posch et al., 1992; Sima et al., 2009; Yoshida et al., 1992). The majority of these kinetic parameters were determined using recombinant mouse protein or enzyme purified from mouse and rat tissue fractions. Due to the variety of enzyme systems, incubation parameters, and lack of a defined nomenclature for many years, the intrinsic capability of each enzyme to form RA is not clear. Even less data is available on RA formation by human ALDH1A, and the RA

formation from retinal by the human ALDH1A isoforms has never been directly compared in the same study.

In humans, ALDH1A1 mRNA has been detected in the liver, kidney, testis, brain, lung, red blood cells, and lens of the eye (Nishimura and Naito, 2006; Sladek et al., 2002; Zhai et al., 2001). In contrast, ALDH1A2 mRNA is found predominantly in the testis, uterus, and skeletal muscle while ALDH1A3 mRNA is localized in the prostate, trachea, intestine, and testis (Nishimura and Naito, 2006). The distinct mRNA expression pattern strongly suggests that all three ALDH1A enzymes contribute to *at*RA synthesis during post-natal life, but their specific role may be tissue specific. Alterations in ALDH1A expression have been observed in a variety of disease states, but it is unclear whether fluctuations in ALDH1A expression contribute to the ailments or are the result of the disease. Specifically, increased ALDH1A1 expression has been associated with poor prognosis in certain types of cancers including clear cell renal, esophageal squamous cell, and papillary thyroid carcinomas (Wang et al., 2013; Xing et al., 2014; Yang et al., 2014). Conversely, ALDH1A2 has been identified as a candidate tumor suppressor in a transgenic animal model of prostate cancer, and gene variants of ALDH1A2 have been found to be associated with osteoarthritis and increased newborn kidney size (El Kares et al., 2010; Kim et al., 2005a; Styrkarsdottir et al., 2014; Touma et al., 2009). However, how the expression of the ALDH1A isoforms is regulated in vivo is unclear. ALDH1A1 expression is believed to be positively regulated by the CCAAT/enchanced binding protein (C/EBPβ) and *at*RA mediated decrease of C/EBPβ expression through activation of RARα was shown to cause a reduction in ALDH1A1 (Elizondo et al., 2000). The ALDH1A2 promoter contains a sterol regulatory element binding protein (SREBP) site and cholesterol has been shown to induce ALDH1A1 and ALDH1A2 mRNA expression in the liver, brain, kidney, and heart (Huq et al., 2006; Wang et

al., 2001). ALDH1A3 mRNA induction (4-fold) has been observed in a prostate cancer cell line treated with dihydrotestosterone (Trasino et al., 2007) implying regulation of ALDH1A3 by androgens in vivo. Taken together these studies point to tissue specific central roles that ALDH1A enzymes play in human physiology and the critical importance for obtaining information concerning the expression and activity of these enzymes in human tissues. To date, methods have not been readily available to determine the specific activity and protein expression of individual ALDH1A enzymes in tissues or for demonstrating that ALDH1A activity influences tissue RA concentrations and net RA formation.

1.4. Quantification of proteins responsible for RA formation

Since the quantitative protein expression and intrinsic RA formation capacity of the ALDH1A enzymes are unknown, the importance of the three ALDH1A enzymes to RA formation in different RA target tissues in humans or animals is currently undetermined. Our current understanding of the relative abundance and localization of ALDH1A has predominantly relied on the use of mRNA quantification approaches. However, it is unclear whether ALDH1A mRNA is directly correlated with protein concentration and/or RA formation activity. Due to a lack of reliable antibodies for the individual ALDH1A isoforms, quantitative or qualitative assessment of protein expression cannot be determined by western blot or ELISA analysis. LC-MS/MS peptide quantification is recognized as a powerful quantitative tool to specifically determine protein expression levels in various biological matrices. While LC-MS/MS peptide quantification offers many advantages compared to western blots and ELISA, the quantification of peptides generated from tissue samples is challenging due to the complexity of different matrices, the steps required to solubilize and digest proteins of interest, and the consideration required for the selection of appropriate quantification standards and internal standards. A robust

LC-MS/MS peptide quantification method would considerably contribute to our understanding of how RA homeostasis is regulated in individual tissues, but LC-MS/MS methods are not currently available to quantify retinoid related proteins.

1.5. Inhibition of RA formation by an ALDH1A inhibitor

In addition to predicting the contribution of ALDH1A enzymes to RA formation using enzyme expression levels and enzymes kinetics, an inhibitor of ALDH1A could be used to determine the role of ALDH1A enzymes in maintaining RA homeostasis during adult life. In addition, a specific ALDH1A enzyme may be a potential therapeutic target for obesity, male contraception or other conditions that are related to RA signaling. WIN 18,446 is a member of a class of compounds known as bisdichloroacetlydiamines (BDADs) that were originally developed as amebicides (Figure 1.6). When WIN 18,446 was tested in rats, a potent reversible inhibition of spermatogenesis was observed (Berberian, 1961). The same reversible inhibition of spermatogenesis was described in humans, but development of the drug for contraception was terminated after one of the subjects experienced severe flushing and nausea after ingesting alcohol along with WIN 18,446 (Heller et al., 1961). While it was unclear at the time, it is now known that the side effect was associated with inhibition of ALDH2 by WIN 18,446 (Amory et al., 2011a). The inhibition of spermatogenesis by WIN 18,446 has been reported in numerous animal species including shrews, cats, rabbits, and mice (Munson et al., 2004; Singh and Dominic, 1980). When WIN 18,446 was administered to mice for 4 weeks (2mg/g of diet) their retinol concentrations increased in both the liver and serum (Paik et al., 2014b), but the intratesticular concentrations of *at*RA were reduced suggesting that WIN 18,446 inhibits RA formation by ALDH1A in vivo (Amory et al., 2011a; Paik et al., 2014b). Yet, it is unclear if WIN 18,446 caused a widespread reduction in tissue *at*RA concentrations or if the decrease in

*at*RA was specific to the testis. Although the inhibition of ALDH1A by WIN 18,446 is believed to suppress spermatogenesis, the inhibition kinetics of ALDH1A by WIN 18,446 are not well understood. In addition, the concentrations of WIN 18,446 have never been determined after administration of the inhibitor, so the effect of WIN 18,446 on in vivo ALDH1A activity can not be predicted with the data currently available.

1.6. Thesis aims

Throughout development and adulthood, RA concentrations need to be tightly regulated in a tissue specific manner. There is evidence to support the role of ALDH1A enzymes in maintaining RA homeostasis in individual tissues, but the protein expression of the ALDH1A enzymes and their intrinsic ability to form RA are not known. Therefore, the pharmacological or toxicological outcomes of decreasing ALDH1A enzyme activity within a specific target or whole body have not been established and methods to predict RA concentrations in vivo are lacking. The hypothesis of this study was that the individual ALDH1A isoforms will have tissue and cell type specific expression and that this localization will cause a distinct effect on tissue RA concentrations when ALDH1A activity is altered by pharmacological inhibition or changes in protein expression. With the data currently available, the contribution of the individual ALDH1A isoforms to tissue RA formation cannot be determined. The contribution of the ALDH1A isoforms to RA formation can be predicted using quantitative protein expression data and in vitro RA formation kinetics. Therefore, a LC-MS/MS peptide quantification method was developed to simultaneously quantify the expression of ALDH1A isoforms in human or mouse tissue samples (**Chapter 2**). Next, the LC-MS/MS peptide quantification method was used to quantify ALDH1A protein expression in human testicular tissue. The testicular ALDH1A protein expression was used along with RA formation kinetics determined with recombinant ALDH1A

protein to accurately predict RA formation by the individual ALDH1A isoforms in human testicular tissue. When the quantified testicular RA concentration was plotted as function of the measured RA formation activity for each study sample, a significant positive association was identified between the testicular RA formation activity and testicular RA concentration. In addition, immunohistochemistry was used to detect a distinct localization pattern for the ALDH1A enzymes within the human testis (**Chapter 3**). Finally, the effect of ALDH1A inhibition by WIN 18,446 on mouse liver and testis RA concentrations was predicted after a single dose or multiple doses of the inhibitor (**Chapter 4**).

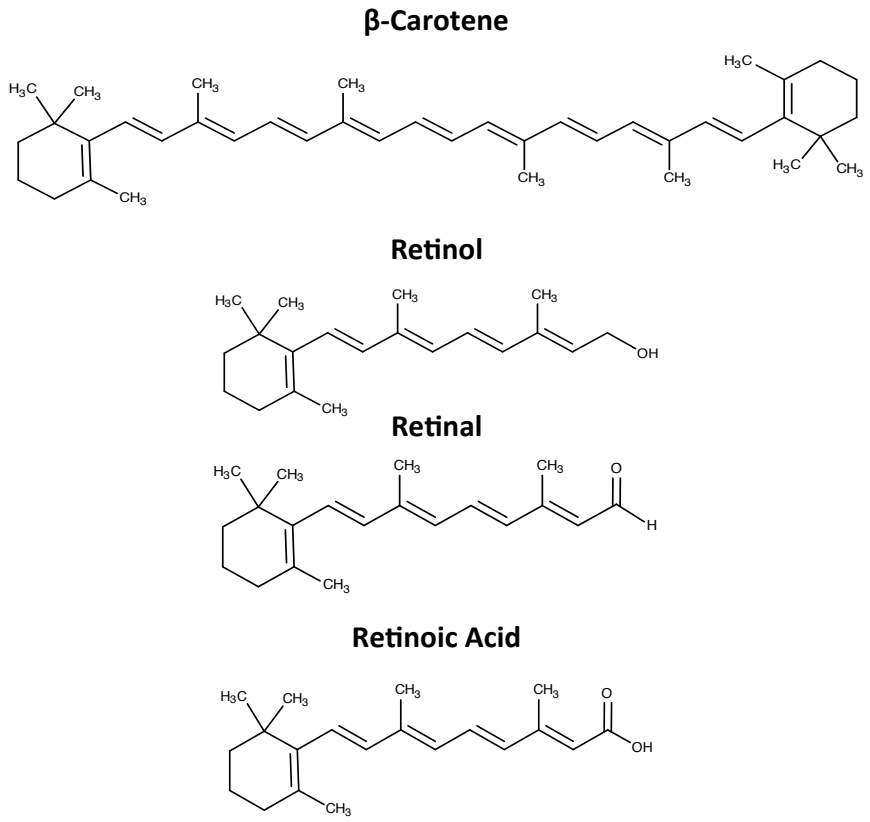

Figure 1.1: The structures of the endogenous retinoids β-carotene, retinol, retinal, and retinoic acid.

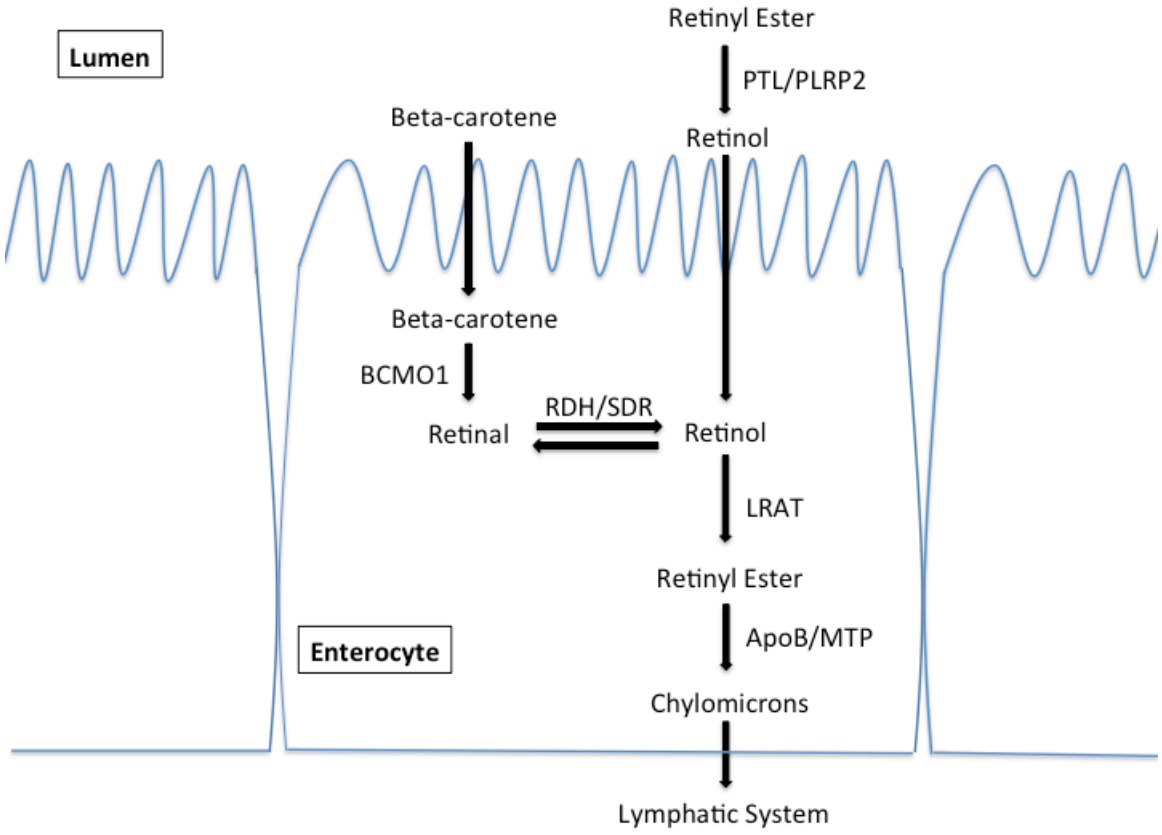

Figure 1.2: Uptake of retinol, retinyl esters, and proretinoid carotenoids in the intestinal lumen.

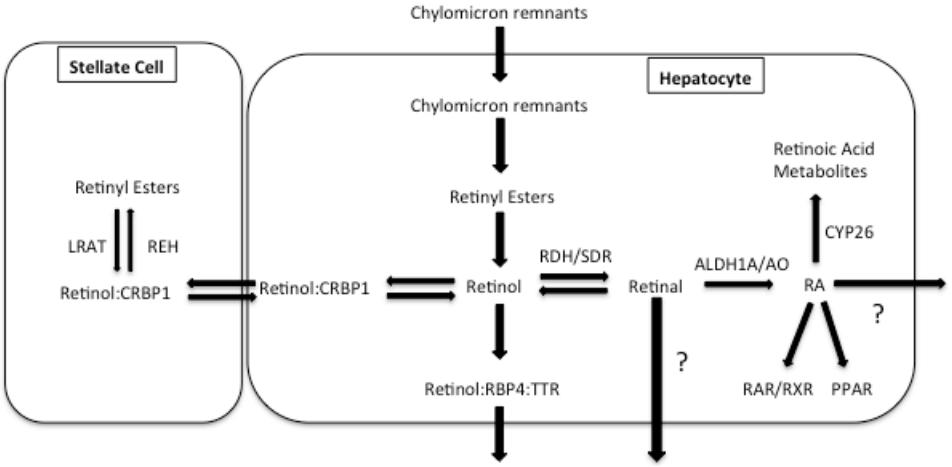

Figure 1.3: Vitamin A storage and metabolism in the liver.

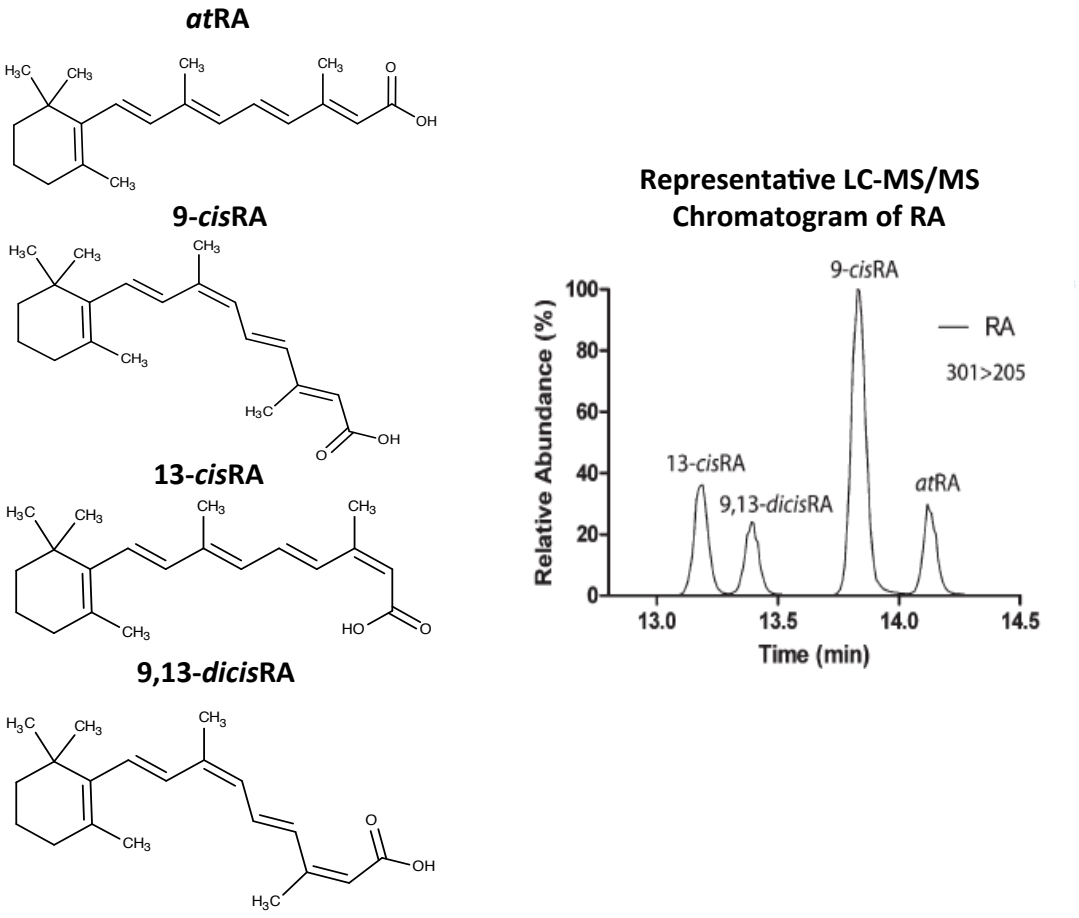

Figure 1.4: The structures of *at*RA, 9-*cis*RA, 13-*cis*RA, and 9,13-*dicis*RA and LC-MS/MS chromatogram of RA in human serum.

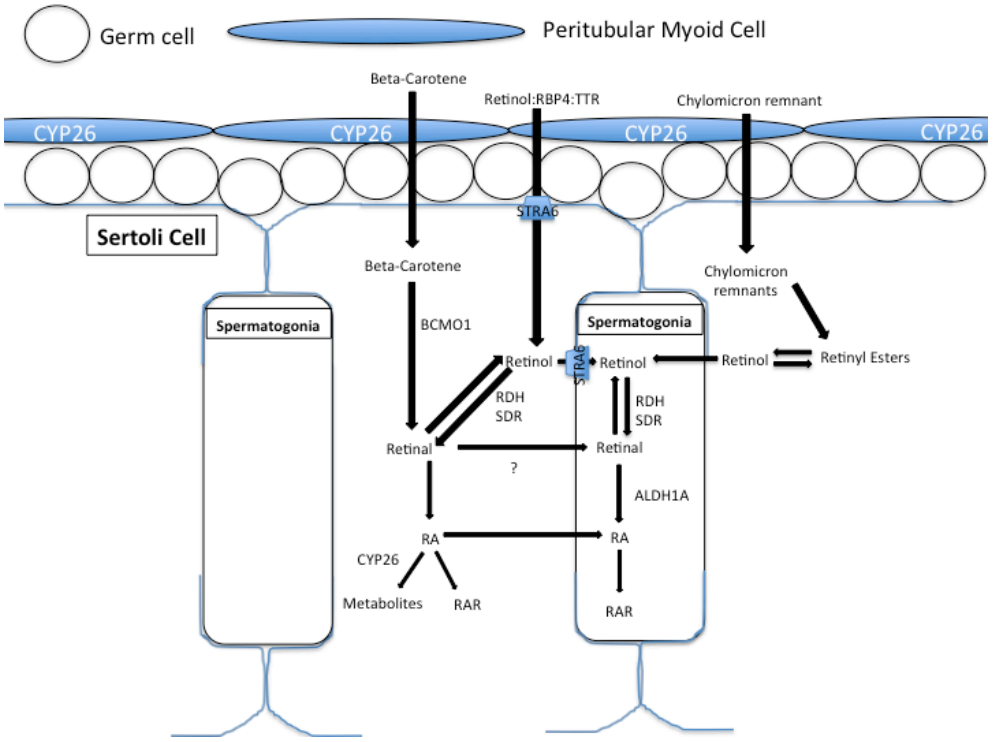

Figure 1.5: Retinoid homeostasis in the testis.

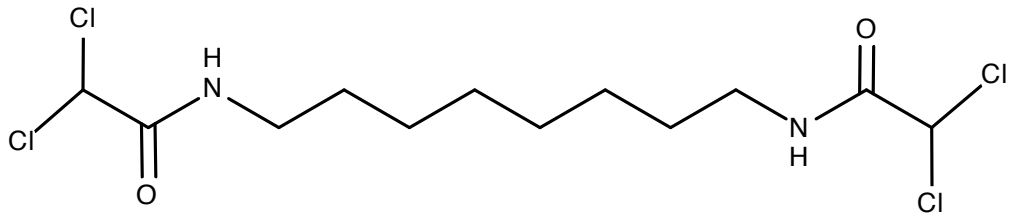

Figure 1.6: The structure of ALDH1A inhibitor WIN 18,446.

Chapter 2

Development and validation of a novel LC-MS/MS method for quantification of RDH11 and ALDH1A expression in human tissues

2.1. Introduction

LC-MS/MS methods have been gaining wide attention and promise as a novel quantitative and specific way of determining protein expression levels in various biological matrices (An et al., 2014; Sakamoto et al., 2011; Seibert et al., 2009). Typically, LC-MS/MS peptide quantification is used to quantify the amount of peptide generated by proteolytic cleavage from a target protein of interest and allows for the simultaneous quantification of multiple proteins. The LC-MS/MS peptide quantification methodology has been validated and applied to therapeutic proteins and biomarkers (An et al., 2014). In addition, methods have been developed for quantification of various catalytic enzymes including CYP enzymes (Heikkinen et al., 2012; Sakamoto et al., 2011; Seibert et al., 2009; Williamson et al., 2011), drug transporters (Li et al., 2008; Sakamoto et al., 2011), UDP-glucuronosyltransferases (Sakamoto et al., 2011), carboxylesterases 1 and 2 (Sato et al., 2012), and aldehyde oxidase (Fu et al., 2013). However, the quantification of protein expression using peptides generated from tissue samples is challenging due to the complexity of different matrices that may result in ion suppression, endogenous matrix interference, and variability in sample recovery and protein digestion. Due to the multiple steps required to solubilize and digest proteins of interest, careful consideration is required for the selection of appropriate quantification standards (calibrators) and internal standards (IS). Therefore, the development of an LC-MS/MS based peptide quantification method for endogenous proteins should involve robust consideration of matrix effects and include steps to compare calibration standards, identify sources of variability, and establish an IS to reduce sources of variability.

Available LC-MS/MS peptide quantification methods generally use one of the following three calibrators: full-length recombinant protein, a synthetic extended peptide, or a synthetic

peptide standard (Keshishian et al., 2007; Pan et al., 2009; Zhu et al., 2010). Of these, recombinant protein has been established as the most accurate and precise calibrator as it must undergo sample preparation steps identical to the target protein (i.e. reduction, solubilization, denaturation, and proteolytic digestion) (Brun et al., 2007; Duan et al., 2012b; Nouri-Nigjeh et al., 2014). However, availability of purified recombinant protein standards is limited and can be challenging especially for membrane proteins. Extended peptides synthesized with additional amino acid residues extending past the site of protease cleavage aim to serve as surrogate calibrators and control for variability in proteolytic digestion and LC-MS/MS analysis. However, it is not clear if proteases interact with extended peptides similarly to whole proteins. In fact, peptide formation from an extended peptide has been observed to occur at a quicker rate than from protein standard resulting in low quantification accuracy (Barnidge et al., 2004; Ocana and Neubert, 2010). Simple synthetic peptides avoid this variability in digestion, but do not report on any of the sample preparation steps necessary for peptide formation from the protein of interest. The use of peptides (Duan et al., 2012a; Nouri-Nigjeh et al., 2014) and extended peptide calibrators (Nouri-Nigjeh et al., 2014) has been shown to generate significant quantification bias in previous studies. Therefore, quantification based on peptide standards is considered relative. An additional strategy to quantify proteins is known as the absolute quantitation (AQUA) method (Gerber et al., 2003). A peptide analogous to the target peptide is synthesized with a stable isotope label (SIL) by incorporating one or more [$^{13}C_6{}^{15}N_2$] residues. The labeled peptide at a known concentration is added to the digested protein sample, and the ratio of unlabeled/labeled peptide measured by LC-MS/MS analysis is used to quantify the amount of peptide formed during the digestion. Although the AQUA method is described as a simple method that facilitates the quantification of multiple proteins, the lack of a calibration curve

prevents both relative and absolute quantification, as it is impossible to know if the peptide ionization used for quantification is within the linear range of the LC-MS/MS.

A considerable challenge in quantification of endogenous proteins is the lack of blank matrix. Generating a calibration curve in a matrix that mimics the study samples is important to minimize bias between the calibration curve and study samples. Membrane bound proteins pose an additional challenge, as they require extraction from a lipid membrane prior to sample digestion. Ideally, the calibration method for membrane proteins will use a matrix allowing for the incorporation of recombinant protein standards into a lipid membrane before sample preparation and digestion. A complication for quantification of endogenous proteins is the lack of availability of a matrix that does not contain the protein of interest. A way to circumvent this problem is to identify peptides that are not conserved between species. For example, if the mouse and human isoforms of the target protein are expressed in the liver cytosol of both species, a peptide for the human protein can be chosen that is specifically formed from the human isoform. Therefore, when human recombinant protein or synthetic peptide is spiked into mouse liver cytosolic protein, an identical peptide from the endogenous mouse protein will not be generated by protease digestion. However, the sample preparation, digestion, and ionization may still be affected by the matrix, and further confirmation of similar peptide formation in the calibration curve matrix and in the study samples is recommended.

In addition to bias generated by different matrices, the protein quantification can be affected by variability within the set of samples. Ideally, the variability between the samples can be reduced by incorporating an IS such as SIL recombinant protein standards (Kumar et al., 2010; Lesur et al., 2010; Nouri-Nigjeh et al., 2014; Seegmiller et al., 2009), extended peptides (Nouri-Nigjeh et al., 2014; Ocana and Neubert, 2010), and peptides (Barnidge et al., 2003; Kuhn

et al., 2004; Nouri-Nigjeh et al., 2014). An ideal IS will correct for variability encountered during the sample preparation, protease digestion, storage, and LC-MS/MS analysis (Jemal et al., 2010). Previously, when LC-MS/MS peptide quantification was used to quantify proteins in human brain tissue, protein extraction from tissue contributed to 72% of variability, short term instrumental variability in instrumental response contributed to 16%, longer term variability in instrumental response contributed to 9%, and protein trypsin digestion contributed to 3% (Piehowski et al., 2013). While the distribution of variability was peptide dependent, this demonstrates that selection of the correct IS is critical to address variability between samples even within a single matrix. A critical aspect of variability relates to extraction of the protein from the matrix prior to incubating the protein with a protease. Therefore, if correctly folded and incorporated into a membrane, SIL protein standards analogous to the target protein would serve as an ideal IS as they require the same sample preparation steps as the target protein. Interestingly when SIL protein standards and SIL peptides were separately used as IS to quantify OATP1B1, OATP1B3, OATP2B1, and P-gp in human liver microsomes (Prasad and Unadkat, 2014), no significant differences in quantification were observed and it was suggested that a SIL peptide structurally analogous to the target peptide would be a sufficient IS. Yet, it is unclear how broadly applicable this strategy is for various peptides and proteins.

The soluble, cytosolic aldehyde dehydrogenase (ALDH) and membrane bound retinol dehydrogenase enzymes (RDH) serve as ideal model proteins for the development of a LC-MS/MS peptide quantification method. In tissues that require retinoic acid (RA) signaling, ALDH and RDH enzymes are essential for maintaining the tight control of RA synthesis (Kurlandsky et al., 1995). RA is formed from retinol by two enzyme dependent steps within each tissue. First, the membrane bound RDH enzymes of the short chain dehydrogenase/reductase

(SDR) superfamily enzymes reversibly form retinal from retinol and at least eleven RDH enzymes have been demonstrated to catalyze the reversible formation of retinal in vitro (Kedishvili, 2013). The conserved nature and overlapping tissue distribution of these enzymes suggests that they are highly functionally redundant and an in vivo role for these enzymes in postnatal RA homeostasis is unclear. Tissue localization data for the RDH enzymes has relied on mRNA and it is not clear if there is a direct correlation between mRNA detection and protein expression. After formation of retinal from retinol by RDH enzymes, the aldehyde dehydrogenase 1A (ALDH1A) family of enzymes is believed to catalyze the irreversible formation of RA from retinal. Yet, the role of the ALDH1A enzymes in postnatal development is unclear due to embryonic lethality of *Aldh1a2*$^{-/-}$ (Niederreither et al., 1999) and *Aldh1a3*$^{-/-}$ (Dupe et al., 2003) mouse models and a lack of studies of the in vivo effect of ALDH1A inhibition. Although mRNA localization has identified a distinct expression pattern for the ALDH1A isoforms in human tissues (Xi and Yang, 2008), the contribution of each isoform to tissue RA formation cannot be determined without knowing the quantitative expression level of each enzyme. However, the lack of selective, stable antibodies for these enzymes has, up to date prevented measurement of their expression by western blot or ELISA. Therefore, LC-MS/MS peptide quantification is a promising approach to allow quantification and characterization of the expression patterns of these proteins in diverse matrices of interest.

The aim of the study was to develop a robust and reproducible LC-MS/MS peptide quantification method using purified protein standard calibrators to measure the expression of RDH and ALDH1A in tissue samples. Based on its wide tissue expression in humans and mice (liver, retina, testis) and the availability of unlabeled and SIL purified protein standards, RDH11 was selected as a model protein for the quantification of RDH enzymes. RDH11 is membrane

bound and localizes to the endoplasmic reticulum, so the results of this study will be applicable to developing LC-MS/MS peptide quantification methods for other membrane bound proteins such as cytochrome P450 enzymes and drug transporters. An in vivo role in regulating RA homeostasis has been demonstrated for the cytosolic, soluble ALDH1A1 and ALDH1A2, but their expression in adult tissues is unclear. To generate a robust quantification method for each of these proteins, stable signature peptides were selected for each protein. Multiple protein matrices for the calibration curve of each protein were compared to eliminate bias introduced due to matrix effects not being represented. For each quantification peptide, variability at each step in the protein quantification method was assessed and different IS options were compared to reduce variability. Finally, the protein quantification methods were applied to human liver tissue to quantify RDH11 and ALDH1A1 protein expression.

2.2 Methods and Materials

Materials

SIL and unlabeled purified RDH11 were acquired from Origene (Rockville, MD). Mass spectrometry grade trypsin, dithiothreitol, iodoacetamide, optima grade water, optima grade acetonitrile, formic acid, and SIL peptides were purchased from Thermo-Fisher (Rockford, IL). Sodium deoxycholate was purchased from Sigma (St. Louis, MO).

Purified recombinant ALDH1A1 and ALDH1A2

Human ALDH1A1 and ALDH1A2 were expressed and purified as previously described (Arnold et al., 2014). Briefly, hexahistidine tagged human ALDH1A1 and ALDH1A2 were expressed in *Escherichia coli* (BL21(DE3)), harvested, and purified using the His.Bind resin and buffer kit (Catalog # 69755-3, Novagen) as previously described (Arnold et al., 2014). Purified enzyme was dialyzed against 20 mM Hepes buffer (pH 8.5) containing 150 mM KCl and 1 mM EDTA. Protein purity was confirmed by SDS-PAGE followed by Coomassie staining and

concentrations were determined using BCA protein assay kit (Thermo Fisher, Waltham, MA) or protein assay kit II (BioRad, Hercules, CA). Enzyme was stored at 4°C in the dialysis buffer with 1mM TCEP (Thermo Fisher, Waltham, MA), a reducing agent.

Preparation of microsomal, cytosolic, and S10 fractions

Livers from 3-5 month old BL/6-129 mice were collected previously, human liver samples were obtained from the University of Washington, School of Pharmacy Human Tissue Bank, and Sf9 cells were grown in Sf-900 II SFM liquid media (Invitrogen, Carlsbad, CA) supplemented with 2.5% fetal bovine serum, harvested, washed once in phosphate buffer solution with 1 mM phenylmethanesulphonylfluoride (PMSF), pelleted, and stored at −80°C prior to subcellular fractionation. Microsomal and cytosolic protein fractions were generated from human liver, mouse liver, and Sf9 insect cells using a previously published method (Paine et al., 1997). Briefly, samples were homogenized on ice using a motor driven Teflon-tipped pestle in a 10 mL Wheaton tube in three times sample volume of tissue homogenization buffer (50 mM Potassium Phosphate (KPi), 250 mM sucrose, pH 7.4) with EDTA free protease inhibitor cocktail (Roche, San Francisco, CA). After homogenization, the Wheaton tube was washed with 2x volume of homogenization buffer and the wash added to the homogenate. The homogenate was transferred to 50 mL centrifuge tubes which were centrifuged at 10,000 g for 15 minutes at 4°C to pellet large organelles and cell membranes. The supernatant (S10 fraction) containing microsomes and cytosol was removed and centrifuged at 110,000 g for 70 minutes to isolate microsomes. The supernatant (cytosolic fraction) was saved, aliquoted, and flash frozen in liquid Nitrogen. The pellet (microsomes) was resuspended in storage solution (50 mM KPi, 250 mM sucrose, pH 7.4) to final concentration of 10- 20 mg/mL. The microsomal protein was

aliquoted, flash frozen in liquid Nitrogen and stored at -80°C. The total protein concentration in each fraction was measured using a BCA assay (Thermo Fisher, Waltham, MA).

In silico protein digestion and initial peptide screening

Initial signature peptide candidates were chosen based on in silico analysis using Skyline software (MacLean et al., 2010). The FASTA files for each protein sequence were downloaded from www.uniprot.org and the accession numbers for the human and mouse proteins respectively, were as follows: RDH11- Q8TC12, Q9QYF1 ALDH1A1- P00352, P24549 and ALDH1A2- O94788-1, Q62148. Enzymes were digested in silico with trypsin and peptides with less than 7 residues or more than 20 residues were excluded from the peptide selection process. In addition, peptides with a predicted $m/z > 1100$ and < 100 were excluded due to the m/z range of the mass spectrometer. Next, human and mouse proteomes obtained from www.uniprot.org were trypsin digested in silico with Skyline. The predicted peptides for the target proteins were screened against the trypsin digested proteomes to ensure peptide selectivity for the protein of interest. For RDH11 and ALDH1A1, specific peptides generated from the human enzymes but not conserved in the mouse protein were chosen to allow spiking the human recombinant proteins to the mouse matrix without endogenous interference from the corresponding mouse protein.

Initial signature peptides can be selected after in silico protein digestion based on their predicted stability (do not contain histidine, tryptophan, cysteine, or methionine). However, since purified protein standards were available for each of the target proteins, peptide stability was assessed experimentally. Peptides generated in silico were avoided if they were reported to contain sites of single nucleotide polymorphisms (SNP) or posttranslational modifications (PTM). Reported sites of SNP or PTM were determined using the information provided by the

www.uniprot.org website. In addition, peptides were discarded if they contained a proline residue on the carboxyl side of the lysine or arginine at the site of cleavage. For the peptides that passed the initial selection criteria, Skyline was used to predict their precursor ions and fragments along with the declustering potentials and collision energies for each transition. A MS/MS method was generated with the *m/z* transitions and mass spectrometric parameters generated with Skyline are shown in Tables 2.1-2.3 for RDH11, ALDH1A1, and ALDH1A2.

Sample preparation, digestion and analysis by UHPLC-MS/MS

Sample preparation and trypsin digestion were performed in 96-well plates according to the following protocol: First, 20 µL of sample (purified protein standards or tissue fraction) were added to each well followed by 4 µL of 100 mM dithiothreitol to reduce disulfide bonds and 10 µL of 100 mM pH 7.8 ammonium bicarbonate buffer. Samples were vortexed and then incubated at room temperature for 20 minutes. Next, 5 µL of 10% sodium deoxycholate (Sigma, St. Louis, MO) were added to each well, and the samples vortexed before incubation at 95°C for 5 minutes. After cooling to room temperature, 4 µL of 200 mM iodoacetamide were added and the samples incubated at room temperature in the dark for 20 minutes to prevent the formation of disulfide bonds. Lyophilized trypsin was reconstituted in 50 mM acetic acid and added at a 1:25 trypsin:protein ratio to each sample. Samples were incubated with trypsin for 15 hours at 37°C unless specified otherwise. The trypsin digestion was quenched by addition of 20 µL ice cold acetonitrile with 8% trifluoroacetic acid. Next, samples were centrifuged at 3,000 g for 25 minutes at 4°C and the supernatants were transferred to a 96-well plate prior to analysis by LC-MS/MS.

The peptides were quantified by mass spectrometry using an AB Sciex 5500 qTrap Q-LIT mass spectrometer (AB Sciex, Foster City, CA) equipped with an Agilent 1290 UHPLC

(Agilent, Santa Clara, CA). The tryptic peptides were separated using an Aeris Peptide XB-C18 column (50 X 2.1 mm) with 1.7 µm particle size at 40°C and a SecurityGuard Ultra UHPLC C18-peptide cartridge (Phenomenex, Torrance, CA). The eluting solvents were A: H_2O + 0.1% formic acid and B: acetonitrile + 0.1% formic acid. For chromatographic separation the following 18 minute linear gradient with a 400 µL/minute flow rate was used: 0 → 3.5 minutes 3% B, then increased to 40% B by 12.0 minutes, 12.0 → 12.1 minutes 95% B and kept 95% B until 15.0 minutes, then 15.0 → 15.1 minutes 3% B, 15.1 → 18 minutes 3% B. The peak areas for each peptide of interest were determined using Analyst (version 1.5.1) (AB Sciex, Foster City, CA). The calibration curve generated for each protein was used to determine the pmol of enzyme in each sample. The final protein concentration was determined by normalizing the amount of enzyme in each sample by the total protein in each digestion.

Selection of signature peptides and protein matrix for calibration curves

To assess the analytical performance of the candidate RDH11 and ALDH1A signature peptides initially selected using Skyline, purified RDH11 and ALDH1A protein standards were digested with trypsin and analyzed by LC-MS/MS. Protein standards were separately spiked to final concentrations of 200 nM RDH11, 600 nM ALDH1A1, and 200 nM ALDH1A2 in homogenization buffer and each digested with trypsin as described above. The single digestion for each protein was quenched after 15 hours and analyzed by LC-MS/MS. To compare the analytical performance of the peptides observed after trypsin digestion, the peak areas were ranked from largest to smallest, and the four peptides that generated the largest peak areas were selected to continue along in the signature peptide selection process. To optimize the duration of the trypsin digestion, assess the stability of the peptides during the trypsin digestion, and determine if mouse and/or insect cell protein could be used as a blank matrix for calibration,

each of the protein standards was spiked in duplicate into homogenization buffer (50 mM Potassium Phosphate, 250 mM sucrose, pH 7.4) or to homogenization buffer with 2 mg/mL of mouse microsomal protein or insect cell microsomal protein for RDH11 and 2 mg/mL mouse cytosolic protein or insect cell cytosolic protein for ALDH1A enzymes. The final spiked concentrations of the protein standards were 200 nM RDH11, 600 nM ALDH1A1, and 200 nM ALDH1A2. In addition, all matrices were digested without the addition of purified protein to visually assess any interferences generated from the matrix during the digestion. The trypsin digestion was quenched at 0, 0.1, 2, 4, 6, 10, 15, and 24 hours to determine the time dependence of peptide formation and stability of each peptide in the various matrices during the trypsin digestion. After 24 hours, the remaining digested protein was quenched and stored at 4°C, 23°C, and 37°C. These stored samples were analyzed in duplicate at 12 and 24 hours after quench to assess the stability of each candidate peptide at temperatures encountered during the sample preparation, digestion, and LC-MS/MS analysis. Peptides that displayed instability during the digestion or post-quench (degradation > 20%) were discarded as signature peptide candidates.

RDH11 peptide formation and stability in human and mouse liver microsomal matrix

To determine if mouse liver microsomal protein could serve as a matrix to simulate the effect of human liver microsomal protein on sample preparation, protein digestion, and peptide ionization, the formation of SIL-VVV and SIL-MLS peptides from SIL-RDH11 purified protein were compared in mouse and human microsomal protein. The SIL-RDH11 contained [$^{13}C_6{}^{15}N_2$]-lysine and [$^{13}C_6{}^{15}N_2$]-arginine residues and was spiked to a final concentration of 50 nM into samples containing homogenization buffer (50 mM Potassium Phosphate, 250 mM sucrose, pH 7.4), 2 mg/mL mouse microsomal protein, or 2 mg/mL human microsomal protein pooled from four human donors. Samples were vortexed and allowed to incubate at room temperature for 20

minutes to allow for incorporation of SIL-RDH11 into mouse and human microsomal membranes. Samples were then aliquoted in quadruplicate, prepared, digested for 15 hours, and analyzed by LC-MS/MS as described above. To confirm the expression of RDH11 in the human liver microsomal protein, the VVV and MLS peptides formed from endogenous RDH11 in the pooled human liver microsomal protein were quantified along with the SIL peptides.

SIL peptide standards

Synthesized SIL peptides analogous to the quantification peptides for each protein contained [$^{13}C_6{}^{15}N_2$]-lysine or [$^{13}C_6{}^{15}N_2$]-arginine residues (Table 2.4). In addition, a SIL-VVV extended peptide was synthesized that contained three additional amino acid residues extending past the site of trypsin cleavage. The peptide, VVVVTGANTGIGKETA, requires cleavage by trypsin to generate the signature VVV peptide for RDH11. The SIL peptides were directly infused with and without the addition of solvent to optimize the MS/MS transitions for the quantitation peptides using the Analyst software (Table 2.4). The purity of the synthetic peptide standards was reported to be >95% by the manufacturer.

Identifying sources of variability during sample preparation/digestion and LC-MS/MS analysis

To identify sources of variability in the method, the instrumental and sample preparation and digestion variances were assessed separately. First, instrumental variance was determined by digesting five separate samples in homogenization buffer (50 mM Potassium Phosphate, 250 mM sucrose, pH 7.4) containing 50 nM RDH11, 325 nM ALDH1A1, and 40 nM ALDH1A2. After the digestions were quenched with solution containing SIL peptides at concentrations similar to their corresponding proteins and centrifuged, the five samples were pooled and analyzed using LC-MS/MS as described. The pooled sample was repeatedly injected 12 times and the instrumental coefficient of variation was determined for each peptide using equation (1)

$$coefficient\ of\ variation = 100 * \frac{\sigma}{\mu} \quad (1)$$

where μ is the average peak area of the observed signature quantification peptides and σ is the standard deviation in peak area. Next, to determine the variability in the sample preparation and digestion, 50 nM of RDH11 was spiked into 2 mg/mL mouse microsomal protein and 325 nM ALDH1A1 and 40 nM ALDH1A2 recombinant protein were spiked into 2 mg/mL mouse cytosolic protein. Each sample was aliquoted into 10 wells and prepared, digested, quenched, and analyzed by LC-MS/MS. In addition, to identify any differences in the formation of the SIL-VVV peptide from the SIL-RDH11 protein or SIL-VVV-extended peptide, SIL-RDH11 and SIL-VVV extended peptide were spiked into 2 mg/mL mouse microsomal protein at a final concentration of 50 nM. The samples were aliquoted to 10 individual wells, prepared, digested, quenched, and analyzed by LC-MS/MS. The coefficient of variation was determined for each peptide using equation (1).

Application of an IS to correct for LC-MS/MS variability

To address the long term variability in LC-MS/MS analysis that can occur over the course of instrumental operation (instrumental stability), SIL peptides were used as an IS to correct for the systematic decline in observed peptide ion intensity. Purified protein standards (50 nM RDH11, 325 nM ALDH1A1, and 40 nM ALDH1A2) were digested in homogenization buffer and quenched with solution that contained 50 nM SIL-VVV, 325 nM SIL-ANN, and 40 nM SIL-ILE peptides. After centrifugation, the sample was injected approximately 700 times until an instrumental instability indicated by a significant negative correlation between the peak area of each quantification peptide and the number of injections was observed. The peak areas for each SIL and unlabeled peptide were assessed separately to determine the rate of signal depreciation for both peptides. To determine if the SIL peptides corrected for the reduction in the

observed peptide responses, the peak areas of the SIL peptides were used to normalize the peak areas of the unlabeled peptides and linear regression was used to determine if significant correlation between the normalized peak areas and the number of injections existed.

Determining the accuracy and precision with different IS

To maximize the accuracy and precision of the protein quantification method, four IS methods were evaluated for RDH11 (Figure 2.1). In three of the methods, 50 nM SIL-RDH11, SIL-VVV extended peptide, or SIL-VVV peptide were added along with the purified RDH11 standard into mouse liver microsomal protein at a final concentration of 2 mg/mL mouse liver microsomal protein matrix. For the fourth and final method, RDH11 protein standard was spiked into 2 mg/mL mouse microsomal protein, prepared, and digested without the addition of a SIL peptide or SIL-RDH11. Upon termination of the trypsin digestion for the fourth method, 50 nM SIL-VVV peptide was added along with the 20 μL of quenching solution. The accuracy and precision of the ALDH1A protein quantification method was maximized by comparing two IS methods (Figure 2.1). 35 nM SIL-ANN-1A1 peptide and 17.5 nM SIL-ILE peptide were added either along with the purified ALDH1A standards into mouse liver cytosolic protein at a final concentration of 0.2 mg/mL mouse liver cytosolic protein matrix or upon termination of the trypsin digestion. All of the samples were analyzed by LC-MS/MS as described above and the peak area of each quantification peptide was normalized to the peak area of the corresponding SIL peptide added to the sample or formed from a SIL purified protein or SIL extended peptide.

To determine the precision of each IS method over a range of protein concentrations, interday and intraday coefficients of variation were determined for three sets of quality control (QC) samples. QC samples were prepared for RDH11 by spiking purified RDH11 to a final concentration of 22.5 nM (QC1) or 55 nM (QC3) in 2 mg/mL mouse microsomal protein. A third

RDH11 QC sample (QC2) was prepared by pooling human liver microsomal protein from four separate donors to a final concentration of 2 mg/mL. For ALDH1A, QC samples were prepared by spiking purified ALDH1A1 into 0.2 mg/mL mouse liver cytosolic protein to final concentrations of 150 nM (QC1), 325 nM (QC2) or 600 nM (QC3) and ALDH1A2 to 10 nM (QC1), 32.5 nM (QC2) and 80 nM (QC3). Next, each QC sample was aliquoted into either four microcentrifuge tubes (RDH11) or two microcentrifuge tubes (ALDH1A). Each of the four microcentrifuge tubes containing RDH11 were separately spiked with either SIL-RDH11, SIL-VVV-extended peptide, SIL-VVV peptide, or homogenization buffer (50 mM Potassium Phosphate, 250 mM sucrose, pH 7.4). The SIL-RDH11, SIL-VVV-extended peptide, and SIL-VVV peptide were added to a final concentration of 50 nM. For the two microcentrifuge tubes containing ALDH1A protein, one tube was spiked with homogenization buffer (50 mM Potassium Phosphate, 250 mM sucrose, pH 7.4) and the other with SIL peptides to a final concentration of 35 nM SIL-ANN-1A1 and 17.5 nM SIL-ILE. After IS or homogenization buffer was added, each sample was aliquoted into twenty separate microcentrifuge tubes, flash frozen in liquid Nitrogen, and stored at −80°C. On three separate days, three to eight replicates of each sample were thawed, digested, and quenched with 20 µl chilled acetonitrile containing 8% trifluoroacetic acid. For samples initially spiked with just homogenization buffer, the quenching solution contained 50 nM SIL-VVV, 35 nM SIL-ANN-1A1, and 17.5 nM SIL-ILE. Samples were analyzed using LC-MS/MS as described above and the peak areas of each quantitation peptide were normalized by the peak area of the corresponding SIL peptide. The interday and intraday variability was calculated using equation (1). On one of the three days of analysis, eight replicates for each QC were digested and used to determine the intraday variability. The interday variability was calculated by determining the coefficient of variance of replicate samples over

the three days of analysis. All samples were included in the final calculation of variability and accuracy.

For quantitation, calibration curves were prepared along with the QC samples. Calibration curves were generated for each protein of interest using purified protein standards at five separate concentrations (RDH11: 7.5-150 nM, ALDH1A1: 50-1000 nM, ALDH1A2: 5-100 nM). The calibration curves were prepared in either 2 mg/mL mouse liver microsomal protein or 0.2 mg/mL mouse liver cytosolic protein. Each sample was aliquoted and spiked with IS or homogenization buffer alongside the QC samples. Next, the samples of each calibration curve were aliquoted into 3 microcentrifuge tubes, flash frozen in liquid Nitrogen, and stored at −80°C. On three separate days, a set of samples for each single calibration curve was thawed, digested, and quenched alongside the QC samples. On each day of analysis, the calibration curve generated with each IS was used to back calculate each point in the calibration curve and calculate the concentration of each QC sample. The accuracy (%) for each data point in the calibration curve was calculated using equation (2)

$$Accuracy\ (\%) = \left(\frac{[measured]}{[actual]}\right) * 100 \quad (2)$$

and the average accuracy was determined for each point in the calibration curve by combining the accuracy over the three days of analysis. The percent error in accuracy for each QC sample was determined using equation (3).

$$Error\ (\%) = \left(\frac{[measured]-[actual]}{[actual]}\right) * 100 \quad (3)$$

The average percent error in accuracy of each of the IS methods was determined by combining the percent error in accuracy for each QC determined over the three days of analysis (n=20 for peptide in quench IS and n=9 for all other IS methods).

Quantification of hepatic RDH11 and ALDH1A1 with purified protein standards and by the AQUA method

To determine the impact of the AQUA method on the quantification of RDH11 and ALDH1A1 in human liver tissue and to establish the applicability of the developed method, RDH11 and ALDH1A1 were quantified in four human livers. To quantify RDH11, 40 μg of microsomal protein from each liver was prepared, digested, and quenched. Each human liver microsomal protein sample was digested in quadruplicate and the SIL-VVV peptide was included in the trypsin quench at a concentration of 50 nM and used as an IS. The ratio of VVV/SIL-VVV was used to quantify the expression of the RDH11 protein based on a five point calibration curve generated with 5-150 nM purified RDH11 concentrations spiked into 2 mg/mL mouse liver microsomal protein. The VVV/SIL-VVV ratio was used to determine the concentration of RDH11 in each sample based on the calibration curve. The final protein concentration was determined by normalizing the amount of enzyme in each sample by the total protein in each digestion. In addition, the AQUA method was used to quantify RDH11 expression in the four livers. For the AQUA method, the concentration of unlabeled VVV peptide was calculated by multiplying the VVV/SIL-VVV ratio measured in each digestion by the known concentration of the SIL-VVV peptide.

To quantify ALDH1A1, 4 μg of cytosolic protein from each liver was digested in triplicate. The trypsin digestion quench solution contained 35 nM SIL-ANN-1A1 peptide which was used as an IS. A single six point calibration curve was generated alongside the samples with 50-1000 nM purified ALDH1A1 spiked into 0.2 mg/mL mouse liver cytosolic protein. The ANN-1A1/SIL-ANN-1A1 ratio was used to determine the concentration of ALDH1A1 in each sample based on the calibration curve. In addition, the AQUA method was used to quantify the

ALDH1A1 expression in the four livers. The concentration of the ANN-1A1 peptide was determined by multiplying the ANN-1A1/SIL-ANN-1A1 ratio by the known concentration of SIL-ANN-1A1. ALDH1A2 was not quantified in human livers as no peptides from this protein were detected in any of the liver samples.

Statistical Analysis

With the exception of the trypsin time course data and the initial peptide peak area ranking, all data are expressed as mean ± standard deviation. The peptide peak areas found in Figure 2.5 are based on a single measurement and all the trypsin time course data is expressed as mean ± range of two measurements. ANOVA analysis was used to determine if there was a significant difference in SIL-VVV and SIL-MLS peptide formation from SIL-RDH11 in human liver microsomal protein, mouse liver microsomal protein, and homogenization buffer. If significance was achieved with the ANOVA analysis, a student's t-test was performed post hoc to identify statistically significant differences between individual groups. A student's t-test was used to determine if purified protein standards and AQUA quantification generated significant differences in measured hepatic RDH11 and ALDH1A1 expression levels.

2.3 Results

In silico digestion and initial signature peptide screening

To identify signature peptide candidates, each target protein was digested in silico with Skyline. As a result, 13 peptides were identified as potential signature peptides for RDH11 along with 21 for ALDH1A1 and 20 for ALDH1A2 (Figures 2.2-2.4). Of the peptides initially identified with Skyline, two peptides for ALDH1A1 and four peptides for ALDH1A2 contained a proline residue on the carboxyl side of the trypsin cleavage site, which can interfere with protease digestion. Therefore, these peptides were discarded as potential signature peptides. In

addition, one of the peptides from RDH11 and four of the peptides from ALDH1A1 were conserved between mouse and human and were removed to prevent interference from endogenous protein in the mouse liver protein fractions. To ensure selectivity in the human proteome for the protein of interest, peptides detected in silico as potential conserved peptides in multiple proteins in the human proteome were discarded as signature peptide candidates. The removal of these peptides resulted in the loss of two peptides for RDH11, three peptides for ALDH1A1, and five peptides for ALDH1A2 (Figure 2.2-2.4). Finally, reported natural variants for each of the proteins were discarded as signature peptide candidates. After the in silico screening, nine peptides remained for RDH11, eleven peptides for ALDH1A1, and eight peptides for ALDH1A2. These remaining peptides for each protein are found in Tables 2.1-2.3 along with the mass spectrometric parameters used for detection of these peptides.

Since relative LC-MS/MS ion abundances of peptides cannot be predicted in silico, the detection sensitivity of the peptides was monitored after trypsin digestion of protein standards and their peak areas ranked from largest to smallest (Figure 2.5). Of peptides identified in the in silico screening as signature peptide candidates, 78% of the RDH11, 83% of the ALDH1A1, and 100% of the ALDH1A2 peptides were observed after trypsin digestion of the purified protein standards. The two peptides not observed in vitro from RDH11 and ALDH1A1 are shown in Tables 2.1 and 2.2, respectively. While it is unclear why these peptides were not observed experimentally, peptide instability may have contributed to their absence as three of the four peptides contained methionine, tryptophan, or histidine residues. Up to 200-fold difference in the LC-MS/MS ion abundances of the candidate peptides from each protein was observed demonstrating the importance of assessing the analytical performance of peptides experimentally, to maximize the sensitivity of the assay. The four peptides for each protein that

generated the largest peak areas were chosen for further evaluation as candidate signature peptides.

Trypsin digestion time course and peptide stability during the digestion

The time required for trypsin to completely digest proteins of interest and generate the signature peptide candidates varied from 2 hours to more than 24 hours (Figure 2.6). The large diversity in the observed rates of peptide formation indicates that the ratio of peptides observed from each protein will depend on the duration of the protease incubation. The peptide formation was not complete at 24 hours for only one of the peptides, YIL. Due to the incomplete digestion to this peptide, it was removed as a signature peptide candidate for ALDH1A1. In addition, one of the four candidate peptides for both RDH11 (LAN) and ALDH1A2 (LAF) displayed instability during the trypsin digestion manifested as decreasing signal with increasing digestion time (Figure 2.6). Therefore, both of these peptides were removed from the signature peptide candidate pool. While the instability of the LAF peptide could have been predicted based on its tryptophan residue, the sequence of the LAN peptide did not contain any of the markers associated with peptide instability. After the removal of the YIL, LAN, and LAF peptides, three signature peptide candidates remained for each of the protein targets.

Matrix effects on RDH11 signature peptides

To determine if the trypsin digestion or signal intensity of RDH11 in tissue fractions was altered by microsomal protein or insect cell microsomal protein also found in recombinant enzyme preparations, the formation of the three remaining peptides for RDH11 in homogenization buffer, mouse liver microsomal protein, and insect cell microsomal protein were compared over a 24 hour trypsin digestion time course (Figure 2.7 A-C). Interestingly, peptide specific instability was observed in insect cell microsomal protein with RDH11. When

recombinant RDH11 was added to insect cell microsomal protein and digested with trypsin, the VVV peptide formed by the protease displayed instability during the digestion that was not observed in homogenization buffer or mouse microsomal protein. Due to this instability, none of the remaining studies with RDH11 were performed with insect cell microsomal protein. In both homogenization buffer and mouse microsomal protein, observed peptide formation was complete by 15 hours for all three peptides, and therefore 15 hours was selected as the optimal length of time for the trypsin digestion of RDH11.

RDH11 is a membrane bound protein that requires extraction and solubilization prior to trypsin digestion. Due to the expression of endogenous RDH11 in human liver microsomal protein, SIL-RDH11 was used to evaluate differences in observed peptide formation in homogenization buffer, mouse liver microsomal protein, and human liver microsomal protein (Figure 2.7D & E). While microsomal protein from both species did not affect SIL-VVV peptide formation, the observed SIL-MLS peptide formation in microsomal protein was significantly less than in buffer ($p < 0.05$) demonstrating the necessity of evaluating appropriate matrices carefully. The reason for this matrix effect is unclear, but the MLS peptide requires alkylation at its cysteine residue in order to be detected by LC-MS/MS and it is possible that differences in alkylation could be responsible for the observed difference in peptide formation. No difference between mouse and human liver matrix was observed demonstrating that mouse liver could be used as a matrix for method validation. In contrast to the SIL-VVV and SIL-MLS peptides, the SIL-EIQ peptide was not observed in the homogenization buffer, mouse liver microsomal protein, or human liver microsomal protein. This is most likely due to low sensitivity for the EIQ peptide compared to the VVV and MLS peptides. To confirm the presence of RDH11 in human liver microsomal protein, the formation of the VVV and MLS peptides from endogenous RDH11

in the pooled human liver microsomal protein was monitored along with SIL peptide formation from the SIL-RDH11 spiked into the human liver microsomal protein (Figure 2.7F). The identification of the endogenous RDH11 was confirmed by the similar VVV/MLS peptide ratio observed from both the endogenous RDH11 and the SIL-RDH in the pooled human liver microsomal protein. Similar to the SIL-EIQ peptide, the EIQ peptide generated from endogenous RDH11 was not detected in the human liver microsomal protein. Therefore, only the VVV and MLS peptides remained as signature peptide candidates.

Matrix effects on observed peptide formation from ALDH1A1 and ALDH1A2

The observed peptide formation from ALDH1A1 and ALDH1A2 was dependent on the digestion matrix (Figure 2.8). Similar to insect cell microsomal protein, use of the insect cell cytosolic protein resulted in peptide instability that was not observed in homogenization buffer or mouse liver cytosol (Figure 2.8B). Therefore, insect cell cytosolic protein was not used for any of the remaining studies. Both mouse and insect cell cytosolic proteins appeared to reduce the observed formation and/or signal intensity of the IFV-1A1 peptide, and hence it was removed as a candidate signature peptide (Figure 2.8C). Similar to RDH11, a 15 hour trypsin digestion was selected for the remaining studies with ALDH1A proteins. Based on the assessment of matrix effects, two peptides, VAF and ANN-1A1, for ALDH1A1, and the three peptides, EMG, EEI, and ILE, for ALDH1A2 appeared as potential signature quantification peptides after evaluation of trypsin digestion.

Peptide stability at 23°C, 4°C, and 37°C

The stability of the remaining signature peptide candidates for the three proteins was assessed at 23°C, 4°C, and 37°C for 12 and 24 hours (Figure 2.9). While the EMG-1A2 peptide was stable at 23°C and 37°C, the ion abundance decreased more than 20% following 24 hour

storage at 4°C. The reason for this peptide instability observed only at 4°C is unclear, but the methionine residue in the EMG peptide may have contributed to the instability. All of the other signature peptide candidates were stable at all three temperatures. After the EMG peptide was removed as a signature peptide candidate, two peptides remained available for each protein. These remaining peptides were chosen as the signature peptides for the protein quantification method. The signature peptides were as follows: VVV and MLS for RDH11, ANN-1A1 and VAF for ALDH1A1, and ILE and EEI for ALDH1A2. Based on the availability of SIL peptide standards, the VVV, ANN-1A1, and ILE peptides were chosen as the quantitation peptides for RDH11, ALDH1A1, and ALDH1A2, respectively.

IS correction for instrumental instability

For each quantitation peptide, the uncertainty due to LC-MS/MS factors was assessed separately from those due to sample preparation by comparing variability of multiple measurements of pooled samples with that of multiple measurements on separate samples. The percent variability introduced by the LC-MS/MS analysis was 5% for VVV, 4% for ANN-1A1, and 7% for ILE. The intraday variability in the sample preparation and digestion combined with potential instrumental variability was determined for each peptide and was 8% for VVV, 7% for ANN-1A1, and 8% for ILE. The instrumental and sample variability were assumed to be independent. Therefore, the variability in the sample preparation for the quantitation peptides was estimated with the propagation of error and was as follows: 6% for VVV, 6% for ANN-1A1, and 4% for ILE. These values were similar to the instrumental variability alone suggesting that sample preparation and digestion are highly reproducible. The corresponding intraday variability for the SIL-VVV peptide formation from the SIL-VVV extended peptide and SIL-RDH11 was 14% and this was 6% higher than from the unlabeled RDH11 protein standard.

In an effort to decrease the instrumental variability introduced by the LC-MS/MS method, a SIL peptide analogous to each quantitation peptide was incorporated into the method as an IS. The SIL peptide was added during the quench of the trypsin digestion. For VVV and ANN-1A1, the instrumental variability was increased when the peak areas of the peptides were normalized by their analogous SIL peptide standard (11%). As such, IS normalization did not decrease the instrumental variance. However, variability in the ratio between the unlabeled peptide and SIL peptide for ILE peptide was lower (5%) than that observed for the ILE peptide alone (8%).

Although the inclusion of a SIL peptide as an IS did not improve the instrumental variability for RDH11 and ALDH1A1, the importance of the SIL peptide as an IS in prolonged MS runs is illustrated by the experiment in which instrumental LC-MS/MS instability was introduced. A single sample containing digested purified protein standards and SIL peptides was repeatedly injected until the ionization of each peptide displayed a significant decrease with the number of injections (Figure 2.10). For each of the three quantitation peptides, the inclusion of a SIL peptide as an IS rectified the observed signal deterioration demonstrating the significant role of an IS in controlling for instrumental instability.

Method validation for quantitative analysis

Multiple IS methods were used for each protein to evaluate the precision and accuracy of the protein quantification method. Over the three days of analysis, all of the calibration curves generated with each IS were linear (coefficients of determination (R^2) ≥ 0.95) with the exception of calibration curves generated for RDH11 with the SIL-VVV extended peptide as an IS (Tables 2.5-2.7). To initially assess the accuracy of each protein quantification method, the accuracy was determined for the data points in each calibration curve over the three days of analysis (Tables

2.5-2.7). Quantitation at each concentration in the calibration curve was considered accurate if the average percent accuracy was within 80-120%. For each protein analyte, only the SIL-peptide in quench IS method had acceptable accuracy for every data point in the calibration curve. The majority of the inaccuracy with the other IS methods was at low protein concentrations demonstrating the significant impact an IS can have on accurate protein quantification in samples with low protein expression.

To further assess the accuracy and precision of each method, the calibration curves generated with each IS were used to determine the accuracy of the protein quantification methods and to generate basic method validation criteria. To pass validation, the accuracy and precision (CV%) for the method had to be less than 20% at all QC concentrations. For RDH11, the individual values for each IS method are shown in Figure 2.11. With the exception of the SIL-VVV peptide added in quench, at least one of the RDH11 QC sample sets failed over the three days of analysis with each IS. Although the average accuracy and precision over the three days of analysis was acceptable for the SIL-VVV peptide and the SIL-RDH11 protein standard, the failure of at least one set of QC samples suggests that they are not an ideal choice as an IS (Table 2.8). While it is not clear why the precision and accuracy were reduced when the SIL-VVV peptide was added prior to the sample preparation, these results demonstrate the importance of selecting the appropriate step to add the IS. For QC2, the concentration of endogenous RDH11 in the human liver microsomal protein was unknown, so only the precision was determined with each IS method. Analogous to QC1 and QC3, the SIL-VVV peptide in quench generated the optimal precision value. The intraday CV% for SIL-VVV peptide in quench for QC1, QC2, and QC3, were 6%, 6% and 7%, respectively. A similar IS trend was observed for ALDH1A1 and ALDH1A2 (Tables 2.9 and 2.10). Compared to the addition of the

SIL-ANN-1A1 and SIL-ILE peptides prior to sample preparation, the accuracy and precision improved when the peptides were added during the quench of the trypsin digestion and used as IS. The intraday CV% for SIL-ANN peptide in quench for QC1, QC2, and QC3 were 9%, 10%, and 6%, respectively. For ALDH1A2, the SIL-ILE peptide in quench IS method was used to determine intraday CV% values of 12%, 8%, and 11% for QC1, QC2, and QC3, respectively. Based on these results, SIL peptides were chosen as the optimal IS for each of the enzymes and were added during the quench of the trypsin digestion for all further analysis. The final validation parameters are summarized in Tables 2.8-2.10.

Quantification of hepatic RDH11 and ALDH1A

As an application of the developed method, RDH11 and ALDH1A expression levels were quantified in human liver (Figure 2.12). The average concentration of RDH11 measured in the four livers was 56 ± 12 pmol/mg microsomal protein when purified RDH11 was used as a calibrator (Figure 2.12E). When ALDH1A was measured in the liver cytosolic fractions, neither of the ALDH1A2 signature peptides was detected. Therefore, only ALDH1A1 expression was quantified in the human liver cytosol. Based on the lowest point in the calibration curve for ALDH1A2 (5 nM) and the amount of cytosolic protein digested (4 μg), if ALDH1A2 is expressed in the liver, its concentration is less than 25 pmol/mg cytosolic protein. The average ALDH1A1 expression in the four livers was 1180 ± 300 pmol/mg cytosolic protein when the ALDH1A1 protein standard was used as a calibrator (Figure 2.12F).

To determine if the AQUA method could be used in lieu of a calibration curve, RDH11 and ALDH1A1 expression was quantified in each of the four livers using the peptide/SIL-peptide ratio. First, the accuracy of the AQUA method was determined with calibration curves for RDH11 and ALDH1A1 that were generated with purified protein standards. When the

AQUA method was used to determine the concentration of each point in the calibration curve for RDH11, the accuracy was 124%, 84%, 80%, 72%, and 82% for RDH11 concentrations of 5 nM, 20 nM, 50 nM, 100 nM, and 150 nM, respectively. Therefore, compared to the purified RDH11 standard, the AQUA method resulted in an approximately 13% lower RDH11 concentration for each liver and this difference was statistically significant ($p < 0.05$) for one of the four livers. When the AQUA method was used to determine the concentration of each point in the calibration curve for ALDH1A1, the accuracy was 55%, 45%, 49%, 48%, 61%, and 44% for ALDH1A1 concentrations of 50 nM, 100 nM, 200 nM, 500 nM, 750 nM, and 1000 nM, respectively. The underestimation of ALDH1A1 concentrations compared to the ALDH1A1 protein standard translated to AQUA generated ALDH1A1 expression levels that were approximately 50% ($p < 0.01$) lower than those determined with the purified ALDH1A1 standard for all four livers in the study.

2.4 Discussion

ALDH1A and RDH enzymes are believed to catalyze the metabolic steps required for RA biosynthesis from retinol in individual tissues. Yet, due to technical limitations of current protein quantification methods, the quantitative expression profiles of the ALDH1A and RDH isoforms in various human tissues are not known (Kasus-Jacobi et al., 2003). The LC-MS/MS peptide quantification method developed in this study can simultaneously quantify the expression of ALDH1A1, ALDH1A2, and RDH11 enzymes with minimal sample preparation. The approach used here to develop the method will be applicable for development of proteomic methods to establish enzyme expression of retinoid and vitamin A metabolism enzymes.

The majority of peptides predicted with in silico protease digestion were observed after in vitro trypsin digestion of RDH11 and ALDH1A. The peptide coverage of the ALDH1A enzymes

was greater than that observed for membrane bound RDH11, but whether the soluble nature of the ALDH1A enzymes contributed to the increased coverage is uncertain. Although trypsin cleavage was not predicted within the N-terminal membrane anchor sequence of RDH11, it is possible that RDH11 contains additional membrane associated regions that may impede the coverage of trypsin digestion even though the sample preparation procedure includes a protein denaturation step to increase the number of sites available for protease digestion. In this study, protein secondary structures were disrupted by heating the samples to 95°C and reducing disulfide bonds with DTT. These steps may affect each protein differently. For example, temperatures above 37°C were reported to negatively affect the coverage of trypsin digestion for proteins larger than 30 kDa possibly due to the formation of insoluble protein aggregates preventing cleavage by the protease (Hildonen et al., 2014). Whether RDH11 (35 kDa) forms protein aggregates at temperatures above 37°C is not known, but aggregation and dimerization of membrane proteins is not uncommon.

The data obtained here for ALDH1A and RDH11 show that the optimal amount of time for the trypsin digestion will depend on the target peptide resulting in time varying ratios of signature peptides. For maximum reproducibility of detection, well optimized digestion times are essential as otherwise small changes in digestion time can greatly impact quantification. Protein digestion protocols often include an "overnight" incubation with trypsin to allow for the complete digestion of protein (Vandermarliere et al., 2013), yet the data shown here suggests that the accurate determination of the optimal digestion time and the stability of each signature peptide candidate during the trypsin digestion is essential. An unnecessarily long trypsin digestion can generate bias in the protein quantification by increasing the probability of slow non trypsin protein cleavage (Keil-Dlouha et al., 1971) and peptide modifications (Geoghegan et al.,

2002; Krokhin et al., 2006). Trypsin has also been shown to preferentially cleave proteins at certain cleavage sites (Siepen et al., 2007) suggesting the amount of time required for each peptide to reach the maximum amount formed will be peptide specific. In good agreement with these observations, the time required to reach the maximum observed peptide ion intensity for the various RDH11 and ALDH1A peptides varied from two hours to more than twenty-four hours. Such variation in peptide abundance can result in discrepant quantification of target proteins if synthetic peptides are used as calibrators instead of purified protein. The different time courses of peptide formation may also result in different quantitation results using different peptides if full protein standards are not available for quantitation. Quantitation based on a synthetic peptide standard assumes that the target protein in each sample is completely digested in respect to the peptide of interest such that 100% of the target protein in the sample produces the quantitation peptide(s). This assumption generates challenges with different digestion efficiencies and stability. Taken together, the data shown in this study strongly supports the use of protein standards for quantitation. Availability of purified protein standards is often a challenge, especially for membrane protein and the AQUA method has been suggested as an alternative quantitation method that does not required purified protein.

In this study, when compared to a purified protein standard, the AQUA method generated inaccurate protein expression levels for RDH11 and ALDH1A1 expression in the human liver. It is generally believed that bias using the AQUA method is due to incomplete digestion efficiency and/or unstable peptide residues (Kettenbach et al., 2011; Kito and Ito, 2008). However, the stability of each quantitation peptide was validated at multiple temperatures, and therefore it is unlikely that the inaccurate protein quantification observed in this study was due to labile peptide residues. Instead, the digestion efficiency may have contributed to the different concentrations

determined for ALDH1A1 with the different methods. Since the AQUA method underestimated the protein quantification, incomplete digestion of ALDH1A1 is the likely reason for the discrepancy. Similar to ALDH1A1, the RDH11 protein concentration in the human liver was underestimated with the AQUA method, but the 13% lower quantification was very modest. While the AQUA method generated similar values for RDH11 expression in the liver compared to the RDH11 protein standard, it resulted in a statically significant different RDH11 concentration for one of the four livers in the study. Taken together, these data show that protein standards are the most appropriate method for accurate quantification regardless of the subcellular localization of the protein.

A bias in quantification can also arise if the calibration curve is subject to different matrix effects than the study samples. While this is typically not a problem for therapeutic proteins, which can be spiked into blank matrix, it is a particularly important consideration for endogenous protein quantification. The data presented here unequivocally shows that matrix effects need to be considered in targeted quantitative proteomics. After peptides were chosen based on their LC-MS/MS performance, the effect of mouse protein matrix caused the disqualification of a peptide candidate that would have been chosen based purely on its peptide ion intensity. If peptide formation had only been compared in homogenization buffer, the matrix effect would have been overlooked in the assay development and potentially generated significant bias in the protein quantification method. The effect of the protein matrix on the digestion of RDH11 is of particular interest due to the subcellular localization of RDH11 to the endoplasmic reticulum. Previously, protein extraction from human brain tissue was shown to contribute to the majority of the variability in protein quantification (72%) (Piehowski et al., 2013). The availability of a SIL protein standard allowed us to demonstrate that RDH11 protein

extraction from mouse and human liver microsomal protein was not a significant source of bias in this study. Yet, despite this, it's noteworthy that the matrix effects were peptide specific and therefore may be due to coeluting peptides in the LC-MS/MS or protein digestion specific effects.

A matrix effect on peptide ionization and/or stability was not limited to mouse and human protein, as the data shown here suggest peptides may be specifically affected by insect cell protein in a peptide dependent manner. A large number of protein standards are commonly expressed in baculovirus infected insect cells (Luckow, 1993), and microsomal fractions generated from insect cell systems have been used to measure protein expression levels by LC-MS/MS peptide quantification (Kawakami et al., 2011; Xu et al., 2014). Therefore, the effect of insect cell protein on peptide stability and ionization was evaluated for a portion of the peptides. Interestingly, presence of insect cell protein in the samples significantly decreased peptide signal and peptide stability for a subset of the analytes for reasons that are not clear. An insect cell specific protease or baculovirus infections may contribute to this phenomenon. Overall, the instability observed in this study suggests careful evaluation of peptide stability must be conducted when signature peptides are selected for a study that has insect cell protein in the calibration curve and/or study samples.

The stability of signature peptide candidates is often predicted in the peptide selection process and peptides containing histidine, tryptophan, cysteine, or methionine residues are routinely disqualified as they are prone to oxidation. Peptide instability can also be caused by number of phenomena including peptide modification, protein aggregation, degradation, and non-specific binding (Agger et al., 2010). Of the initial potential signature peptides for all three proteins, half of the twenty-eight peptides could have been excluded based on a priori predicted

stability. While the stability of all twenty-eight peptides was not directly tested in vitro, it is plausible that peptide oxidation contributed to the observation that only three of the twelve top performing signature peptide candidates contained a labile residue (Figure 2.5). Furthermore, when the stability of these twelve remaining peptide candidates was tested experimentally, three of the peptides were determined to be unstable and two of these would have been discarded a priori based on their peptide sequence. As a result, although they contributed to half of the initial signature peptide candidates, only one of the final six signature peptides contained a histidine, tryptophan, cysteine, or methionine residue. While these results support the utility of screening peptides based on predicted stability when purified protein standards are not available, the selection of the MLS peptide as a signature peptide for RDH11 demonstrates that in some cases peptide candidates should not be prematurely discarded from the signature peptide selection process. If the MLS peptide had been immediately discarded due to its methionine residue, confirmation of RDH11 expression would not have been possible since the VVV peptide would have been the only peptide sensitive enough to be detected in the human liver samples. Overall, these data suggest that peptide candidates should not be preemptively discarded from the signature peptide selection process without experimental assessment. This is especially important for smaller proteins with limited number of potential peptides as exemplified with RDH11.

Another important aspect of method development addressed by the analysis of recombinant proteins is the ionization efficiency and sensitivity of the individual peptides as the relative magnitude of LC-MS/MS response for each peptide cannot be predicted in silico. In general, the synthesis of every potential peptide candidate is cost prohibitive, making availability of recombinant protein important. The impact of a protein standard was demonstrated with the quantification of RDH11 in the human liver. Based on the more than 200-fold difference in

peptide ionization between the RDH11 peptides, in vitro assessment of peptide analytical performance was essential for RDH11 quantification. With any other combination of signature peptides for RDH11, quantitation of protein expression in the human liver would not have been possible.

The selection of the best IS to use in peptide quantification methods has been evaluated in several previous studies (Nouri-Nigjeh et al., 2014; Pailleux and Beaudry, 2012; Prasad and Unadkat, 2014). A decrease in precision with SIL protein IS compared to SIL peptides was observed for multiple proteins (Prasad and Unadkat, 2014), and in agreement with previous findings, when SIL-RDH11 was used as the IS, the precision of the quantification method decreased compared to the SIL-VVV peptide standard. This may be due to the fact SIL protein standards do not always mimic the native protein, but whether this is generally applicable is not clear (Pritchard et al., 2011). In addition, due to the extensive signature peptide selection process, the cumulative variability in sample preparation/digestion and instrumental performance was below 15% suggesting an IS controlling for the steps preceding LC-MS/MS analysis can provide only limited improvement in the quantification. The SIL-VVV extended peptide IS provided the lowest precision of all the IS methods, a finding in good agreement with previous studies using extended peptides as IS (Barnidge et al., 2004; Bronsema et al., 2013). SIL peptides were used as IS in two separate methods for RDH11, ALDH1A1, and ALDH1A2 by adding the SIL peptides at either the start of the sample preparation or in the quench of the trypsin digestion. For all of the peptides, the precision and accuracy were lower when the SIL peptide was added at the start of the sample preparation. It is possible that this is due to the fact that simple peptides do not behave identically to full proteins in the denaturation and digestion steps of the protocol. As

such, adding the IS at the end of the sample preparation is recommended in simple protocols without extractions.

The reproducibility and accuracy of the protein quantification method is of critical importance and can be addressed via method validation. The final quantification method used a SIL-peptide in the quench and the overall variability (CV%) of the method was below 15% for each of the quantification peptides. The low variability of the method is well within the current method validation parameters set forth by the FDA and EMA for protein ligand binding assays and small molecule LC-MS/MS methods (Jenkins et al., 2015) and demonstrates that rigorous validation criteria can be used for protein quantification methods. While validation criteria do not currently exist for LC-MS/MS peptide quantification, recommended parameters for method validation are similar to those established for ligand binding assays (Jenkins et al., 2015). Previously, LC-MS/MS analysis has been reported to introduce up to 13% variability in peptide abundance between individual sample analysis (instrumental variance) and 17% variability over two weeks of continued analysis (instrumental instability) (Piehowski et al., 2013). In this study, the instrumental variability and sample preparation were both below 10% for all of the quantitation peptides. It is important to note that this variability was obtained by selecting signature peptides that had optimal sample preparation and detection characteristics.

In conclusion, a novel LC-MS/MS peptide method was developed that uses a judicious selection of signature peptides together with protein standard calibrators to determine the concentration of RDH11 and ALDH1A1 in the human liver. This method provides a foundation for the development of LC-MS/MS peptide quantification methods to simultaneously quantify the expression of enzymes responsible for maintaining RA homeostasis and will be an invaluable resource to study how RA concentrations are selectively controlled in a tissue dependent manner.

The method also shows a workflow for the development of validated methods for quantifying endogenous proteins in human tissues.

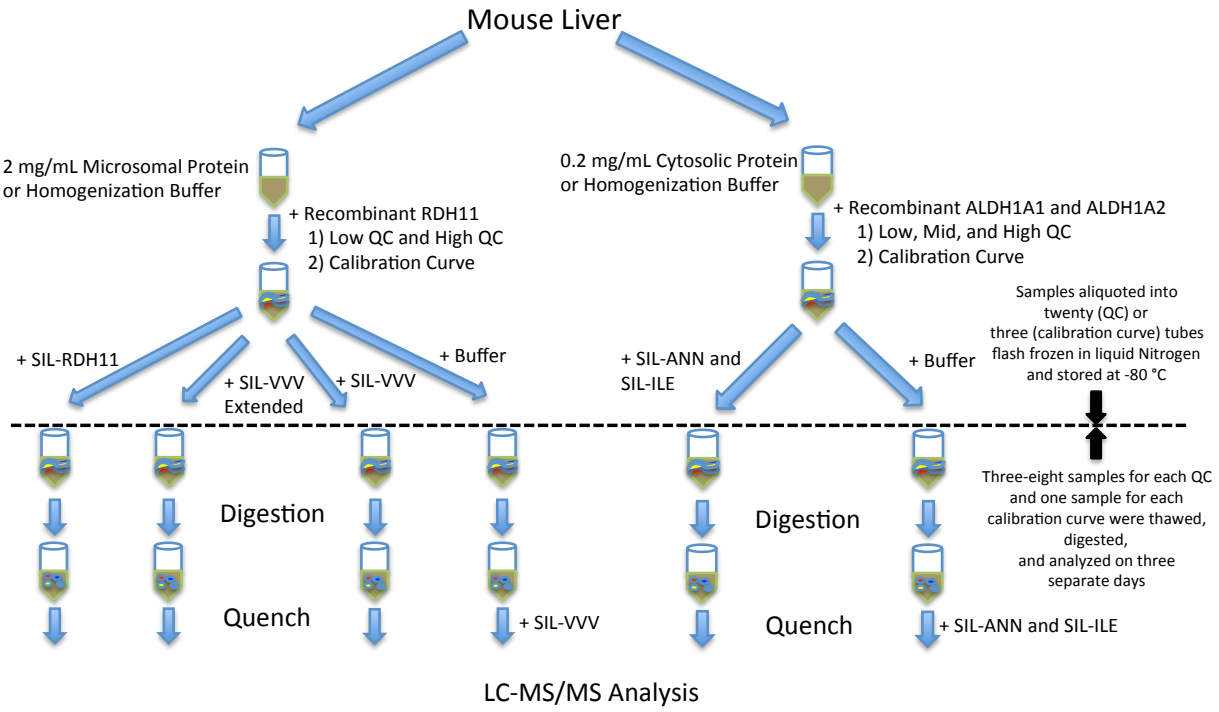

Figure 2.1: **Experimental design for determining the precision and accuracy of RDH11 and ALDH1A quantification with each IS method.** Mouse liver microsomal and cytosolic tissue fractions were generated from mouse livers. Recombinant RDH11 was spiked into 2 mg/mL mouse liver microsomal protein and recombinant ALDH1A enzymes into 0.2 mg/mL mouse liver cytosolic protein. Next, SIL-RDH11, SIL-VVV extended peptide, SIL-VVV peptide, or homogenization buffer were spiked into samples containing mouse liver microsomal protein and purified RDH11 protein. Samples containing ALDH1A protein standards were spiked with either SIL-ANN and SIL-ILE peptides or homogenization buffer. Each sample was further aliquoted as described in the material and methods and flash frozen in liquid Nitrogen. On three separate days, samples were thawed, digested, and analyzed by LC-MS/MS as described in the materials and methods.

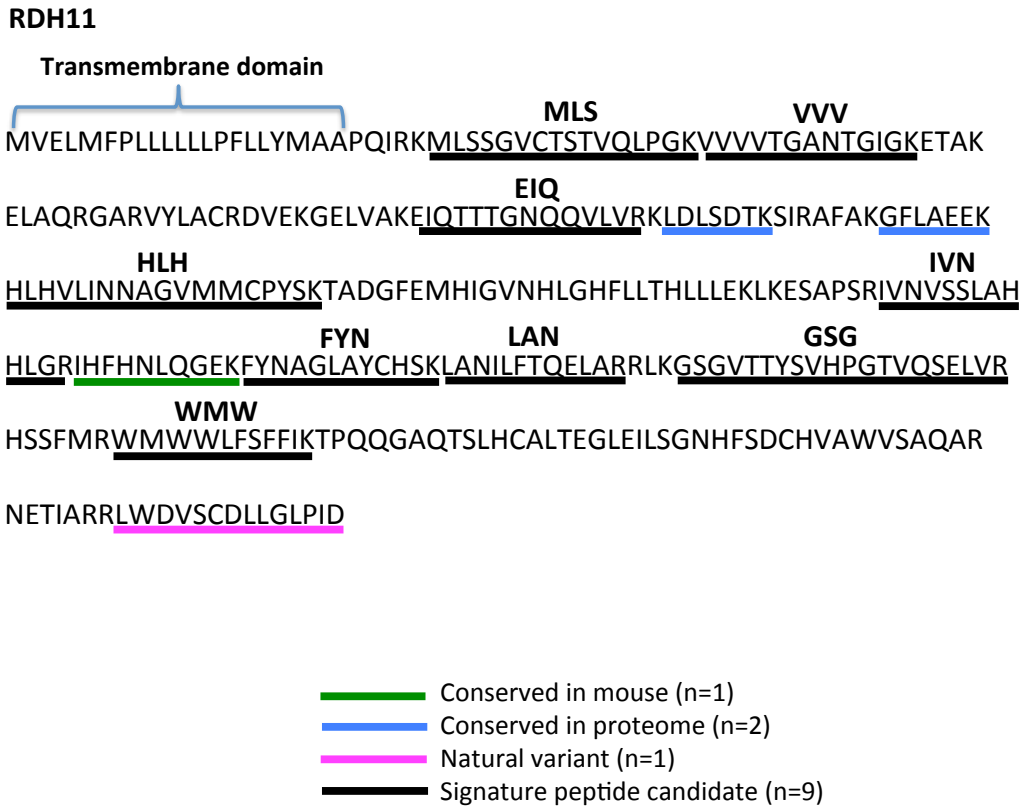

Figure 2.2: **The sequence of RDH11 and signature peptide candidates.** The first twenty-one residues of the RDH11 sequence constitute the N-terminal membrane anchor of the enzyme. Peptides for RDH11 were initially selected based on the length of the peptide (longer than six residues, but shorter than twenty residues) and the dynamic range of the mass spectrometer. These peptides were then screened as described in the methods and materials. As a result, nine of the original thirteen peptides remained as signature peptide candidates.

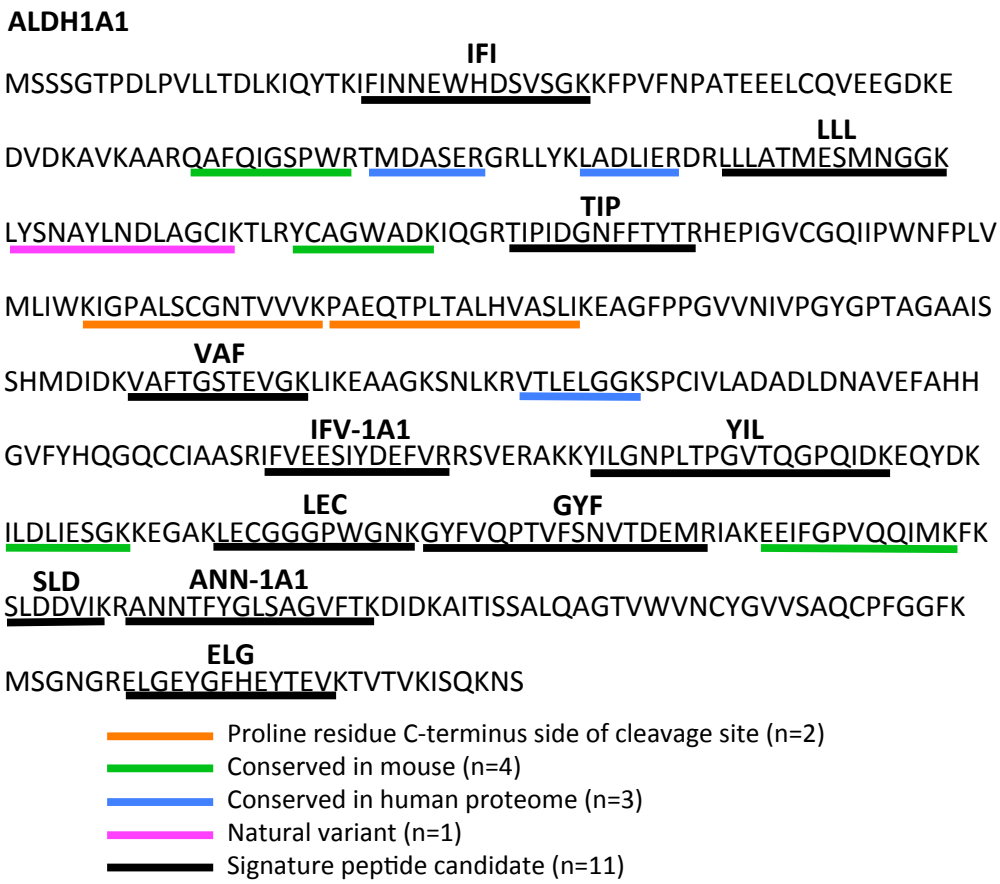

Figure 2.3: **The sequence of ALDH1A1 and signature peptide candidates.** Peptides for ALDH1A1 were initially selected based on the length of the peptide (longer than six residues, but shorter than twenty residues) and the dynamic range of the mass spectrometer. These peptides were then screened as described in the methods and materials. As a result, eleven of the original twenty-one peptides remained as signature peptide candidates for ALDH1A1.

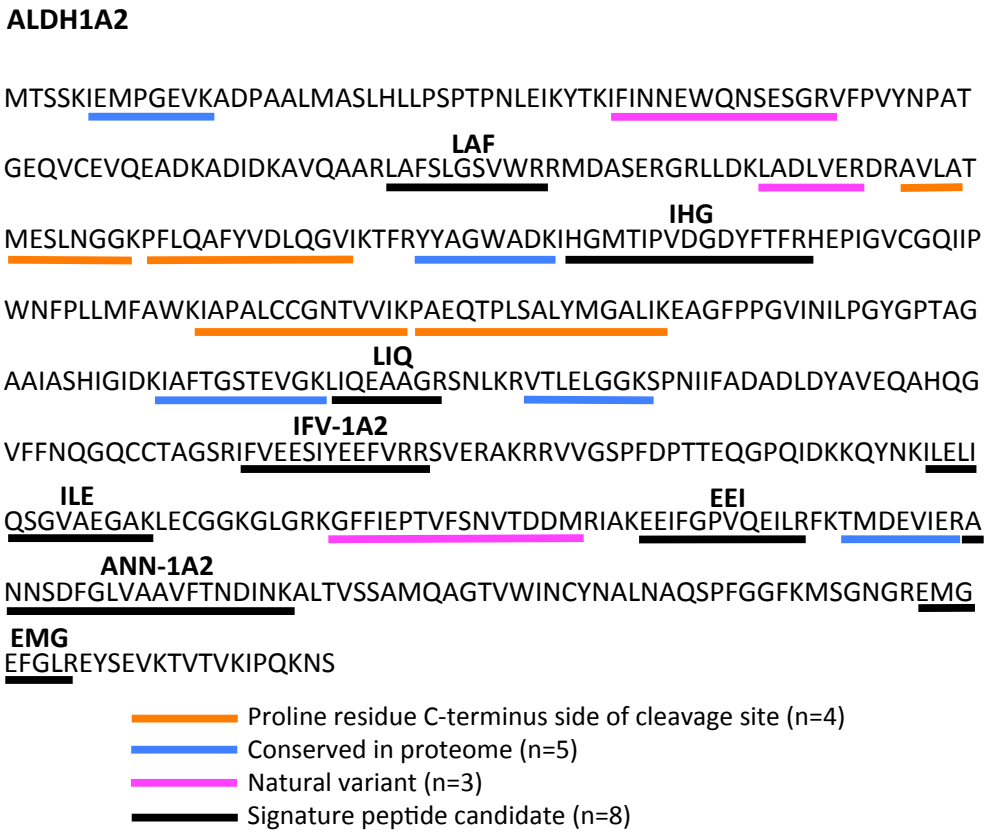

Figure 2.4: **Sequence of ALDH1A2 and signature peptide candidates.** Peptides for ALDH1A2 were initially selected based on the length of the peptide (longer than six residues, but shorter than twenty residues) and the dynamic range of the mass spectrometer. These peptides were then screened as described in the methods and materials. As a result, eight of the original nineteen peptides remained as signature peptide candidates for ALDH1A2.

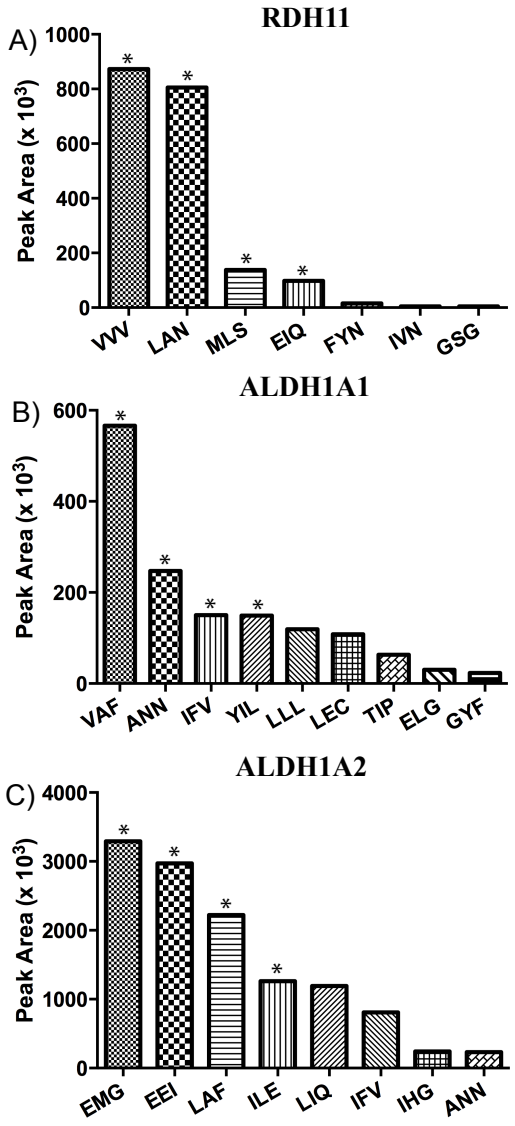

Figure 2.5: **The analytical performance and detection sensitivity of the signature peptide candidates.** The detection of the peptides identified in silico was tested by digesting recombinant RDH11 (A), ALDH1A1 (B), and ALDH1A2 (C) protein standards in homogenization buffer and evaluating detection of all signature peptides as described in materials and methods. For each protein, the peak areas of the observed peptides were ranked from largest to smallest. The peptides are labeled according to Tables 2.1-2.3 and Figures 2.2-2.4. For each protein, the peptides (*) that generated the four largest peak areas were allowed to continue in the signature peptide selection process.

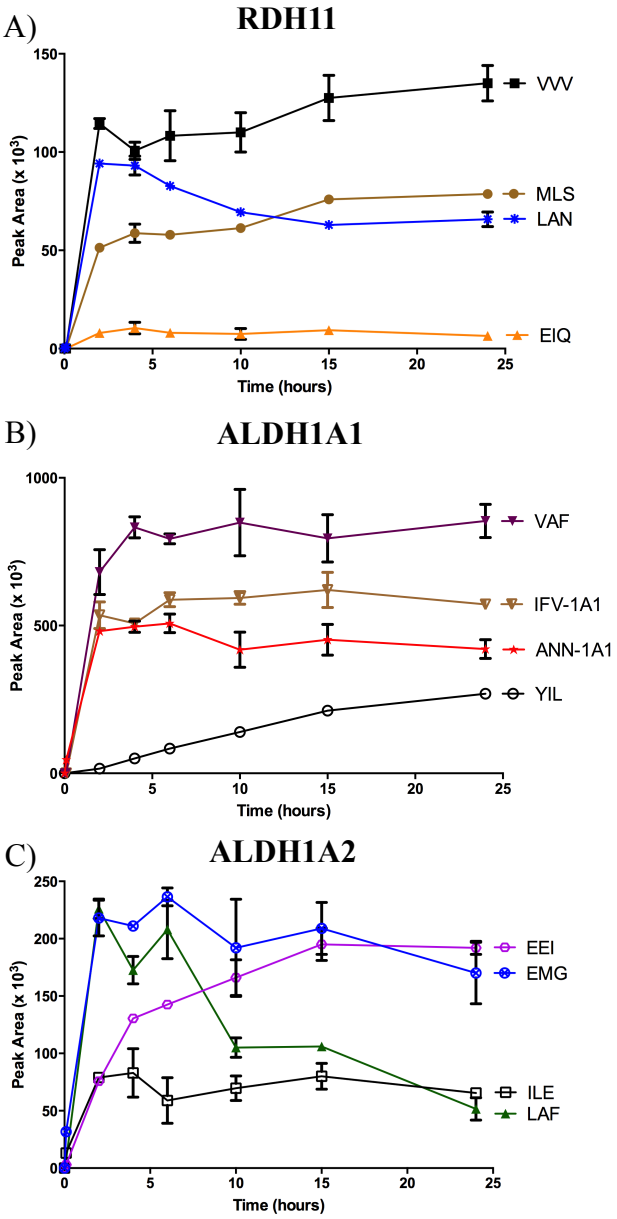

Figure 2.6: The time course of peptide formation and stability in homogenization buffer for target proteins. The formation of the top four signature peptide candidates for RDH11 (A), ALDH1A1 (B), and ALDH1A2 (C) selected from data in Figure 2.5 was monitored after recombinant protein standards were spiked into homogenization buffer and digested with trypsin. The peak area for each peptide was determined at 0, 0.1, 2, 4, 6, 10, 15, and 24 hour time points in duplicate protein digestions. The symbols and corresponding error bars represent the mean and range of the peak areas measured from the duplicate digestions. Peptide labels are according those listed in Tables 2.1-2.3 and Figure 2.2-2.4.

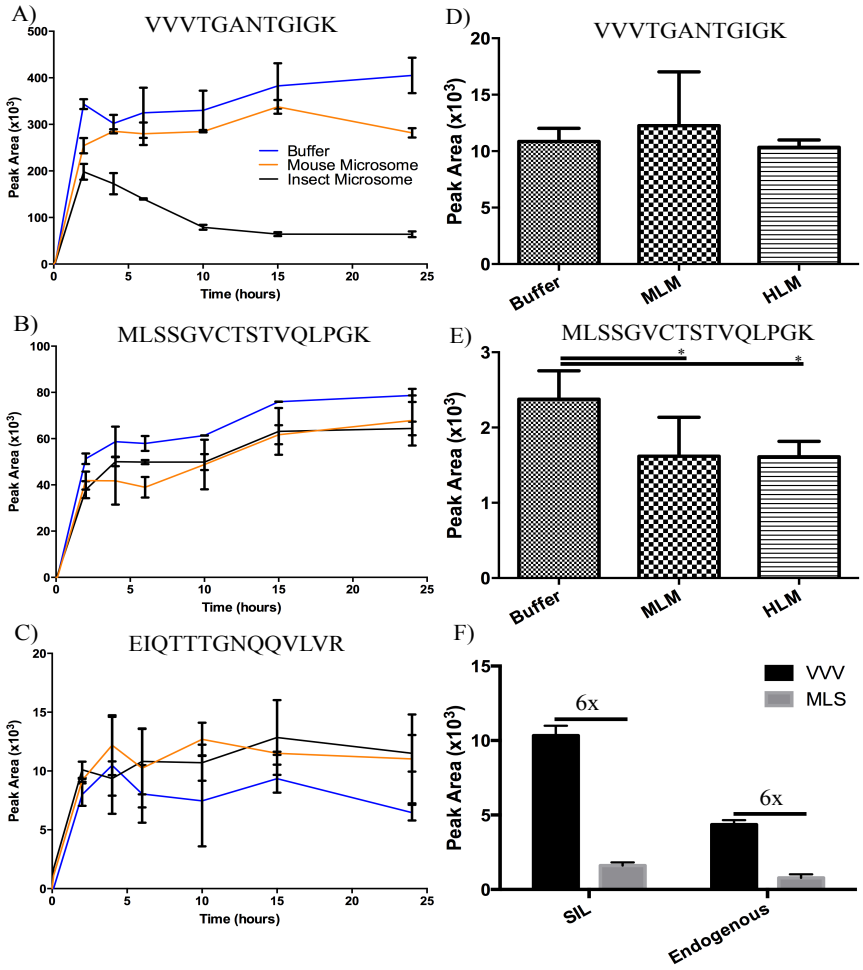

Figure 2.7: The effect of microsomal protein on peptide formation from RDH11 was determined using microsomal protein generated from mouse livers, human livers, and insect cells. The time course of VVV (A), MLS (B), and EIQ (C) peptide formation from RDH11 was observed after RDH11 was spiked in homogenization buffer, 2 mg/mL mouse liver protein matrix, or 2 mg/mL insect cell protein matrix. Each sample was digested in duplicate, and the peak area for each peptide was determined at 0, 0.1, 2, 4, 6, 10, 15, and 24 hour time points. The symbols and corresponding error bars represent the mean and range of the peak areas measured from the duplicate digestions. The formation of SIL-VVV and SIL-MLS peptides were monitored after SIL-RDH11 was spiked in either homogenization buffer, 2 mg/mL mouse liver microsomal protein (MLM), and 2 mg/mL human liver microsomal protein (HLM). There was no difference in the observed formation of the SIL-VVV peptide between the three matrices (D). However, the formation of the SIL-MLS peptide from SIL-RDH11 in MLM and HLM protein was significantly decreased when compared to homogenization buffer (E). The identification of RDH11 in the human liver microsomal protein was confirmed by the similar VVV/MLS peptide ratio generated by the SIL-RDH11 and endogenous RDH11 (F). (*: $p < 0.05$)

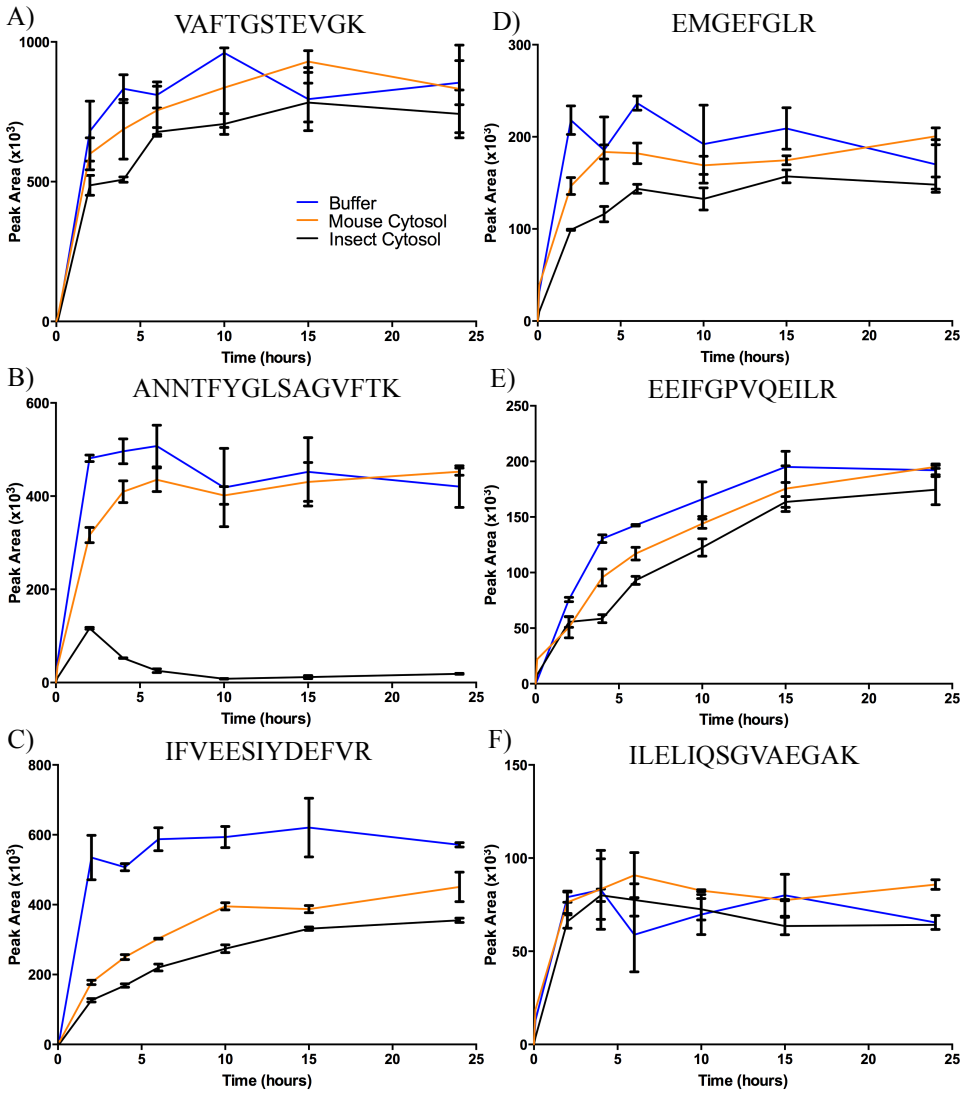

Figure 2.8: Time course of peptide formation from ALDH1A1 and ALDH1A2 spiked into mouse liver and insect cell cytosolic protein. The time course of peptide formation was observed after purified ALDH1A1 (A-C) and ALDH1A2 (D-E) were spiked in homogenization buffer, 2 mg/mL mouse liver cytosol, and 2 mg/mL insect cell cytosol. The peak area for each peptide was determined at 0, 0.1, 2, 4, 6, 10, 15, and 24 hour time points in duplicate protein digestions. The symbols and corresponding error bars represent the mean and range of the peak areas measured from the duplicate digestions. The ANNTFYGLSAGVFTK peptide formed from ALDH1A1 displayed instability in insect cell cytosolic protein, but not in mouse liver cytosolic protein or homogenization buffer (B). In cytosolic protein from insect cells and mouse livers, the amount of IFVEESIYDEFVR formed from ALDH1A1 during the trypsin digestion was suppressed compared to homogenization buffer (C).

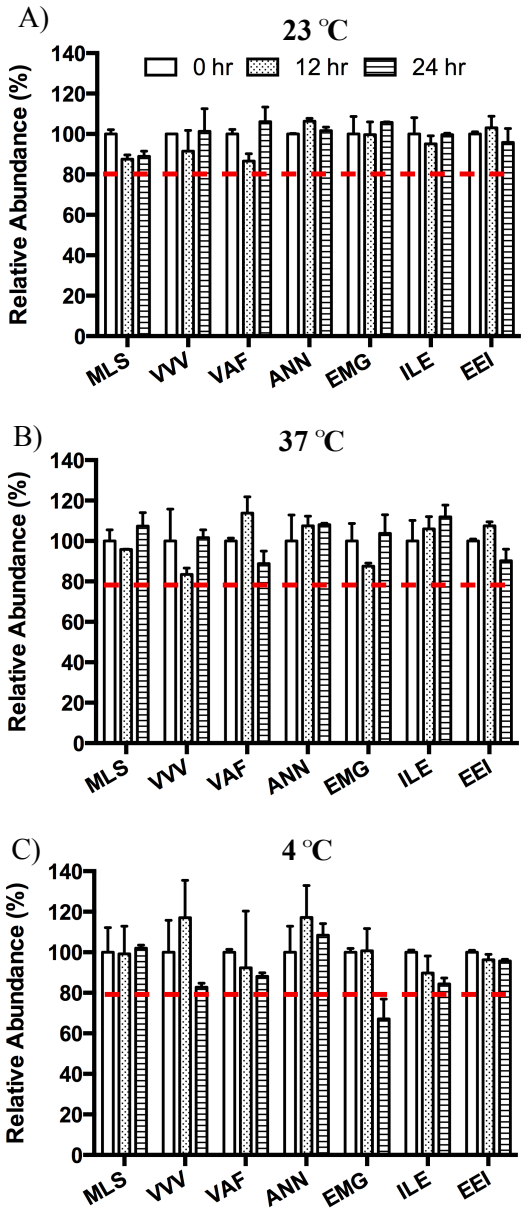

Figure 2.9: The stability of the peptides was assessed at temperatures encountered during the sample preparation, digestion, and LC-MS/MS analysis. Since samples are kept at 23°C and 37°C for prolonged periods of time during sample preparation and digestion, the stability of each peptide was determined at these temperatures for up to 24 hours (A and B). If the relative abundance of all the peptides did not decrease more than 20% during the 24 hour period, the peptides were considered stable at these temperatures. During LC-MS/MS analysis, samples are kept at 4°C to prevent peptide degradation, so the stability of the peptides was determined at 4°C for up to 24 hours. Although the majority of the peptides were stable at this temperature, the average abundance of the EMGEFGLR decreased more than 20%. Since the peptide was unstable at 4°C, it was discarded as a signature peptide candidate for ALDH1A2.

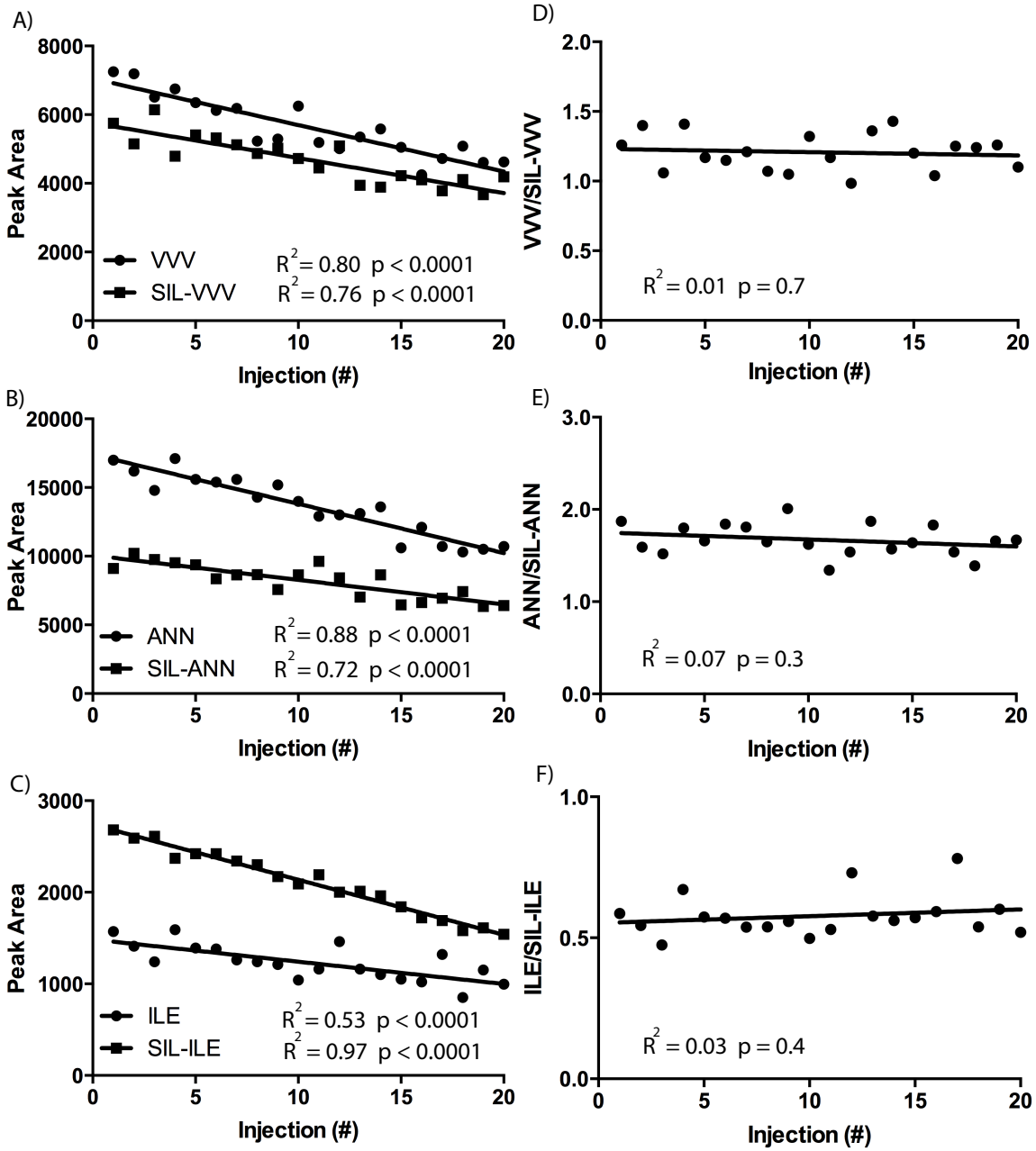

Figure 2.10: The importance of an IS for peptide quantification. A sample containing digested RDH11 (A), ALDH1A1 (B), and ALDH1A2 (C) protein standards and SIL peptide standards analogous to the quantitation peptides was repeatedly injected until a significant decrease in LC-MS/MS signal was observed for the VVV (A), ANN (B), and ILE (C) unlabeled and SIL peptides. When the peak area for each unlabeled peptide was normalized by the peak area of the corresponding SIL peptide standard and plotted as a function of injection number for VVV (D), ANN (E), and ILE (F), the peak area ratio was stable and unaffected by decreased signal intensity.

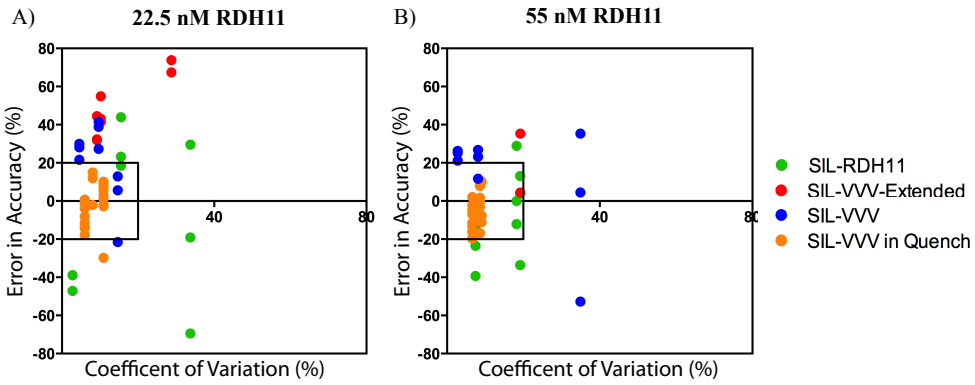

Figure 2.11: The accuracy and precision of RDH11 protein quantification using four different IS methods. The precision and accuracy of RDH11 quantification was determined with the four IS methods at a low QC of 22.5 nM (A) and high QC of 55 nM (B) sample. The intra-day coefficient of variation (precision) was determined for each set QC samples and the CV% for the day plotted on the x-axis. The error in accuracy was determined for each individual sample on three separate days. Therefore, each sample within a set of quality controls will have its own accuracy, but the precision will be shared amongst the other samples analyzed that day. A method that has perfect accuracy and precision will result in values of 0% on the x-axis and y-axis.

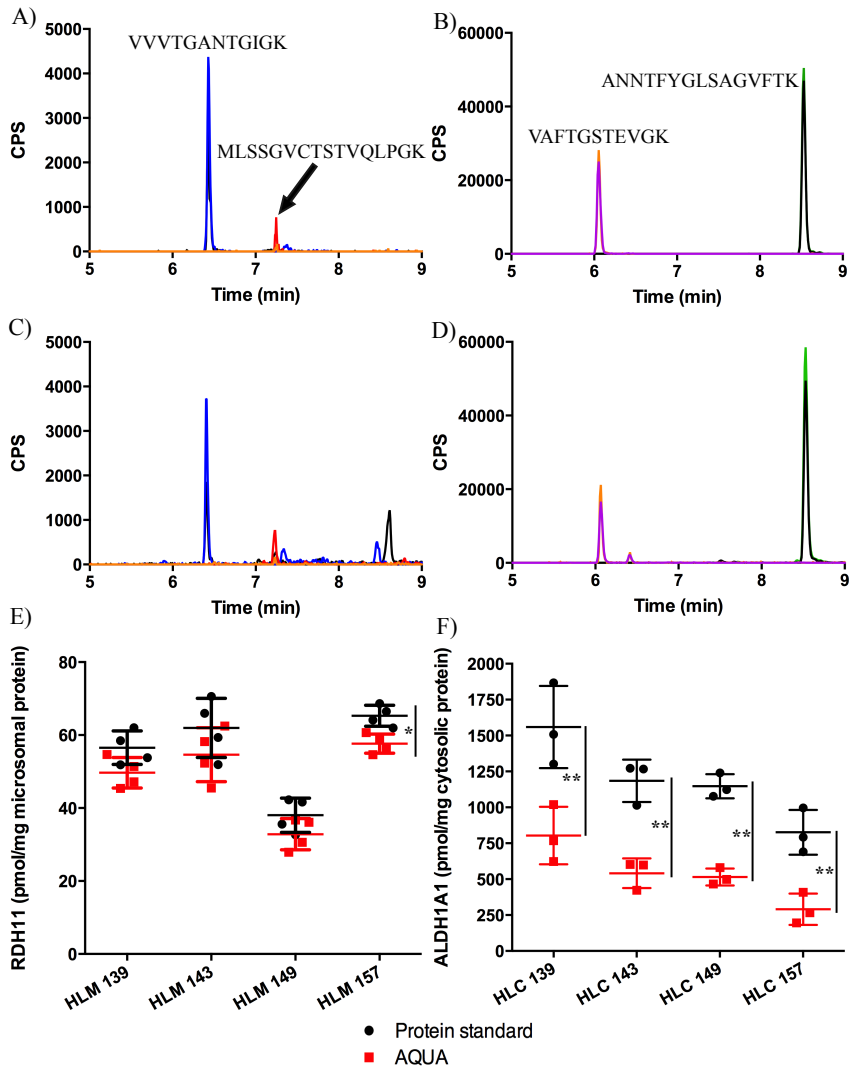

Figure 2.12: Quantification of RDH11 and ALDH1A1 from human liver tissue fractions. RDH11 and ALDH1A1 concentrations were measured using the optimized LC-MS/MS based peptide quantification method. Two peptides (each with two *m/z* transitions) were chosen for each protein to measure recombinant RDH11 (A) and ALDH1A1 (B) protein standards digested with 40 µg mouse liver microsomal protein (RDH11) or 4 µg mouse liver cytosolic protein (ALDH1A1). Each peptide was observed in all four donors and representative chromatograms of detection of RDH11 in 40 µg human liver microsomal protein (C) and 4 µg human liver cytosolic protein (D) are shown. All peaks displayed in the chromatograms are scaled to counts per second (CPS). RDH11 (E) and ALDH1A1 (F) expression levels were quantified in four human livers using either a protein standard (Black) or the AQUA method (Red). For two of the livers, the AQUA method significantly overestimated the RDH11 expression level (E). When the ALDH1A1 expression was quantified with the AQUA method, the measured expression level was significantly less than that determined with the ALDH1A1 protein standard (F). (* $p < 0.05$, **: $p < 0.01$)

Table 2.1 Mass spectrometric parameters for RDH11 peptides selected after in silico screening.

Peptide (Residue #)	Precursor Ion (*m/z*)	Fragments (*m/z*)	Declustering Potential	Collision Energy
MLSSGVCTSTVQLPGK* "MLS" (26-41)	832.9	1197.6 1098.6	92	39
VVVVTGANTGIGK* "VVV" (42-54)	607.9	818.4 717.4	75	31
EIQTTTGNQQVLVR "EIQ" (83-96)	793.9	1014.6 913.5	89	37
HLHVLINNAGVMMCPYSK "HLH" (119-139)	1042.5	654.3 494.3	107	46
IVNVSSLAHHLGR "IVN" (171-183)	701.9	977.2 803.6	78	34
FYNAGLAYCHSK "FYN" (194-205)	715.8	935.4 765.3	83	35
LANILFTQELAR "LAN" (206-217)	694.9	864.5 977.5	82	34
GSGVTTYSVHPGTVQSELVR "GSG" (221-240)	1037.5	1085.6 603.3	107	46
WMWWLFSFFIK "WMW" (247-257)	795.9	641.4 554.3	89	38

Italicized peptides not observed from the digested protein standard, * denotes signature peptides, bolded peptide used for quantitation

Table 2.2 Mass spectrometric parameters for ALDH1A1 peptides selected after in silico screening.

Peptide (Residue #)	Precursor Ion (*m/z*)	Fragments (*m/z*)	Declustering Potential	Collision Energy
IFINNEWHDSVSGK "IFI" (22-35)	823.3	915.6 477.4	91	39
LLLATMESMNGGK "LLL" (100-112)	682.8	593.3 375.2	180	47
TIPIDGNFFTYTR "TIP" (143-155)	772.9	665.8 540.3	180	47
VAFTGSTEVGK* "VAF" (241-251)	548.3	778.4 677.3	71	29
IFVEESIYDEFVR "IFV-1A1" (308-320)	823.4	1028.5 1157.5	91	39
YILGNPLTPGVTQGPQIDK "YIL" (329-347)	1006.0	1139.6 725.9	105	45
LECGGGPWGNK "LEC" (367-377)	587.8	932.4 318.2	74	30
GYFVQPTVFSNVTDEMR "GYF" (378-394)	995.5	698.3 435.2	104	45
SLDDVIK "SLD" (412-418)	395.4	589.1 474.3	60	23
ANNTFYGLSAGVFTK* "ANN-1A1" (420-434)	795.4	879.5 1042.6	120	20
ELGEYGFHEYTEVK "ELG" (476-489)	850.9	246.2 147.1	93	40

Italicized peptides not observed from the digested protein standard, * denotes signature peptides, bolded peptide used for quantitation

Table 2.3 Mass spectrometric parameters for ALDH1A2 peptides selected after in silico screening.

Peptide (Residue #)	Precursor Ion (*m/z*)	Fragments (*m/z*)	Declustering Potential	Collision Energy
LAFSLGSVWR "LAF" (85-94)	568.3	604.3 547.3	73	29
IHGMTIPVDGDYFTFTR "IHG" (156-172)	657.3	834.4 524.3	79	33
LIQEAAGR "LIQ" (269-276)	429.2	374.2 303.2	62	24
IFVEESIYEEFVR "IFV-1A2" (325-337)	830.4	1042.5 1171.6	92	39
ILELIQSGVAEGAK* "ILE" (370-383)	714.4	846.4 959.5	120	35
EEIFGPVQEILR* "EEI" (415-426)	715.4	911.5 854.5	83	35
ANNSDFGLVAAVFTNDINK "ANN-1A2" (437-455)	670.7	489.3 261.2	80	34
EMGEFGLR "EMG" (493-500)	469.7	492.3 345.2	65	26

* denotes signature peptides and bolded peptide used for quantitation

Table 2.4: SIL peptide standards for the quantitation peptides and optimized mass spectrometric parameters. Synthesized SIL peptides analogous to the quantification peptides for each protein contained [$^{13}C_6{}^{15}N_2$]-lysine or [$^{13}C_6{}^{15}N_2$]-arginine residues. In addition, a SIL-VVV extended peptide was synthesized that contained three additional amino acid residues extending past the site of trypsin cleavage. The peptide, VVVVTGANTGIGKETA, requires cleavage by trypsin to generate the signature VVV peptide for RDH11 (bolded). The declustering potential and collision energy parameters for the quantitation peptides were optimized by infusing SIL peptide standards into the mass spectrometer with and without solvent. The same declustering potential and collision energy was also used for the unlabeled peptides.

Protein	SIL Peptide	SIL Extended Peptide	Precursor Ion (*m/z*)	Fragments (*m/z*)	Declustering Potential	Collision Energy
RDH11	VVVVTGANTGIGK	**VVVVTGANTGIGK**ETA	611.9	826.5 725.4	75	30
ALDH1A1	ANNTFYGLSAGVFTK	N/A	799.4	1050.6 887.5	120	35
ALDH1A2	ILELIQSGVAEGAK	N/A	718.4	854.4 967.4	120	30

Table 2.5: The average error at each concentration of the calibration curve and coefficient of determination (R^2) for the calibration curve over the three days of QC analysis for RDH11. The quantification was considered accurate if the average value was between 80 and 120%. The VVV peptide was used for RDH11 quantification.

Internal Standard	Accuracy of calibration curve (%)					Coefficient of determination (R^2)
	7.5 nM	20 nM	50 nM	100 nM	150 nM	
SIL-RDH11	75 ± 28	85 ± 20	98 ± 15	116 ± 5	93 ± 3	0.97 ± 0.01
SIL-VVV extended peptide	28 ± 16	74 ± 18	118 ± 5	123 ± 21	87 ± 11	0.91 ± 0.10
SIL-VVV peptide	54 ± 14	63 ± 15	115 ± 18	81 ± 60	92 ± 2	0.96 ± 0.01
SIL-VVV peptide (quench)	92 ± 1	103 ± 2	107 ± 9	95 ± 2	102 ± 8	0.98 ± 0.01

Table 2.6: The average error at each concentration of the calibration curve and coefficient of determination (R^2) for the calibration curve over the three days of QC analysis for ALDH1A1. The quantification was considered accurate if the average value was between 80 and 120%. The ANN-1A1 peptide was used for ALDH1A1 quantification.

Internal Standard	Accuracy of calibration curve (%)					Coefficient of determination (R^2)
	50 nM	100 nM	500 nM	750 nM	1000 nM	
SIL-ANN-1A1 peptide	124 ± 40	126 ± 23	89 ± 10	96 ± 19	93 ± 28	0.96 ± 0.02
SIL-ANN-1A1 peptide (quench)	104 ± 22	90 ± 4	102 ± 12	92 ± 13	101 ± 5	0.99 ± 0.01

Table 2.7: The average error at each concentration of the calibration curve and coefficient of determination (R^2) for the calibration curve over the three days of QC analysis for ALDH1A2. The quantification was considered accurate if the average value was between 80 and 120%. The ILE peptide was used for ALDH1A2 quantification.

Internal Standard	Accuracy of calibration curve (%)					Coefficient of determination (R^2)
	5 nM	15 nM	50 nM	75 nM	100 nM	
SIL-ILE peptide	132 ± 22	70 ± 18	97 ± 34	112 ± 6	96 ± 5	0.96 ± 0.02
SIL-ILE peptide (quench)	115 ± 16	102 ± 7	100 ± 4	108 ± 20	97 ± 6	0.98 ± 0.01

Table 2.8: The error in accuracy and the precision (interday variability) values for RDH11 with each IS method. If the accuracy error or precision was greater than 20% or less than -20% with any QC, the method was determined to be invalid. The VVV peptide was used for RDH11 quantification.

	SIL-RDH11	SIL-VVV extended	SIL-VVV	SIL-VVV (Quench)
QC1 (22.5 nM)				
Accuracy Error (%)	-11	53	20	-2
Precision (%)	17	16	10	8
QC2 (40 µg HLM)				
Precision (%)	16	12	13	8
QC3 (55 nM)				
Accuracy Error (%)	-9	22	13	-6
Precision (%)	15	11	15	8

Table 2.9: The error in accuracy and the precision (interday variability) values for ALDH1A1 QC samples with each IS method. If the accuracy error or precision was greater than 20% or less than -20% with any QC, the method was determined to be invalid. The ANN-1A1 peptide was used for ALDH1A1 quantification.

	SIL-peptide	SIL-peptide (Quench)
QC1 (150 nM)		
Accuracy Error (%)	-26	10
Precision (%)	33	10
QC2 (325 nM)		
Accuracy Error (%)	-7	11
Precision (%)	23	14
QC3 (600 nM)		
Accuracy Error (%)	27	11
Precision (%)	20	11

Table 2.10: The error in accuracy and the precision (interday variability) values for ALDH1A2 QC samples with each IS method. If the accuracy error or precision was greater than 20% or less than -20% with any QC, the method was determined to be invalid. The ILE peptide was used for ALDH1A2 quantification.

	SIL-peptide	SIL-peptide (Quench)
QC1 (10 nM)		
Accuracy Error (%)	9	5
Precision (%)	26	14
QC2 (32.5 nM)		
Accuracy Error (%)	20	-8
Precision (%)	4	11
QC3 (80 nM)		
Accuracy Error (%)	16	-11
Precision (%)	16	15

Chapter 3

Importance of ALDH1A enzymes in determining human testicular retinoic acid concentrations

Chapter 3 was published

in

Journal of lipid research. 2015;56:342-57.

3.1 Introduction

all-trans-retinoic acid (*at*RA) is essential for a multitude of biological processes including reproduction, maintenance of the immune system, skin integrity, fetal development, and cell cycle regulation (Chapellier et al., 2002; Chung et al., 2009; Clagett-Dame and Knutson, 2011; Noy, 2010b; Ross, 2007). Most importantly, in all of these processes, the concentrations of *at*RA are tightly regulated to obtain time and location specific signaling. This requires careful control of the expression of enzymes responsible for synthesizing and eliminating *at*RA. Yet, the specific enzymology of how *at*RA concentrations are regulated in a tissue and cell type specific manner is not well established (D'Ambrosio et al., 2011; Kedishvili, 2013; Napoli, 2012). In various in vitro systems, three aldehyde dehydrogenases (ALDHs), ALDH1A1, 1A2, and 1A3 have been shown to generate *at*RA from retinaldehyde (Graham et al., 2006; Posch et al., 1992; Wang et al., 1996), but the tissue and cell type specific localization, ontogeny, and specific activity of these enzymes is poorly understood.

The importance of ALDH1A2 and ALDH1A3 in *at*RA formation during fetal development has been established by the fact that ALDH1A2$^{-/-}$ mice die during embryonic development displaying classic malformations associated with *at*RA deficiency, and ALDH1A3$^{-/-}$ mice die shortly after birth (Niederreither et al., 1999; Vernet et al., 2006). In contrast, ALDH1A1$^{-/-}$ mice are viable, fertile, and protected against obesity (Ziouzenkova et al., 2007). The significance of ALDH1A1 in *at*RA formation in mice is implied from the increased serum retinal concentrations when the ALDH1A1$^{-/-}$ mice are treated with retinol (Fan et al., 2003; Molotkov and Duester, 2003). Yet, as the quantitative protein expression and intrinsic RA formation capacity of these enzymes in specific tissues is unknown, the importance of the three ALDH1A enzymes to *at*RA formation in different *at*RA target tissues in humans or animals is currently undetermined.

In humans, ALDH1A1 mRNA has been detected in the liver, kidney, testis, brain, lung, red blood cells, and lens of the eye (Nishimura and Naito, 2006; Sladek et al., 2002; Zhai et al., 2001). In contrast, ALDH1A2 mRNA is found predominantly in the testis, uterus, and skeletal muscle while ALDH1A3 mRNA is localized in the prostate, trachea, intestine, and testis (Nishimura and Naito, 2006). These mRNA expression patterns strongly suggest that all three ALDH1A enzymes contribute to *at*RA synthesis during post-natal life. In addition, ALDH1A1 expression has been proposed as a cancer stem cell marker and associated with poor prognosis in certain types of cancers including clear cell renal, esophageal squamous cell, and papillary thyroid carcinomas (Wang et al., 2013; Xing et al., 2014; Yang et al., 2014). Conversely, ALDH1A2 has been identified as a candidate tumor suppressor in a transgenic animal model of prostate cancer, and gene variants of ALDH1A2 have been found to be associated with osteoarthritis and increased newborn kidney size (El Kares et al., 2010; Kim et al., 2005a; Styrkarsdottir et al., 2014; Touma et al., 2009). Taken together these studies point to tissue specific central roles that ALDH1A enzymes play in human physiology, and the critical importance for obtaining information concerning the expression and activity of these enzymes in human tissues.

One of the major challenges in evaluating vitamin A and *at*RA homeostasis and the importance of ALDH1A enzymes in these processes has been the fact that serum concentrations do not readily reflect tissue retinoid concentrations as *at*RA is believed to be synthesized in the target tissues (Napoli, 1996). Because of this, measurements of tissue *at*RA concentrations, and expression and activity of *at*RA synthesizing enzymes in small tissue fractions such as biopsies from humans is critically important. To date, methods have not been readily available to determine the specific activity and expression of ALDH1A enzymes in human tissues or for

demonstrating that ALDH1A activity influences tissue *at*RA concentrations and net *at*RA formation velocity. As such it has not been possible to predict the pharmacological outcomes within a specific target tissue or globally in the whole body in response to specific ALDH1A enzyme inhibition or induction.

An excellent model organ for the tissue specific synthesis of *at*RA is the testis (Hogarth and Griswold, 2010), as *at*RA synthesis within the testis is required for male fertility (Raverdeau et al., 2012; Tong et al., 2013). For example, there is no initiation of spermatogenesis in mice which lack ALDH1A1, ALDH1A2, and ALDH1A3 in the Sertoli cells (Raverdeau et al., 2012). Similarly, an inhibitor of the ALDH1A enzymes, WIN 18,446, has been shown to affect the ability of multiple mammalian species, including humans, to produce sperm (Amory et al., 2011b; Heller et al., 1961; Munson et al., 2004), likely due to decreased *at*RA concentrations in the testes (Amory et al., 2011b). However, the specific role of the individual ALDH1A enzymes in *at*RA formation in the testis has not been evaluated. Hence, the human testis was chosen as a model tissue to establish how *at*RA synthesis is orchestrated by the three ALDH1A enzymes in a tissue and cell type specific manner to regulate *at*RA concentrations in the organ. A novel LC-MS/MS peptide quantification method was developed that allows accurate quantification of the expression levels of ALDH1As in small biopsy scale samples. This method was coupled with measurements of ALDH1A activity, the formation of *at*RA in tissue samples from 18 human donors, and measurements of *at*RA concentrations in paired samples from the same donors. In addition, the effect of CRBP on *at*RA synthesis in the testis was evaluated. These novel methods allowed the prediction of the relative contribution of each of the ALDH1A enzymes to overall intratesticular RA formation. The relative contribution of the ALDH1As to *at*RA formation was confirmed via specific inhibition studies. The importance of individual ALDH1A enzymes to

*at*RA formation in specific cell types in the testis was evaluated via tissue localization studies of ALDH1A enzymes. The approach used can also be applied to measuring *at*RA formation in any human tissue biopsy by combining quantitative proteomics and sensitive kinetic analyses.

3.2 Materials and Methods

Human Samples used in the Study:

Samples of testicular tissue used to characterize ALDH1A expression and activity were obtained from 18 anonymous donors at the Centre of Reproductive Medicine and Andrology in Munster, Germany. 15 of the testes were from men who underwent orchiectomy as an androgen depletion therapy for the treatment of prostate carcinoma and all samples were anonymized following informed consent. All of the men had qualitatively normal spermatogenesis based on histological analysis. The men were 62-87 years old (mean: 70.7). In addition, three samples from individuals undergoing male to female sex re-assignment surgery after at least two years of estrogen treatment were analyzed. These samples were also anonymized following informed consent and the age range of this group was 49-75 years (mean 58.3 years). Due to the estrogen treatment, spermatogenesis was severely reduced on histological analysis of the tissue from these individuals. The tissues were collected into ice-cold Leibovitz medium at the surgery site, protected from light and taken to the laboratory. The testes were decapsulated and fragmented by scalpels and scissors. The fragments were snap frozen in liquid nitrogen and stored at -80°C until RA measurements or preparation of S10 fractions.

Quantification of ALDH1A1, ALDH1A2 and ALDH1A3 in human testes using LC-MS/MS

Tissue biopsies (33-102 mg) from 18 donors were homogenized on ice using a drill powered 2 mL Potter-Elvehjem glass homogenizer (Kimbel Glass, Vineland, NJ). Samples were homogenized in 3x volume tissue homogenization buffer (50 mM Potassium Phosphate 250 mM

sucrose) with an EDTA free protease inhibitor cocktail (Roche, San Francisco, CA). The samples were transferred to a 1.5 mL microcentrifuge tube, the homogenizer washed with 2x volume of homogenization buffer, and the wash added to homogenate. The homogenate was centrifuged at 10,000 g for 25 minutes at 4°C to pellet large organelles and cell membranes. The resulting supernatant (S10 fraction) that contains microsomes and cytosolic proteins was collected, aliquoted, flash frozen in liquid Nitrogen and stored at -80°C. Total protein concentration in each S10 fraction was measured using a BCA assay (Thermo Fisher, Waltham, MA).

ALDH1A expression in human testicular tissue was measured by peptide quantification using LC-MS/MS. Peptides were chosen based on *in silico* analysis of their selectivity and analytical performance (MacLean et al., 2010). The FASTA files for each ALDH1A sequence were downloaded from www.uniprot.org with the accession numbers P00352, O94788-1, and P47895. The human ALDH1A enzymes were first trypsin digested *in silico* and peptides with a predicted *m/z* greater than 1100 were excluded due to the *m/z* range limitations of the mass spectrometer. Next, the predicted peptides were screened against a trypsin digested human proteome to ensure selectivity. Additionally, sites predicted or reported to have post-translational modifications or mutations were avoided. Purified recombinant ALDH1A enzymes were trypsin digested in vitro to determine the coverage of ALDH1A digestion. Of the predicted peptides that were within the detectable mass range of the MS, 100% were detected for ALDH1A1, 100% for ALDH1A2, and 93% for ALDH1A3.

For the peptides that passed the initial criteria described above, the predicted precursor ion and fragments were incorporated into an LC-MS/MS method. Human testicular S10 protein and purified recombinant ALDH1A were trypsin digested to determine which remaining peptides were detected in human testicular tissue and were specific for ALDH1A. For each

ALDH1A, one peptide was selected as a quantification peptide and a second for verification (Table 3.1). For the quantification peptide, a matching heavy labeled peptide was synthesized as an internal standard (Pierce, Rockford, IL). In order to account for the efficiency of the trypsin digestion, a heavy labeled peptide with extended sequence over the trypsin cleavage site (lagging end) was synthesized for ALDH1A2 and ALDH1A3. These peptides were labeled at the N terminal with a [$^{13}C_6{}^{15}N_2$]-lysine or [$^{13}C_6{}^{15}N_2$]-arginine. Each lagging end peptide requires two cleavages by trypsin to produce the target peptide. In addition, a separate labeled internal standard for ALDH1A1 and ALDH1A2 quantification peptides was incorporated that does not require trypsin cleavage (Table 3.1). For each peptide, 2 fragments from each of the two peptides were used for detection and to confirm the presence of the protein. The stability of the peptides was validated by confirming there was no significant sample degradation after 3 freeze thaw cycles, 24 hours at 37°C, and 24 hours at room temperature.

Trypsin digestion of purified ALDH1As and testicular S10 fractions was done in 96-well plates according to the following protocol: First, 15 µL of sample (0-400 nM of ALDH1A or 5.33 mg/mL S10 fraction) were added to each well. Next, 5 µL of 700 nM ALDH1A2 lagging end peptide and 300 nM ALDH1A3 lagging end peptide were added together with 4 µL dithiothreitol (100 mM) and 10 µL of ammonium bicarbonate buffer (100 mM, pH 7.8). Next, 5 µL of 10% sodium deoxycholate (Sigma, St. Louis, MO) was added in the well, and the sample was mixed before incubation at 95 °C for 5 minutes. After cooling to room temperature, 4 µL of iodoacetamide (200 mM) was added and the sample incubated at room temperature in the dark for 20 minutes. Trypsin was added at a 1:25 trypsin:protein ratio, and the sample was digested for 24 hours at 37°C. The incubation was quenched by addition of 20 µL chilled acetonitrile with 8% trifluoroacetic acid containing the non lagging end heavy labeled ALDH1A1 and ALDH1A2

peptide internal standards. Samples were centrifuged at 3,000 g for 25 minutes at 4°C and analyzed by LC-MS/MS.

The peptides were quantified by mass spectrometry using an AB Sciex 5500 qTrap Q-LIT mass spectrometer (AB Sciex, Foster City, CA) equipped with an Agilent 1290 UHPLC (Agilent, Santa Clara, CA). The tryptic peptides were separated using an Aeris Peptide XB-C18 column (50 X 2.1 mm) with 1.7 µm particle size at 40 °C and a SecurityGuard Ultra UHPLC C18-peptide cartridge (Phenomenex, Torrance, CA). The eluting solvents were A: H_2O + 0.1% formic acid and B: ACN + 0.1% formic acid. For chromatographic separation the following 18 minute linear gradient with a 400 µL/minute flow rate was used: 0 → 3.5 minutes 3% B, then increased by 12.0 minutes to 40% B, 12.0 → 12.1 minutes 95% B and stayed 95% B until 15.0 minutes, then 15.0 → 15.1 minutes 3% B, 15.1 → 18 minutes 3% B.

For quantification of ALDH1As, purified ALDH1A1, ALDH1A2, and ALDH1A3 were used as standards. A 9 point standard curve was generated with values of 0.018-7.2 pmol for ALDH1A1, 0.005-1.35 pmol for ALDH1A2, and 0.002 – 0.72 pmol ALDH1A3. The amount of enzyme detected in each sample was normalized to total S10 protein (0.08 mg).

Mass spectrometric quantification of atRA, 13-cisRA, and retinal

The concentrations of *at*RA, 13-*cis*RA, and retinal were measured using an AB Sciex 5500 qTrap Q-LIT mass spectrometer (Foster City, CA) equipped with an Agilent 1290 UHPLC (Santa Clara, CA) as previously described (Arnold et al., 2012) with several minor modifications. Briefly, *at*RA and 13-*cis*RA were monitored using positive ion APCI and MS transitions of 301→ 205 and 301→ 123 *m/z* with the 205 fragment used for quantification. For quantification, *at*RA and 13-*cis*RA peak areas were normalized to the *at*RA-d_5 internal standard area.

For in vitro incubation samples, the analytes were separated using a Kinetex C18 column (100 X 2.1 mm, 1.7 µm particle size) heated to 40°C with a SecurityGuard Ultra UHPLC C18 cartridge (Phenomenex, Torrance, CA) and a linear gradient with A: H_2O + 0.1% Formic Acid and B: Acetonitrile + 0.1% Formic Acid. The mobile phase flow was 600 µL/min with the following linear gradient: 0.0→ 0.25 minutes 40% B, then increased to 95.0% at 4.0 minutes, 4.0 → 5.0 minutes 95.0% B, 5.0 → 6 minutes 40% B. A standard curve consisting of RA spiked into buffer containing 0.05 mg/mL S10 protein at concentrations of 0, 1, 5, 10, 25, 50, and 100 nM was prepared simultaneously with all incubations. Analyst software (AB SCIEX, Foster City, CA) was used to quantify peak areas for each analyte.

For determining the in vitro retinal fraction unbound, the concentration of retinal was measured using positive ion APCI and the MS transition 285→161 *m/z*. The liquid chromatography settings were identical to those used for the RA in vitro incubation samples and the mass spectrometer parameters were set at 66.0 for declustering potential, 13.0 for collision energy, and 4.0 for the collision cell exit potential. *at*-retinal-d_5 was used as an internal standard and was monitored using the 290→161 *m/z* transition.

For testicular tissue analysis, the extraction of RA from tissue was optimized to increase the recovery of RA without causing any isomerization, and chromatographic separation was optimized to avoid endogenous interference from tissue. Briefly, tissue was homogenized with a 2 mL Potter-Elvehjem glass homogenizer (Kimbel Glass, Vineland, NJ) in a 1:1 volume of 0.9% NaCl. After transferring the sample to a 15 mL glass culture tube, a 2:1 volume of ACN with 1% formic acid was added followed by 10 µL of 1 µM *at*RA-d_5, which served as an internal standard. 10 mL of hexanes were used to extract RA, the organic layer was transferred to a glass tube and dried under nitrogen at 37°C. The sample was reconstituted in 60:40 ACN/H_2O. A

standard curve and quality control samples were generated with RA standards spiked into homogenized dog testicular tissue (A kind gift from Dr. Mary Zoulas of the Seattle Animal Shelter) exposed to UV light to destroy endogenous RA. Dog testicular tissue was homogenized in a 1:1 volume with 0.9% NaCl and 198 µL were placed in a 15 mL glass culture tube. 2 µL of *at*RA and 13-*cis*RA standards were added to each tube to final concentrations of 0, 1, 2.5, 5, 7.5, and 10 nM for each standard. The quality control samples were prepared at 1.5, 3.75, and 8.75 nM, and duplicate quality control samples were included together with the standard curve in all analytical assays. *at*RA and 13-*cis*RA were separated from endogenous interferences using a 150 mm x 2.1 mm Supelco Ascentis Express reverse phase amide column (Sigma, St. Louis, MO) with 2.7 µm particle size and an Ascentis Express reverse phase amide 2.7 µm guard cartridge. The solvents for the UHPLC analysis were A: H_2O + 0.1% formic acid and B: ACN/ MeOH (60/40) + 0.1% formic acid. The solvent flow was 500 µl/minute and the following linear gradient was used: 0.0 → 2.0 minutes 40% B, then increased to 95% B at 10.0 minutes, 10.0 → 15.0 minutes 95% B, 15.0 → 17.0 minutes 40% B. *at*RA and 13-*cis*RA peak areas were normalized to the *at*RA-d_5 internal standard and peak area ratios were used for quantification using Analyst software (AB SCIEX, Foster City, CA). A signal:noise of 9 was set as the minimum threshold for quantitation.

To further confirm the identity of retinoids detected in the testes, MS^3 (MS/MS/MS) was used. To collect reference spectra *at*RA and 13-*cis*RA standards were spiked into 60:40 acetonitrile:water + 0.1% formic acid. The standards and two separate 75 mg testicular tissue samples were extracted and analyzed as described above with following modifications on the MS settings. The *m/z* 205.3^+ fragment generated from *m/z* 301.2^+ (RA) was fragmented using the linear ion trap of the API 5500 with a scan rate of 10,000 daltons/second, Q3 entry barrier of 8.0

volts, and a dynamic fill time set for the ion trap. All the fragments generated from m/z 205.3^+ between *m/z* 50-200 *m/z* were collected in the trap and subsequently sent to the detector. The MS^3 product ion spectrum was collected for each chromatographic peak and the spectra of compounds eluting from the tissue sample was compared to the RA standards. Based on the fact the *m/z* 159.1^+ fragment was the main fragment generated from RA, the *m/z* 159.1^+ fragment was extracted from the MS^3 total ion chromatograms and monitored as a function of time to generate a chromatogram of the *m/z* $301.2^+>205.3^+>159.1^+$ transition.

Formation of all-trans and retinoic acid by recombinant ALDH1A enzymes and human testis S10 fractions

Human *ALDH1A1* cDNA was purchased from OriGene (SC321535). Full-length human *ALDH1A2* cDNA was cloned from human testis RNA using RT-PCR. An open reading frame of ALDH1A1 was subcloned into a pETite expression vector (Lucigen Middleton, WI) with a 5' hexahistidine tag and that of *ALDH1A2* into a pET28 bacterial expression vector (Novagen, Billerica, MA) containing a 3' hexahistidine tag. The resulting plasmids were verified through DNA sequencing for correct frame and sequences. Enzymes were expressed in *Escherichia coli* (BL21(DE3)) grown to an OD600 of 0.6-1.0. Expression was induced with 0.5 mM IPTG and continued for 4 hours at 37°C before harvest. ALDH1A1 and ALDH1A2 were purified using the His.Bind resin and buffer kit (Catalog # 69755-3, Novagen) as previously described (Fierce et al., 2008). Purified enzyme was dialyzed against 20 mM Hepes buffer (pH 8.5) containing 150 mM KCl and 1 mM EDTA. Protein purity was confirmed by SDS-PAGE followed by Coomassie staining and concentrations were determined using BCA protein assay kit (Thermo Fisher, Waltham, MA) or protein assay kit II (BioRad, Hercules, CA). Enzyme was stored at 4°C in the dialysis buffer with 1mM TCEP (Thermo Fisher, Waltham, MA), a reducing agent.

Purified recombinant human ALDH1A3 was purchased from Life Technologies (Grand Island, NY). The lyophilized protein was reconstituted to a final concentration of 0.2 mg/mL with filtered water according to manufacturer's directions and stored at -80 °C.

To characterize the kinetics of *at*RA formation by ALDH1A1 and ALDH1A3 enzymes, *at*-retinal (0-5000 nM) was incubated with 18 nM ALDH1A in 100µL of buffer consisting of 750 mM KCl and 50 mM Hepes at a pH of 8.0 with 2 mM NAD^+. Following a preincubation of 5 min at 37°C, the incubations were initiated with addition of substrate. The incubations were terminated at 5 minutes by transferring 75 µL of the incubation into an equal volume of chilled acetonitrile with 100 nM *at*RA-d_5 (internal standard). In order to characterize the *at*RA formation kinetics by ALDH1A2, the protein concentration was decreased to 2 nM, and the incubations were terminated after 2 minutes. The formation kinetics of 13-*cis*RA by ALDH1A1 were characterized by incubating 13-*cis*-retinal (0-7500 nM) with 15 nM ALDH1A1 and quenching after 5 minutes. After termination, all plates were spun at 3,000 g for 25 minutes, the samples were transferred to a 96 well plate and analyzed by LC-MS/MS for *at*RA and 13-*cis*RA concentrations. In order to determine if 13-*cis*-retinal was a substrate of ALDH1A2 or ALDH1A3, 5,000 nM 13-*cis*-retinal was incubated with 50 nM ALDH1A2 and ALDH1A3 for up to 45 minutes. Over the course of 45 minutes, no enzyme dependent 13-*cis*RA formation greater than 0.0007 pmol/min/pmol (based on assay lower limit of detection) was detected. All incubations were conducted under protein and time linearity and as triplicate measurements. The Michaelis-Menten equation was fitted to the velocity of *at*RA formation as a function of substrate concentration data to obtain kinetic parameters for each enzyme. When ALDH1A1 was incubated with 13-*cis*-retinal, 13-*cis*RA formation demonstrated substrate inhibition kinetics, and substrate inhibition equation was used to fit the data according to

$$v = \frac{Vmax*[S]}{K_m+[S]*\left(1+\left(\frac{[S]}{K_i}\right)\right)}$$

where v is the predicted velocity, V_{max} is the maximum observed velocity, [S] is the substrate concentration, K_m is the affinity constant of 13-*cis*-retinal with the ALDH1A1, and K_i is the disassociation constant for 13-*cis*-retinal binding in a way that allows for the enzyme to bind two substrates. All kinetic analyses were done using Graphpad Prism (La Jolla,CA)

*at*RA and 13-*cis*RA formation from the corresponding retinals was measured in the individual human testis S10 preparations using a similar method as that described for recombinant ALDH1As. Briefly, *at*-retinal at nominal concentrations of 100 nM and 1000 nM or 13-cis-retinal (1000 nM) were incubated with S10 fractions (5 µg S10 protein / 0.1 mL) from each donor. The incubations were initiated with substrate and terminated after 10 minutes and analyzed as described above. The protein binding of *at*-retinal and 13-*cis*-retinal to the nonspecific proteins and membranes in the activity assay was determined by ultracentrifugation as described before (Thatcher et al., 2010). Retinal was added to 0.05 mg/mL pooled S10 protein to final concentrations of 100 and 1000 nM *at*-retinal and 1000 nM 13-*cis*-retinal. The samples were aliquoted into ultracentrifuge tubes (Beckman 343775) and spun at 435,000g at 37°C for 90 minutes using a Sorval Discovery M150 SE ultracentrifuge with a Thermo Scientific S100-AT3 rotor (Waltham, MA) or incubated at 37°C for 90 minutes in a water bath. The incubated sample or supernatant was added to 100 µl ice cold acetonitrile containing 100 nM *at*-retinal-d_5. The samples were centrifuged at 3,000 g for 20 minutes at 4°C. Samples were transferred to a 96 well plate and analyzed using the LC-MS/MS method described. The unbound (free) fraction of retinal in the incubations was calculated as ratio of retinal concentration with or without ultracentrifugation. This calculation assumes minimal CRBP concentration and binding in the

incubations. The insignificant concentration of CRBP was confirmed via direct measurement of CRBP concentrations in the S10 fractions (*vide infra*).

ALDH1A inhibition by WIN 18,446

In order to determine reversible inhibition of ALDH1A1, ALDH1A2, and ALDH1A3 by WIN 18,446, recombinant purified enzymes were incubated with 100 nM of *at*-retinal and increasing concentrations (1-5,000 nM) of WIN 18,446. All activity assays with recombinant enzymes included 18 nM ALDH1A, 2 mM NAD^+, and were terminated after 5 minutes by transferring 75 µL of the incubation into an equal volume of chilled acetonitrile with 100 nM *at*RA-d_5. The samples were prepared and analyzed by LC-MS/MS as described for incubations with recombinant purified ALDH1A. A screen for time dependent inhibition (TDI) used the dilution method and *at*-retinal as a substrate (Grimm et al., 2009). Briefly, TDI was determined by incubating 180 nM ALDH1A enzyme with and without 1 µM WIN 18,446 in the presence of 2 mM NAD^+ in a final volume of 100 µL of buffer (750 mM KCl and 50 mM Hepes at a pH of 8.0). At time points of 0.25, 3, and 5 minutes, 10 µL aliquots were diluted 10 fold into 100 µL of buffer (750 mM KCl and 50 mM Hepes at a pH of 8.0) containing NAD^+ (2 mM) and a saturating concentration of *at*-retinal (5000 nM). All incubations were performed in triplicate with a no NAD^+ control for the WIN 18,446 and *at*-retinal incubations. Since WIN 18,446 was a TDI for ALDH1A2, but not ALDH1A1 or ALDH1A3, the kinetics of ALDH1A2 TDI with WIN 18,446 were characterized using 8 concentrations of WIN 18,446 (0-5000 nM). The dilution method was used with timepoints of 0.25, 1, 3, and 5 minutes. The k_{inact} and K_I were determined by fitting equation 1 to the data in Graphpad Prism.

$$\Lambda = \frac{k_{inact} * [I]}{K_I + [I]} \quad (1)$$

[I] is the inhibitor concentration, λ is the observed apparent inactivation rate (min^{-1}), k_{inact} is the maximum inactivation rate, and K_I is the concentration of inhibitor when the inactivation rate is half of the k_{inact}.

Quantification of CRBP1 Expression in human testes and determination of the effect of CRBP1 to RA formation in human testis

Testicular CRBP1 protein expression was quantified in all tissue donors using an ELISA kit obtained from Cloud Clone Corp (Houston, TX). Standards and samples were prepared according to the manufacturer's instruction. Testicular S10 protein fractions were diluted 1:20 fold into phosphate buffer pH 7.4 and CRBP1 quantified based on the standard provided. The amount of CRBP1 in each sample was normalized to milligrams of S10 protein, and the expression was scaled to the concentration of CRBP1 as pmol/gram testis using the S10 recovery (mg S10 protein /g testes). In addition the concentration of CRBP1 in the incubations with testicular S10 protein was calculated using the measured concentration in each donor.

The effect of CRBP1 (purchased as purified protein from Origene, Rockville, MD) on *at*RA formation by ALDH1A was determined using recombinant ALDH1A proteins and testicular S10 protein. Holo-CRBP1 was generated by preincubating 3,000 nM *at*-retinal for 5 minutes at room temperature with 3,000 nM CRBP1 in buffer (10% glycerol, 100 mM glycine, 25 mM Tris-HCl pH 7.3). 10 µL of holo-CRBP1 (3,000 nM) or 3,000 nM *at*-retinal in buffer was used to initiate incubations with 0.05 mg/mL pooled S10 protein from 5 donors, 18 nM ALDH1A1, 18 nM ALDH1A3, or 2 nM ALDH1A2 in a 100 µL volume. All of the incubations were performed in quadruplicate and contained 2 mM NAD^+. Incubations were quenched after 5 minutes (ALDH1A enzymes) or 10 minutes (S10 protein) by transferring 75 µL of the incubation

into an equal volume of chilled acetonitrile with 100 nM *at*RA-d_5 (internal standard). After termination, the samples were analyzed by LC-MS as described above.

Contribution of individual ALDH1A enzymes to retinoic acid formation in human testes

To establish the relative importance of each ALDH1A enzyme in RA formation in human testis, the ALDH1A concentrations for each subject and the in vitro kinetics of RA formation from retinal by the recombinant ALDH1A enzymes were used to predict the overall *at*RA and 13-*cis*RA formation velocity in each donor. Due to the different K_m and k_{cat} values for each ALDH1A enzyme with *at*-retinal as a substrate, their contribution to *at*RA formation was predicted at two different substrate concentrations, while 13-*cis*RA formation was predicted only at one concentration. *at*RA formation in each testis S10 sample was predicted using equation (2)

$$v = \frac{[ALDH1A1]*k_{cat}*f_u[S]}{K_m+f_u[S]} + \frac{[ALDH1A2]*k_{cat}*f_u[S]}{K_m+f_u[S]} + \frac{[ALDH1A3]*k_{cat}*f_u[S]}{K_m+f_u[S]} \quad (2)$$

in which v is the predicted velocity, [ALDH1A] is the measured expression level of each individual ALDH1A enzyme, k_{cat} is the maximum product formation velocity measured with recombinant enzymes, f_u is the experimentally determined free fraction in S10 preparation, [S] is the total substrate concentration, and K_m is the affinity constant of *at*-retinal with the ALDH1A. Due to the fact 13-*cis*RA formation by ALDH1A1 from 13-*cis*-retinal demonstrated substrate inhibition, an equation accounting for substrate inhibition was used (3). K_i is the disassociation constant for 13-*cis*-retinal binding in a way that allows for the enzyme to bind two substrates.

$$v = \frac{[ALDH1A1]*k_{cat}*f_u[S]}{K_m+f_u[S]*(1+\left(\frac{f_u[S]}{K_i}\right))} \quad (3)$$

In order to determine the contribution of each ALDH1A enzyme to the total formation of *at*RA, the predicted velocity of *at*RA formation by the given ALDH1A was divided by the

predicted total velocity at multiple substrate concentrations. The accuracy of the ALDH1A activity predictions was evaluated by comparing the measured velocity to the predicted velocity of *at*RA and 13-*cis*RA formation in each subject (S10 fraction) at the different concentrations. The average fold error (afe) of the predictions was calculated for each prediction using equation (4):

$$\text{afe} = 10^{\frac{1}{n}\sum log\frac{Predicted}{Measured}} \quad (4)$$

An afe between 0.5 and 2.0, which indicates the 2-fold prediction error cutoff, was set as the limit for acceptable predictions according to previous studies on clearance predictions (Brown et al., 2005).

The relative importance of ALDH1A2 and ALDH1As to *at*RA formation in the testis was confirmed using WIN 18,446. Due to the fact WIN 18,446 inactivates ALDH1A2, but not ALDH1A1 or ALDH1A3, the contribution of ALDH1A2 to *at*RA formation can be determined using the TDI characteristics of WIN 18,446 and the dilution method described above. Briefly, 625 nM WIN 18,446 and pooled human testes S10 (250 µg S10 protein / 0.1mL) were incubated for 0.25, 15, and 30 minutes after initiating the reaction with 10 µL of 20 mM NAD^+. At the set timepoints, 2 µL aliquots were diluted 1:50 fold into activity assays containing a final concentration of 2 mM NAD^+ and 5000 nM *at*-retinal. After 10 minutes, incubations were terminated by transferring 75 µL of the incubation into an equal volume of chilled acetonitrile with 100 nM *at*RA-d_5. The concentration of WIN 18,446, incubation time, and the dilution were chosen so that 98% of ALDH1A2 was inactivated in 30 minutes and minimal reversible inhibition of ALDH1A1 and ALDH1A3 would be present. This concentration was determined using equations 1 and 5:

$$\text{Activity Remaining (\%)} = 100 * e^{-\lambda t} \quad (5)$$

A concentration of 625 nM WIN 18,446 results in an inactivation rate of 0.14 min^{-1} and a decrease of 87% and 98% in ALDH1A2 activity at 15 and 30 minutes. The 12.5 nM WIN 18,446 remaining after the 1:50 dilution results in minimal reversible inhibition with saturating substrate conditions.

The effect of CRBP1 on ALDH1A activity in the testis was predicted by incorporating the measured in vitro effect of CRBP1 on *at*RA formation by ALDH1A1 and ALDH1A2 at the physiologically relevant *at*-retinal concentration of 100 nM. In addition to ALDH1A expression levels and *at*RA formation kinetics, the observed 52% decrease in *at*RA formation by ALDH1A1 and 2.7-fold increase of *at*RA formation by ALDH1A2 in the presence of CRBP1 was incorporated into equations 2 and 3 to predict the contribution of each enzyme to *at*RA formation.

Immunohistochemistry

Testicular tissue from three healthy, fertile subjects was used to determine ALDH1A localization. These men volunteered to be part of this research study that was approved in advance by the University of Washington Institutional Review Board. All subjects provided signed written consent prior to any study procedures. Three healthy men aged 28, 52, and 43 years consented to donating testicular biopsies for the study. The tissue slices shown are from a 43 year old subject with left spermatocele, normal sperm counts, and normal hormone levels. Immunohistochemistry was performed using human testis tissue fixed in Bouin's fixative using commercial rabbit polyclonal antibodies raised against ALDH1A1 (Abcamplc, ab24343), ALDH1A2 (Proteintech Group, 13951-1-AP), and ALDH1A3 (Abgent, AP7847a) as previously described (Hogarth and Griswold, 2013). Antigen retrieval was achieved using citrate buffer (pH 6) at a rolling boil for 5 min. Sections were incubated in primary antibody at a concentration of

0.5 µg/mL (ALDH1A1), 4 µg/mL (ALDH1A2), 2.5 µg/mL (ALDH1A3), or 0.1 µg/mL in 5% normal goat serum/ 0.1% bovine serum albumin in phosphate buffered saline at room temperature overnight (~16 hrs). Control sections were incubated without primary antibody. Biotinylated goat-anti-rabbit secondary antibody (Invitrogen, 956143b) was applied for 1 hour at room temperature, following the manufacturer's instructions. Streptavidin conjugated horseradish peroxidase (Invitrogen, 956143b) was subsequently applied for 1 hr at room temperature. Localization was determined by a brown precipitate formed by horseradish peroxidase activity in the presence of 3,3′-diaminobenzidine tetrahydrochloride (Invitrogen, 002020). Sections were counterstained with a 1:3 dilution Harris Heamotoxilin (Sigma-Aldrich, HHS32-1L), dehydrated, and mounted under glass coverslips using DPX mounting media (VWR International, 360294H). Cell types were determined using nuclear morphology and location within the testis. Immunohistochemistry was performed on three samples for three individuals to ensure consistent results.

Statistical analysis

Linear regression analysis was used to test for any associations between ALDH1A expression levels and measured *at*RA and 13-*cis*RA formation velocities. Linear regression was also used to test whether the measured and predicted 13-*cis*RA and *at*RA formation correlated. The correlation between measured *at*RA concentrations and *at*RA and 13-*cis*RA formation velocities was used to test whether in vitro data could predict in vivo *at*RA concentrations. Unpaired two-tailed student's t-test was used to determine any significant differences between transgender individuals and the rest of the sample set. P values of less than 0.05 were considered significant for all analyses. All statistical tests and kinetic analyses were performed using Graphpad Prism (La Jolla, CA).

3.3 Results

ALDH1A protein quantification

In order to simultaneously quantify all three ALDH1A enzymes in human tissue, a novel LC-MS/MS based peptide quantification method was developed. Recombinant purified ALDH1A enzymes were used as standards and [$^{13}C_6{}^{15}N_2$]-lysine or [$^{13}C_6{}^{15}N_4$]-arginine labeled peptides as internal standards. For each ALDH1A enzyme, two trypsin digested peptides were chosen for measurement. One of the peptides was used for quantification and the second for verification of peptide identification. The peptides and the MS/MS transitions used for quantification of the ALDH1A enzymes are listed in Table 3.1. The peptides were chosen based on their predicted specificity and the observed sensitivity. In order to account for the efficiency of the trypsin digestion, heavy labeled peptides used as an internal standard for ALDH1A2 and ALDH1A3 were synthesized with an extended end over the trypsin cleavage site, and hence their detection required cleavage by trypsin (Table 3.1). Chromatograms of the digested recombinant proteins and the internal standards showing the specific quantified peptides are depicted in Figure 3.1.

The expression of ALDH1A1, ALDH1A2, and ALDH1A3 was quantified from 33-102 mg samples of testicular tissue collected from 15 men undergoing orchiectomy for treatment of prostate cancer and from 3 male to female transgendered individuals undergoing orchiectomy as part of their gender reassignment surgery. S10 fractions containing the cytosolic and microsomal proteins were generated from each individual donor sample. The average yield of S10 protein was 48 ± 11 mg S10 protein/gram testis tissue. 80 μg of this S10 protein was used for ALDH1A quantification. Representative chromatograms of the detection of ALDH1A1, ALDH1A2, and ALDH1A3 in the human testis, and the quantification of the three enzymes in the human testis

are shown in Figure 3.1. Based on the expression levels, ALDH1A1 was the major ALDH1A enzyme present in the human testis. In the non-transgendered individuals, the average expression of ALDH1A1 (70.9 ± 15.1 pmol/mg testis) was approximately 42-fold higher than that of ALDH1A2 (1.7 ± 0.3 pmol/mg testis) and 51-fold higher than ALDH1A3 (1.4 ± 0.5 pmol/mg testis). A positive correlation was observed between the expression levels of ALDH1A1 and ALDH1A2 ($R^2 = 0.27$, $p = 0.05$) and ALDH1A1 and ALDH1A3 ($R^2 = 0.30$, $p = 0.04$). However, there was no correlation between the expression levels of ALDH1A2 and ALDH1A3.

Metabolism of at-retinal and 13-cis-retinal by ALDH1As

The formation kinetics of *at*RA from *at*-retinal and 13-*cis*RA from 13-*cis*-retinal by purified ALDH1A1, ALDH1A2, and ALDH1A3 was characterized to determine the specific activity of each of these enzymes in *at*RA and 13-*cis*RA formation (Table 3.2). All three ALDH1A enzymes formed *at*RA from *at*-retinal, but only ALDH1A1 showed detectable formation of 13-*cis*RA from 13-*cis*-retinal (Figure 3.2). Of the ALDH1A enzymes, *at*-retinal had the highest affinity for ALDH1A2 (K_m= 56 nM), and the affinities of *at*-retinal to ALDH1A1 and ALDH1A3 were both five-fold lower (K_m= 285 and 261 nM). In addition, ALDH1A2 had the greatest efficiency to form *at*RA. The intrinsic clearance (k_{cat}/K_m) of *at*RA formation by ALDH1A2 was 27-fold greater than that by ALDH1A1 and 60-fold greater than that by ALDH1A3 (Table 3.2). Interestingly, 13-*cis*RA formation by ALDH1A1 demonstrated substrate inhibition kinetics (Figure 3.2). The k_{cat}, K_m, and K_i values relevant for a substrate inhibition model together with kinetic constants obtained for *at*-retinal with the ALDH1A enzymes are listed in Table 3.2.

Characterization of 13-cisRA and atRA formation in human testis samples

To establish the relative importance of the ALDH1A enzymes in the human testis, and to test whether the measured ALDH1A expression levels and the determined in vitro *at*RA formation kinetics predict the net *at*RA formation velocity in the human tissue, *at*RA formation from *at*-retinal was measured and predicted at two nominal concentrations (100 nM and 1000 nM) of *at*-retinal for each individual in the study (Figure 3.3). The substrate concentrations in the in vitro system were corrected for the protein binding of *at*-retinal measured at 100 and 1000 nM *at*-retinal. The free (unbound) fraction (f_u) of *at*-retinal was 7.8 ± 0.7% at 100 nM and 18.1 ± 7.8% at 1000 nM. The measured concentration of CRBP in the in vitro incubations was < 0.5nM (*vide infra*) and hence the effect of CRBP binding was considered insignificant for *at*-retinal in the incubations. Therefore, the free concentrations used in the predictions were 7.8 and 181 nM. Due to the sole contribution of ALDH1A1 to 13-*cis*RA formation from 13-*cis*-retinal, the formation of 13-*cis*RA was measured and predicted only at the nominal concentration of 1000 nM 13-*cis*-retinal. The 13-*cis*-retinal concentration was corrected for the measured unbound fraction in the in vitro system (f_u=60.0 ± 5.1%), and the free concentration of 600 nM 13-*cis*-retinal was used for all predictions. The average observed and predicted velocities for *at*RA formation from 7.8 nM free *at*-retinal in the human testis were 5.6 ± 3.2 pmol/min/mg S10 protein and 2.6 ± 0.6 pmol/min/mg S10 protein, respectively. At 181 nM free *at*-retinal, the mean observed and predicted velocities were 33.3 ± 7.7 pmol/min/mg S10 protein and 28.9 ± 15.9 pmol/min/mg S10 respectively (Figure 3.3). The average observed and predicted 13-*cis*RA formation velocities at 600 nM 13-*cis*-retinal were 25.5 ± 9.1 pmol/min/mg S10 and 15.2 ± 3.2 pmol/min/mg S10, respectively. The correlations between the predicted and observed *at*RA and 13-*cis*RA formation velocities are shown in Figure 3.3. RA formation (ALDH1A activity) was

accurately predicted at each free retinal concentration with average fold error values of 0.6 (7.8 nM *at*-retinal), 1.3 (181 nM *at*-retinal), and 0.8 (600 nM 13-*cis*-retinal).

Relative importance of individual ALDH1A enzymes to atRA formation in human testis samples

The relative importance of each ALDH1A enzyme in *at*RA formation (fraction of retinal metabolized by a given enzyme, f_m) was predicted using ALDH1A expression levels and *at*RA formation kinetics as a function of substrate concentration. The predicted relative importance of each ALDH1A enzyme at increasing *at*-retinal concentrations is shown in Figure 3.4. Overall ALDH1A1 is predicted to be the main enzyme forming *at*RA in the testis with >80% contribution to the overall *at*RA formation. ALDH1A2 was predicted to play a role in *at*RA formation (~15%), while the contribution of ALDH1A3 appeared insignificant. Due to the different K_m-values for *at*-retinal with ALDH1A2 and ALDH1A1, the predicted contribution of ALDH1A2 increases with decreasing retinal concentrations. The published concentration of retinal in the mouse testis (90.7 pmol/gram) (Kane and Napoli, 2010) is similar to ALDH1A2 K_m. However, the free concentration of retinal in the testis is unknown as well as the fraction of retinal bound to CRBP in the testis and hence the contribution of ALDH1A2 could be greater.

Based on the selective formation of 13-*cis*RA by ALDH1A1, ALDH1A1 was predicted to be the only contributor to 13-*cis*RA formation in incubations with *at*-retinal. In agreement with this, a significant ($p < 0.01$) correlation between ALDH1A1 protein expression and 13-*cis*RA formation ($R^2 = 0.41$) was observed (Figure 3.5). In addition, ALDH1A1 protein concentration had a significant correlation with *at*RA formation velocity measured with 181 nM *at*-retinal ($p = 0.02$, $R^2 = 0.28$) (Figure 3.5). However, only ALDH1A2 expression had a positive correlation ($p = 0.02$, $R^2 = 0.33$) with *at*RA formation measured at 7.8 nM *at*-retinal Figure 3.5).

To further evaluate the relative contributions of ALDH1A enzymes to *at*RA formation, an inhibitor of ALDH1A enzymes, WIN 18,446, was used as a selective ALDH1A inhibitor. WIN 18,446 was found to be a potent reversible inhibitor of ALDH1A1 and ALDH1A3 (IC_{50} values 102 ± 2 and 187 ± 1 nM), and an efficient time dependent inhibitor (k_{inact}= 22.0 ± 2.4 hr^{-1}, K_I= 1,026 ± 374 nM) of ALDH1A2 (Figure 3.4). Based on the strong inhibition of all three ALDH1A enzymes by WIN 18,446, the effect of WIN 18,446 on *at*RA formation in human testis S10 fractions was also evaluated. Using a pooled testis S10 fraction of 5 men, the IC_{50} for WIN 18,446 against testicular ALDH1A activity (*at*RA formation) was 88 ± 1 nM. This IC_{50} value is in excellent agreement with the IC_{50} with recombinant ALDH1A1 suggesting that this enzyme contributes the majority of *at*RA formation in the in vitro system (Figure 3.4). At concentrations in which WIN 18,446 inhibits recombinant ALDH1A activity >90%, the *at*RA formation in the testis was inhibited >90% demonstrating that ALDH1A enzymes are the predominant enzymes involved in *at*RA formation from *at*-retinal in the testis. To evaluate the specific contribution of ALDH1A2 to *at*RA formation, the time dependent inhibition of *at*RA formation in the testes samples was determined. After a 30 minute incubation with WIN 18,446, 97% of the ALDH1A2 is predicted to be inactivated and TDI by WIN 18,446 can be used to determine ALDH1A2 contribution to the *at*RA formation. The observed decrease in *at*RA formation after 30 min preincubation with WIN 18,446 was 28 ± 15% (Figure 3.4). This observed 28% contribution of ALDH1A2 to testicular *at*RA formation is consistent with the average 15% contribution predicted from the recombinant enzyme data.

The effect of CRBP-1 on retinoic acid formation by ALDH1A enzymes and in testes S10 fractions

To determine whether CRBPs affect the formation of *at*RA in human testis the formation of *at*RA by recombinant ALDH1A and testes S10 protein was measured with holo-CRBP1. The

formation of *at*RA was increased 3.0-fold in incubations of testis S10 protein with holo-CRBP1 in comparison to *at*-retinal (Figure 3.6A). In order to determine the enzyme(s) responsible for the increase in *at*RA formation, the effect of holo-CRBP1 on *at*RA formation with each ALDH1A enzyme was determined (Figure 3.6A). *at*RA formation by ALDH1A1 was decreased 52% when holo-CRBP1 was used as a substrate compared to *at*-retinal. In contrast *at*RA formation by ALDH1A2 was increased 2.7-fold in the presence of CRBP1 when compared to free *at*-retinal. *at*RA formation by ALDH1A3 was unchanged in the presence of CRBP1. CRBP1 expression in the human testis was quantified in each study subject and the average concentration of CRBP1 was 445 ± 85 pmol/gram testis (445 nM) (Figure 3.6B). The effect of CRBP1 on the contribution of each ALDH1A enzyme to *at*RA formation in the testis was predicted using a physiologically relevant concentration of 100 nM *at*-retinal. In the absence of CRBP1, ALDH1A1 is predicted to be the main contributor to *at*RA formation (84%). However, if all *at*-retinal is bound to CRBP1, ALDH1A2 is predicted to contribute to the majority of *at*RA formation (52%) (Figure 3.6C).

Alterations in the intratesticular ALDH1A activity in transgender individuals

To further evaluate the function of ALDH1A enzymes in the human testis, the ALDH1A activity and protein concentrations were measured in a sample set of three transgender individuals who had undergone hormonal sex reassignment therapy. The average protein concentrations of ALDH1A1, ALDH1A2, and ALDH1A3 were 54.0 ± 14.7 pmol/mg S10 protein, 1.3 ± 0.2 pmol/mg S10 protein, and 1.3 ± 0.5 pmol/mg S10 protein in the transgender donors (Figure 3.7). ALDH1A2 expression was significantly ($p < 0.05$) decreased in the testes of the transgendered individuals compared to the men. Additionally, the ALDH1A1 expression level was 20% lower in these donors than in the other donors, but this difference did not achieve significance ($p > 0.05$). The ALDH1A mediated *at*RA formation was significantly ($p < 0.02$)

lower in the testis from transgender donors than in the men undergoing orchiectomy at both concentrations of *at*-retinal (1.8 ± 0.6 pmol/min/mg S10 protein at 7.8 nM and 9.0 ± 3.4 pmol/min/mg S10 protein at 181 nM) (Figure 3.7). Additionally, the formation of 13-*cis*RA from 13-*cis*-retinal was significantly ($p < 0.01$) decreased (8.9 ± 4.1 pmol/min/mg S10 protein) in these individuals when compared to the other donors.

ALDH1A localization in the human testis

The predicted relative contribution of ALDH1A1 to *at*RA formation in the testis must be reconciled with the fact that male ALDH1A1 knock-out mice are fertile (Ziouzenkova et al., 2007). Hence, it was hypothesized that the tissue localization of the ALDH1A enzymes within the testis may explain this phenotypic discrepancy. To test this, immunohistochemistry was performed to investigate the cell type specific expression pattern of the three ALDH1A enzymes within testicular tissue from three healthy, fertile men (Figure 3.8). The three ALDH1A enzymes were expressed in distinct cell types and the expression patterns were different for each isozyme. Sertoli and peritubular myoid cells were all positive for ALDH1A1, but this enzyme could not be detected within any germ cell type (Figure 3.8A). In contrast, ALDH1A2 localized to pachytene spermatocytes and round spermatids with signal also present in some spermatogonia and peritubular myoid cells (Figure 3.8B-D). The third isoform, ALDH1A3, displayed a similar expression pattern, with protein detected in pachytene spermatocytes, spermatogonia, and Sertoli cells (Figure 3.8E). Under these conditions, cells of the interstitium are positive without primary antibody, and therefore are possibly non-specifically stained in all. Taken together, the localization patterns of the individual ALDH1A enzymes suggest that the various cell types of the testis can all synthesize RA, but do so utilizing distinct ALDH1A isoforms.

Correlation of intratesticular retinoic acid concentrations with ALDH1A activity

To test whether tissue *at*RA and 13-*cis*RA concentrations were affected by ALDH1A activity in the same tissue, intratesticular *at*RA and 13-*cis*RA concentrations were measured in the testes samples from the 15 donors with prostate cancer (Figure 3.9). The intratesticular RA concentrations were 4.3 ± 0.5 pmol/gram for *at*RA and 5.1 ± 0.6 pmol/gram for 13-*cis*RA, and concentrations of *at*RA and 13-*cis*RA were positively correlated (R^2= 0.36, p = 0.02). An unknown peak was observed in each sample that eluted between the *at*RA and 13-*cis*RA isomers. Based on the fact the 9-*cis*RA isomer elutes between the *at*RA and 13-*cis*RA isomers, MS^3 was used to determine if the unknown peak was a RA isomer (Arnold et al., 2012). The fragmentation pattern of the *at*RA and 13-*cis*RA isomers were identical and generated fragments of *m/z* 159^+, 119^+, 131^+, and 105^+(Figure 3.9B). An identical fragmentation pattern was observed for the RA peaks measured from human testicular tissue. However, the fragments generated from the unknown peak were distinctly different and suggest it is not a RA isomer. Based on the abundance of the *m/z* 159^+ fragment formed from RA and not the unknown peak, the 159^+ fragment was extracted from the MS^3 data (Figure 3.9C). The extraction of the fragment allows for clear identification of RA isomers from matrix components observed using MRM. The ALDH1A activity (*at*RA formation) measured at the biologically relevant 7.8 nM concentration of *at*-retinal correlated positively with intratesticular 13-*cis*RA concentrations (R^2= 0.40, p =0.01) and total RA concentration (R^2= 0.30, p =0.03). However, intratesticular *at*RA concentrations did not correlate significantly with ALDH1A activity at either of the *at*-retinal concentrations (p = 0.22 at 7.8 nM and 0.94 at 181 nM) (Figure 3.9D).

3.4 Discussion

The current study describes the development of novel methods necessary to study the formation of RA by ALDH1A enzymes and the application of these methods to characterization

of RA formation in human testis. While the indispensible nature of RA in the testis is well established, the complement of human enzyme(s) responsible for RA formation has been poorly characterized. The methods developed in this study provide the foundation to determine the tissue specific importance of each ALDH1A enzyme to RA formation, and establish novel tools to evaluate the cell and tissue specific mechanisms that allow for generation of RA gradients required for the regulation of biological processes. The developed methods are particularly useful for evaluating the role of altered RA homeostasis in human diseases, as all these methods can be used to study ALDH1A localization, expression level, activity, and RA concentration using a single tissue biopsy of 100 mg.

The testis ALDH1A expression levels reported in this study present for the first time the quantitative expression levels of ALDH1A1, ALDH1A2, and ALDH1A3 in any human tissue. Human tissue specific mRNA expression profiles of each ALDH1A enzyme have been previously shown and based on the mRNA levels, the rank order of ALDH1A expression in the testis is ALDH1A2 (59%) > ALDH1A1 (29%) > ALDH1A3 (12%) (Nishimura and Naito, 2006). This is in contrast to the current study showing ALDH1A1 being the predominant enzyme and emphasizes the need to measure protein expression levels instead of mRNA. Another previous study used in situ hybridization to determine the localization of Aldh1a enzymes in the mouse testis. In that study, ALDH1A1 was found in Leydig cells and Sertoli cells, ALDH1A2 in pachytene spermatocytes and step 1-6 spermatids, and ALDH1A3 in Leydig cells (Vernet et al., 2006). The protein localization reported here is in generally good agreement with the previous mouse mRNA data although unlike in mouse mRNA studies ALDH1A2 protein was found in the spermatogonia of the human testis. The distinct ALDH1A localization in human testicular tissue suggests that each ALDH1A may play a different role in RA formation in different cell types of

the testis. Previous work in knockout mice has shown that ALDH1A enzymes in Sertoli cells are responsible for the initial source of RA during spermatogenesis, while ALDH1A in spermatocytes may help maintain RA formation after the first wave of spermatogenesis (Raverdeau et al., 2012).

This study shows that overall in the human testis, ALDH1A1 and ALDH1A2 contribute significantly to formation of *at*RA from *at*-retinal and their relative contributions will depend on the interactions of the ALDH1A enzymes with CRBP1 in the specific cell types. The WIN 18,446 inhibition data unequivocally shows that RA formation in the testis is dependent on ALDH1A enzymes and not other enzymes such as aldehyde oxidases or xanthine oxidases. Together with the correlation between ALDH1A expression and *at*RA and 13-*cis*RA formation in vitro, the WIN 18,446 inhibition confirms the validity of the protein quantification and recombinant enzyme kinetic data. The correlation between ALDH1A2 expression and *at*RA formation together with the predicted importance of ALDH1A2 in the presence of CRBP, suggests that ALDH1A2 makes a significant contribution to *at*RA formation, and that its expression is at least in part responsible for the interindividual variability in RA formation in the testis. As shown by the expression of CRBP1 in the human testes and the ALDH1A isoform specific effects of CRBP1 on RA formation, prediction of the in vivo contribution of each individual ALDH1A enzyme is complex and likely also affected by the fraction of CRBP1 that is bound by retinol in vivo. The expression of cellular retinoic acid binding proteins that may affect product release from ALDH1As may also alter the predicted contributions in vivo. Previously, rat ALDH1A1 has been shown to recognize holo-CRBP1 as a substrate (Posch et al., 1992), but the effect of CRBP1 on *at*RA formation by human ALDH1A has never been reported. Similarly CBRP1 expression in the Sertoli cells of mice and rats (Kato et al., 1985b) has been shown

suggesting that CRBPs play an important role in modulating intratesticular RA metabolism. While ALDH1A1 was predicted to be the major contributor to *at*RA formation in the absence of CRBPs, when the inhibition of ALDH1A1 and activation of ALDH1A2 by CRBP1 was accounted for, ALDH1A2 was predicted to be the predominant enzyme forming *at*RA in the testis. The observed increase in RA formation in the presence of CRBP1 in the testis S10 fractions is in agreement with the effects observed in the recombinant enzymes and supports the role of ALDH1A2 in RA formation in the testis. The predicted primary contribution of ALDH1A2 to RA formation in the presence of CRBP1 is also in agreement with the fact that ALDH1A1$^{-/-}$ mice are fertile and no obvious defects are detected in these mice at adulthood.

Interestingly, ALDH1A1 was the only ALDH1A enzyme capable of forming 13-*cis*RA from 13-*cis*-retinal. The 13-*cis*RA formation by ALDH1A1 displayed substrate inhibition kinetics suggesting multiple 13-*cis*-retinal molecules may be able to simultaneously bind ALDH1A1. Despite this, the kinetics determined from the substrate inhibition model could be used to predict 13-*cis*RA formation velocity in individual human samples in vitro. The fact ALDH1A1 was the one enzyme able to form 13-*cis*RA is of interest since in a preliminary study of 24 men, an association between intratesticular 13-*cis*RA and abnormal semen was revealed suggesting that altered intratesticular RA homeostasis may be present in infertile men (Nya-Ngatchou, 2012). In addition, 13-*cis*RA treatment has been shown to increase sperm production in humans (Hoting VE, 1992). Based on the results of this study, the decreased intratesticular 13-*cis*RA concentration may suggest a decreased expression of ALDH1A1 in men with abnormal semen. However, at present the source of intratesticular 13-*cis*RA is not known and it could be formed either via isomerization from *at*RA or enzymatically from 13-*cis*-retinal if it is present in

human tissues. Also, it is unknown if 13-*cis*RA is necessary for spermatogenesis, and the cause of the differences in RA concentrations with different fertility diagnoses has not been identified.

A significant decrease in the RA formation velocity was observed in the testicular tissue of transgender individuals possibly due to the significant decrease in ALDH1A2 expression. It seems likely that the pre-surgical hormonal therapy with estradiol commonly given prior to gender reassignment surgery may have affected ALDH1A2 expression. In support of this notion, a mouse model lacking a functional androgen receptor has significantly decreased mRNA for both *Aldh1a1* and *Aldh1a2* (O'Shaughnessy et al., 2007). Additionally, ALDH1A2 expression is significantly decreased in infertile men diagnosed with Sertoli cell only syndrome on testicular biopsy (Amory et al., 2014). The reduced expression of ALDH1A2 in these men is likely related to the reduction in the numbers of developing sperm cells, consistent with our observation that spermatogonia, spermatids, and spermatocytes were the main cell type staining for ALDH1A2 in the histological analysis. Although the donors in this study were men with prostate cancer undergoing orchiectomy the good agreement with this data and prior clinical findings suggests these men reflect healthy, fertile men in terms of testicular function. Yet, further studies in different populations of men, including young healthy men and infertile men are needed to fully characterize the role of the different ALDH1A enzymes in male reproduction. Taken together, these data demonstrate the critical importance of understanding the specific enzymology of RA synthesis in the testis.

The correlation discovered between RA formation activity and RA concentration in the human testis described here is to our knowledge the first published example of a correlation between human tissue concentrations of an endogenous substance and the activity of the enzyme responsible for its formation. With the evidence suggesting intratesticular RA is formed within

the tissue and assuming no interindividual differences in the clearance of intratesticular RA, a correlation between the RA synthesis rate and the measured intratesticular RA is expected. The reason intratesticular 13-*cis*RA correlated with ALDH1A activity and *at*RA did not, may be due to the fact 13-*cis*RA is a poor substrate for CYP26 enzymes compared to *at*RA (Helvig et al., 2011). Therefore, interindividual differences in CYP26 expression are more likely to affect the intratesticular concentration of *at*RA. Additionally, differences in RA elimination between the individuals in the study would explain why a stronger positive correlation was not observed.

The results of this study demonstrate the usefulness of novel mass spectrometry approaches to model RA formation in human tissue using the testis as an example. RA formation kinetics was accurately characterized using two novel methods to measure ALDH1A concentrations and determine RA formation by ALDH1A in human tissue biopsies. ALDH1A1 is the predominant enzyme in the formation of RA in the Sertoli cells while the specific localization of ALDH1A2 in the developing sperm indicates a critical role for ALDH1A2 in these cell types. The distinct localization of the ALDH1A enzymes together with their different interactions with CRBP1 suggest specific, cell-type specific roles of the different ALDH1A enzymes in intratesticular *at*RA formation. Further studies are needed to establish the full biological relevance of these findings. These results illustrate the need to determine the contribution of each ALDH1A to RA formation and the localization of each enzyme in individual target tissues. Tissue RA concentrations by themselves will not give an accurate representation of how RA formation is controlled within the tissue. Furthermore, given the indispensible role of RA in many other biological functions, the methods described will provide a valuable tool in understanding how RA homeostasis is altered by or potentially leads to disorders associated with changes in ALDH1A expression.

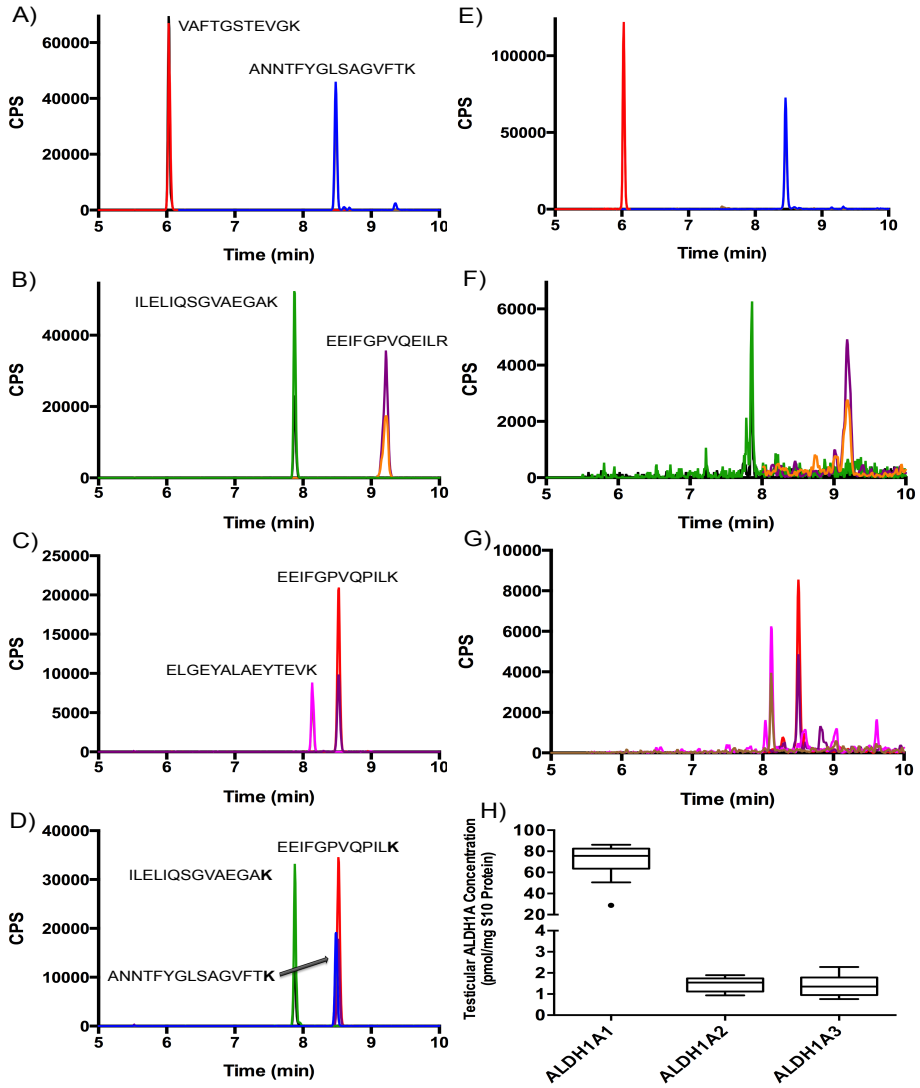

Figure 3.1: Quantification of ALDH1A1, ALDH1A2, and ALDH1A3 from testicular tissue S10 fractions. ALDH1A concentrations were measured using a novel LC-MS/MS based peptide quantification method. Recombinant protein was digested and two peptides (each with two *m/z* transitions) were chosen for each protein to measure ALDH1A1 (A), ALDH1A2 (B), and ALDH1A3 (C) using LC-MS/MS. The peptide used for quantification was normalized to a corresponding stable isotope labeled peptide with a [$^{13}C_6{}^{15}N_2$]-lysine or [$^{13}C_6{}^{15}N_2$]-arginine bolded (D). Each peptide was observed in all 18 men and representative chromatograms of detection of ALDH1A1 (E), ALDH1A2 (F), and ALDH1A3 (G) in human testis are shown. The expression levels of the three proteins in the human testes of non-transgendered men are shown in (H). All peaks displayed in the chromatograms are scaled to counts per second (CPS).

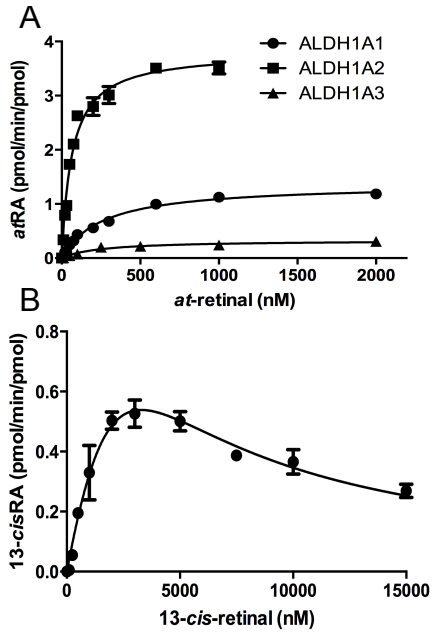

Figure 3.2: Kinetics of RA formation by recombinant ALDH1A proteins. Recombinant purified human ALDH1A was used to determine the kinetics of *at*RA formation for each ALDH1A enzyme (A). Since only ALDH1A1 formed 13-*cis*RA from 13-*cis*-retinal, only 13-*cis*RA formation by ALDH1A1 was characterized (B).

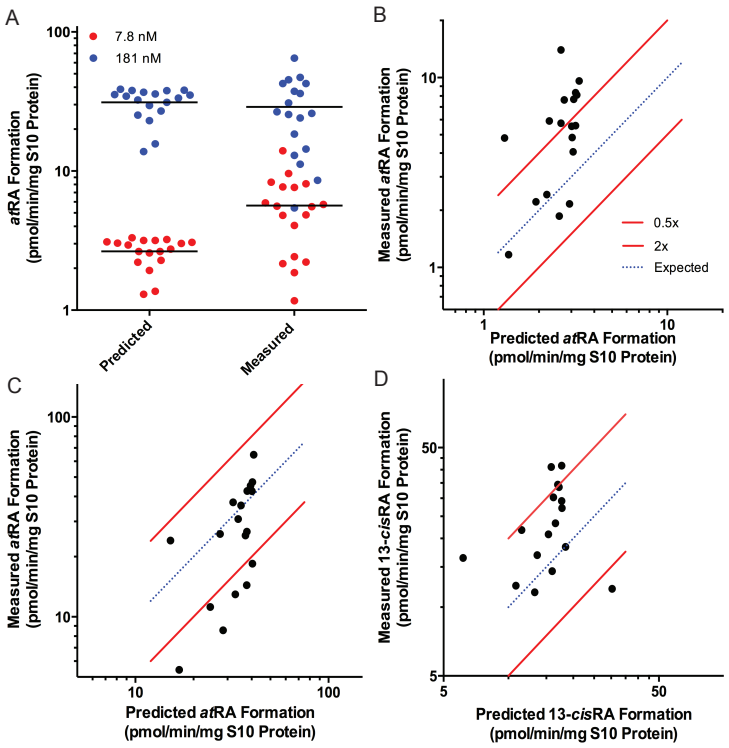

Figure 3.3: Comparison of the predicted and measured ALDH1A activity in human testis. *at*RA formation was measured and predicted for the 18 subjects with 8 nM (red circles) and 181 nM (blue circles) *at*-retinal as the substrate (Panel A). Each dot represents an individual in the study. The measured activity was plotted as a function of predicted activity in each subject with 7.8 nM *at*-retinal (B), 181 nM *at*-retinal (C), and 600 nM 13-*cis*-retinal (D). The blue dotted line represents an exact correlation between predicted and measured RA formation (ALDH1A activity). The red lines represent the range between 2-fold overprediction and 0.5-fold underprediction.

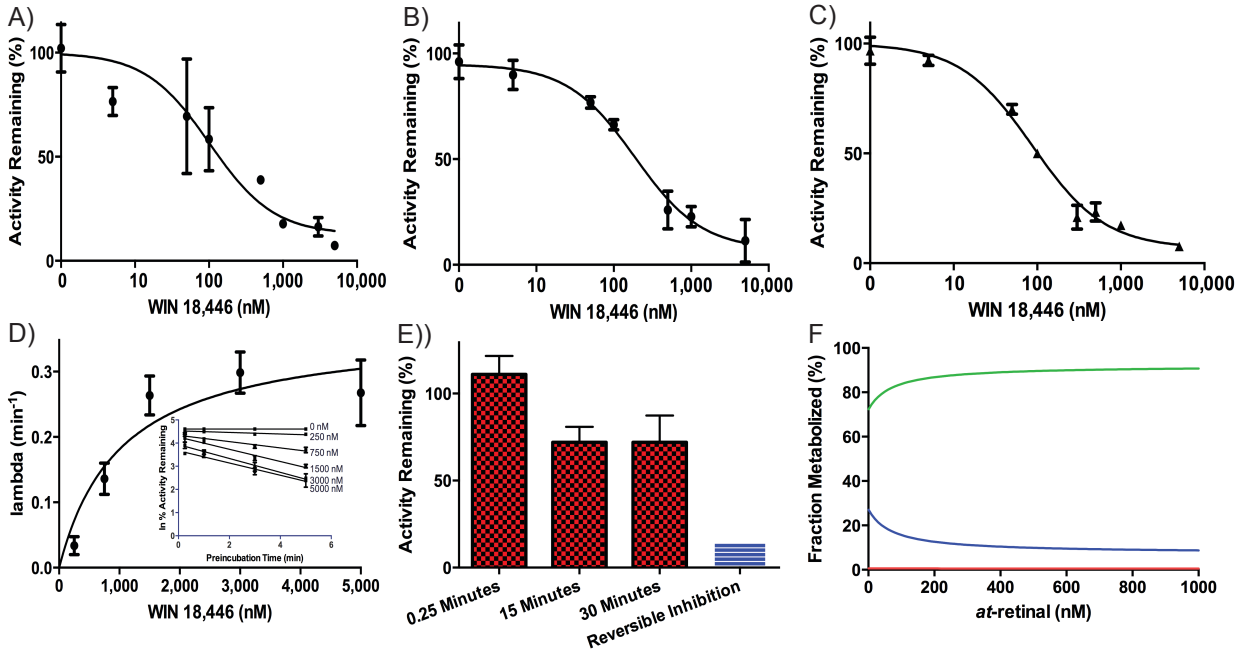

Figure 3.4: Inhibition of ALDH1A and RA formation by WIN 18,446. The inhibition kinetics of WIN 18,446 were characterized and used to determine the fraction of *at*RA formation by ALDH1A2 in the human testis. The reversible inhibition kinetics of WIN 18,446 with recombinant ALDH1A1 (A, IC_{50}= 102 nM) and ALDH1A3 (B, IC_{50}= 187 nM) were determined together with the effect of WIN 18,446 on *at*RA formation in testicular S10 fractions (Panel C, IC_{50}= 88 nM). Due to the time dependent inhibition of ALDH1A2 by WIN 18,446, the rate of inactivation was determined with increasing concentrations of inhibitor (D inset) and plotted as a function of inhibitor concentration (D) to determine the K_I and k_{inact}. In order to measure the f_m for ALDH1A2 in the testis, S10 protein was preincubated with inhibitor for 0.25, 10, and 30 minutes to inactivate any ALDH1A2 protein (E). The preincubation was diluted out to remove reversible inhibition, and the ALDH1A activity was determined. The 25% decrease in ALDH1A activity (E) can be attributed to the contribution by ALDH1A2. The predicted relative contribution of each ALDH1A enzyme (Green- ALDH1A1, Blue- ALDH1A2, Red- ALDH1A3) to atRA formation as a function of at-retinal concentration is shown in Panel F.

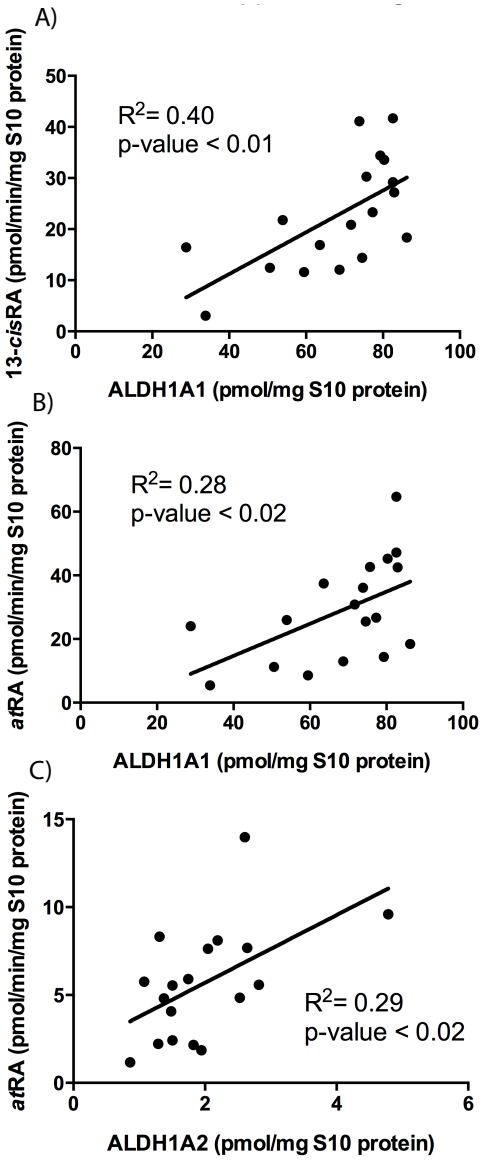

Figure 3.5: The correlation between ALDH1A protein expression and in vitro RA formation by testicular S10 protein. When testicular S10 protein was incubated with nominal 1000 nM 13-*cis*-retinal or *at*-retinal, there was a significant positive correlation between the formation of RA and ALDH1A1 protein concentration (A, B). The expression of ALDH1A2 had a significant positive correlation with the formation of *at*RA when testicular S10 protein was incubated with nominal 100 nM *at*-retinal (C).

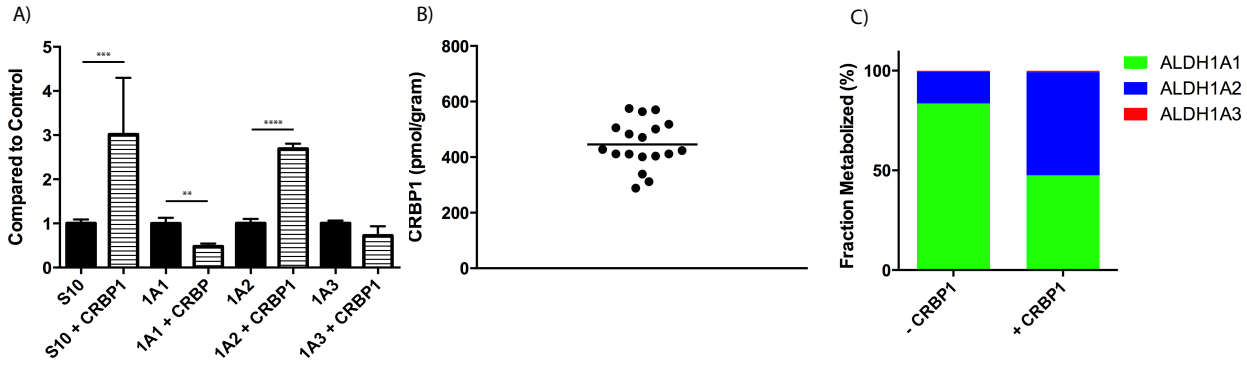

Figure 3.6: The effect of CRBP1 on *at*RA formation and expression level in the testis. The effect of CRBP1 on *at*RA formation by testicular S10 protein, ALDH1A1, ALDH1A2, and ALDH1A3 was determined (A). Next, CRBP1 expression in testicular tissue was quantified by ELISA (B). In addition, the contribution of each ALDH1A enzyme to *at*RA formation in the presence or absence of CRBP1 was determined with a physiologically relevant substrate concentration of 100 nM (C).

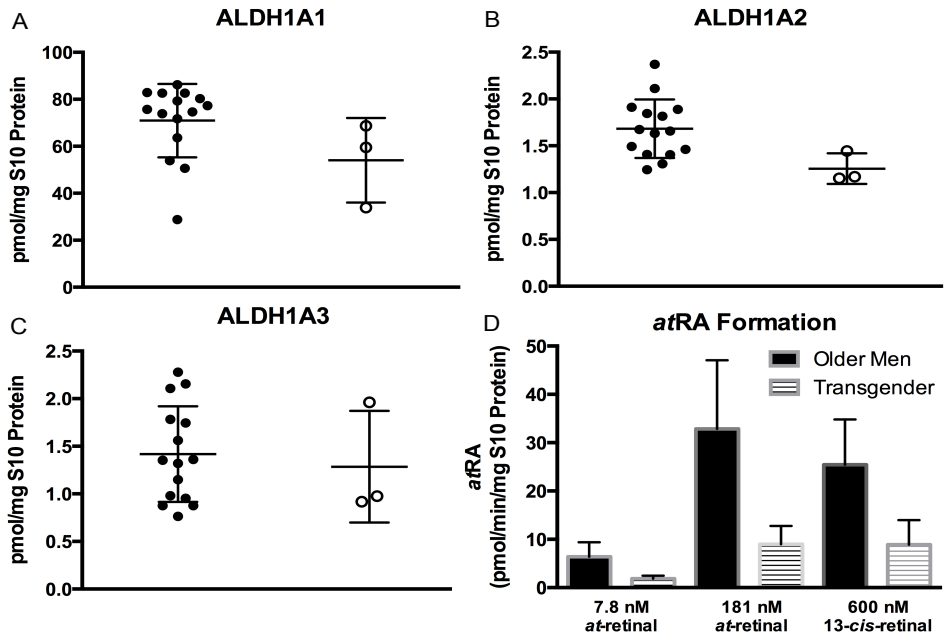

Figure 3.7: Comparison of the ALDH1A protein expression and activity between men and transgender individuals. There was a significant decrease in the ALDH1A2 protein concentration in the three transgender individuals (clear) compared to the men (black) (B). However, there was no observed difference in the testicular protein concentration of ALDH1A1 (A) or ALDH1A3 (C). Additionally, testicular ALDH1A activity was significantly lower in the transgender individuals at both 7.8 and 181 nM *at*-retinal ($p < 0.02$) as well as 600 nM 13-*cis*-retinal ($p < 0.01$).

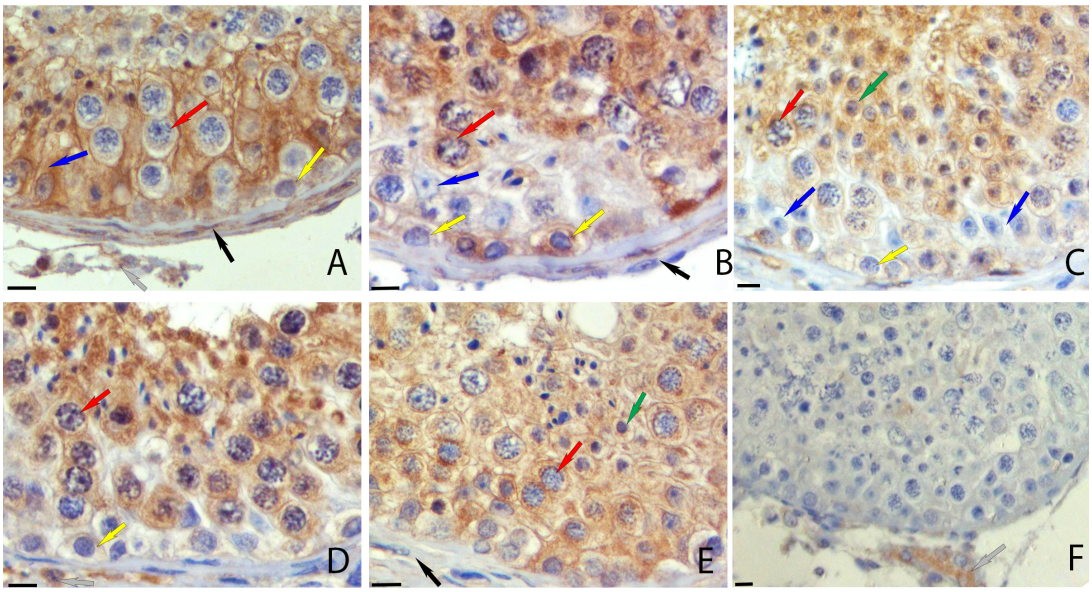

Figure 3.8: **Localization of ALDH1A enzyme in the human testis.** ALDH1A1, 1A2 and 1A3 have distinct localization patterns in the human testis. Each panel is representative of immunohistochemical results from three different human testes. All were fixed in Bouin's fluid and embedded in paraffin. Brown stain indicates immunopositive reaction for ALDH1A1 (A), ALDH1A2 (B-D), and ALDH1A3 (E). A negative control (F) used Rabbit IgG instead of primary rabbit antibody. Original magnification was 225x for each. The bar at lower left of each panel represents 10 microns. Cell types are indicated by arrows as follows: Blue, Sertoli cells; Yellow, spermatogonia; Red, primary spermatocytes; Green, round spermatids; Black, peritubular cells; Gray, interstitial cells.

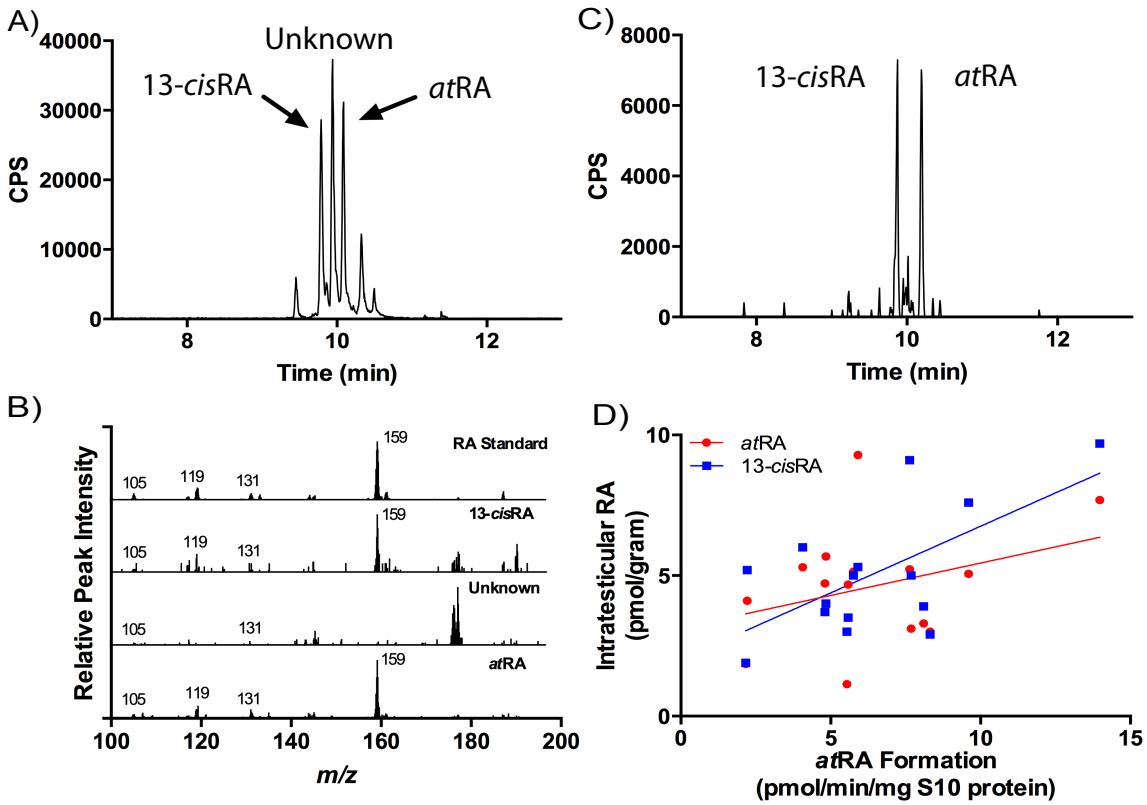

Figure 3.9: Quantification of intratesticular RA and correlation of RA concentration and measured RA formation in human testes. Intratesticular *at*RA and 13-*cis*RA were measured using LC-MS/MS and a representative chromatogram is shown (A). Panel B shows the correlation between *at*RA formation and 13-*cis*RA. In addition, total RA had a significant positive correlation with *at*RA formation.

Table 3.1: Two signature peptides were chosen for quantification and confirmation of ALDH1A proteins. The peptides used for quantification of ALDH1A1 and ALDH1A2 were synthesized with a heavy labeled terminal lysine or arginine and functioned as an internal standard. A heavy labeled peptide for ALDH1A3 was synthesized to control for the variability in trypsin digestion across the sample set. For each peptide, values of 10 and 13 were used for the entrance and collision exit potential.

Protein	Peptide (Amino Acid #)	Precursor Ion (*m/z*)	Fragments (*m/z*)	Declustering Potential	Collision Energy
ALDH1A1	ANNTFYGLSAGVFTK[A] (420-434)	795.4	879.5 1042.6	120	20
	VAFTGSTEVGK (241-251)	548.3	778.4 677.3	71	28
ALDH1A2	ILELIQSGVAEGAK[A] (370-383)	714.4	846.4 959.5	120	30
	LAFSLGSVWR (85-94)	568.3	604.3 717.4	73	30
ALDH1A3	EEIFGPVQPILK[A,B] (409-420)	685.4	851.5 794.5	81	34
	ELGEYALAEYTEVK (487-500)	807.9	839.4 952.5	90	38

An ([A]) denotes the peptide used for the quantitation of each ALDH1A enzyme. A heavy labeled peptide (EVTDNMRIAKEEIFGPVQPILK) that required trypsin cleavage to generate the labeled target peptide (EEIFGPVQPILK) was synthesized for ALDH1A3 ([B]).

Table 3.2: Enzyme kinetic parameters for RA formation from retinal by ALDH1A enzymes

	at-retinal			13-*cis*-retinal			
Enzyme	k_{cat} (min^{-1})	K_m (nM)	Cl_{int} (mL/min/pmol)	k_{cat} (min^{-1})	K_m (nM)	K_i (nM)	Cl_{int} (μL/min/pmol)
ALDH1A1	1.1 ± 0.1	285 ± 24	3.9	3.0 ± 2.2	7434 ± 6700	1468 ± 1320	0.4
ALDH1A2	3.7 ± 0.1	56 ± 5	66.1	N/A	N/A	N/A	N/A
ALDH1A3	0.3 ± 0.01	261 ± 18	1.1	N/A	N/A	N/A	N/A

Chapter 4

Pharmacological inhibition of ALDH1A in mice decreases *all-trans* retinoic acid concentrations in a tissue specific manner

Chapter 4 was published

in

Biochemical Pharmacology. In press.

4.1 Introduction

The central role of the vitamin A active metabolite *all-trans* isomer (*at*RA) is well established in many post natal biological processes including spermatogenesis (Chung et al., 2009; Raverdeau et al., 2012), the gut-homing specificity of both T cells and B cells (Iwata et al., 2004; Mucida et al., 2007), regulation of apoptosis (Noy, 2010a), energy homeostasis (Kiefer et al., 2012), and stem cell differentiation (Gudas and Wagner, 2011). *at*RA acts as a signaling molecule by activating the nuclear retinoic acid receptors (RARs) (Idres et al., 2002) and peroxisome proliferator-activated receptor (PPAR) β/δ (Mark et al., 2006; Schug et al., 2007). Of the tissues responsive to *at*RA signaling, the liver and testis are of particular interest. The liver is the primary storage organ for vitamin A playing a central role in regulating vitamin A homeostasis. Loss of *at*RA signaling in a liver specific RAR negative mouse model has also been shown to cause steatosis and increased risk of liver cancer (Shiota, 2005). In the testis, *at*RA is critical to initiate and maintain spermatogenesis (Raverdeau et al., 2012) and loss of *at*RA signaling in the testis leads to male infertility (Lohnes et al., 1993; Lufkin et al., 1993). Yet, the enzymology of how *at*RA concentrations are regulated in these organs and how inhibiting *at*RA formation would effect *at*RA concentrations in specific tissues remains to be determined.

In most organs, the primary source of *at*RA is in situ synthesis (Kurlandsky et al., 1995). As a result, tissue concentrations of *at*RA do not necessarily correlate with circulating *at*RA concentrations, although it is likely that alterations in tissue *at*RA synthesis or metabolism will be reflected in altered serum concentrations (Obrochta et al., 2014). The concentrations of *at*RA in each tissue are regulated by the availability of the precursors retinol and β-carotene which are enzymatically converted to the *at*RA precursor *all-trans* retinal (*at*-retinal). The final irreversible step in *at*RA synthesis is the oxidation of *at*-retinal to *at*RA, and multiple enzymes of the

aldehyde dehydrogenase (ALDH), aldehyde oxidase (AOX), xanthine oxidase (XOX), and cytochrome P450 (Gagnon et al., 2002, 2003; Graham et al., 2006; Huang et al., 1999; Raner et al., 1996; Roberts et al., 1992; Taibi et al., 2001; Watanabe et al., 1991) families have been shown to catalyze the formation of *at*RA from *at*-retinal in vitro. Of these enzymes, the ALDH1A enzymes (ALDH1A1, ALDH1A2, and ALDH1A3) are generally believed to be the most important. This is due to the fact that *Aldh1a2*$^{-/-}$ and *Aldh1a3*$^{-/-}$ mice die during embryonic development and have typical malformations relating to vitamin A deficiency (Dupe et al., 2003; Niederreither et al., 1999). *Aldh1a1*$^{-/-}$ mice are viable and fertile and have increased circulating concentrations of retinal, but whether tissue *at*RA concentrations are decreased in *Aldh1a1*$^{-/-}$ mice is unclear (Molotkov and Duester, 2003). Despite the distinct phenotypes of the these mice, it is not known whether decreased activity of ALDH1A enzymes will alter tissue *at*RA concentrations in adult animals or if other enzymes are important in *at*RA formation in postnatal life.

Cytosolic enzymes appear to be responsible for the overwhelming majority of *at*RA formation from *at*-retinal (Dockham et al., 1992; Lee et al., 1991; Napoli and Race, 1987, 1990). The ALDH enzymes along with AOX and XOX are cytosolic soluble enzymes that form *at*RA from *at*-retinal (Garattini et al., 2008; Yoshida et al., 1998). While ALDH enzymes are $NAD(P)^+$ dependent, AOX and XOX do not require a pyridine nucleotide cofactor for their activity (Garattini et al., 2008; Taibi et al., 2001), and the necessity of $NAD(P)^+$ for the majority of *at*RA formation in the mouse liver was used to show that ALDH enzymes contribute to the majority of *at*RA formation (Lee et al., 1991). An AOX inhibitor, pyridoxal, only inhibited approximately 5% of the *at*RA formation. Similarly, 80% of the *at*RA formation in human liver cytosol was NAD^+ dependent and the overall contribution of AOX was approximately 10% (Dockham et al.,

1992). Whether microsomal NADPH dependent enzymes such as cytochrome P450s contribute to in vivo *at*RA synthesis is poorly studied. This is mainly because the K_m values for *at*-retinal with cytochrome P450 are nearly 70-fold higher than endogenous concentrations of *at*-retinal suggesting they most likely do not have a significant role in *at*RA biosynthesis (Obrochta et al., 2014; Raner et al., 1996). In contrast, the K_m values for *at*-retinal with ALDH1A1-1A3 are low nanomolar (Arnold et al., 2014). The ALDH1A enzymes also catalyze the formation of *at*RA from *at*-retinal bound to cellular retinol binding protein 1 (CRBP1) which is expressed ubiquitously across the body (Kato et al., 1985a; Posch et al., 1992; Zhai et al., 2001).

The ALDH1A enzymes appear to have tissue and cell type specific roles in *at*RA synthesis. To date, methods have not been readily available to determine the specific activity and protein expression of individual ALDH1A enzymes in tissues or for demonstrating that ALDH1A activity influences tissue *at*RA concentrations and net *at*RA formation. In mice, ALDH1A1 and ALDH1A2 enzymes show tissue specific localization based on western blots. ALDH1A1 is expressed in the liver, testis, and lung with highest expression in the liver, while ALDH1A2 expression is highest in the testis followed by the uterus and ovary (Haselbeck et al., 1999). The tissue specific expression patterns suggest that each ALDH1A plays a unique role in regulating *at*RA concentrations but the pharmacological or toxicological outcomes of decreasing ALDH1A enzyme activity within a specific target or whole body have not been established and methods to predict *at*RA concentrations in vivo are lacking. WIN 18,446 is a potent reversible inhibitor of ALDH1A1 and ALDH1A3 and a time dependent inhibitor of ALDH1A2 (Arnold et al., 2014). Due to its broad and potent ALDH1A inhibition, it provides a unique, novel tool to alter ALDH1A activity in vivo and to test the tissue specific effects of ALDH1A inhibition to *at*RA concentrations. In rabbits and mice, WIN 18,446 treatment leads to lack of sperm

production, a finding correlated with decreased testicular *at*RA concentrations (Amory et al., 2011a; Paik et al., 2014a). However, the in vivo exposure and ALDH1A inhibition of WIN 18,446 has never been studied. The aim of this study was to determine how inhibition of ALDH1A affects tissue *at*RA concentrations and whether this effect could be predicted from in vitro data. To predict the effect of ALDH1A inhibition on *at*RA formation in the mouse testis and liver, ALDH1A expression and *at*RA formation in mouse testis and liver were measured. Inhibition of *at*RA formation in each tissue was predicted based on in vivo WIN 18,446 pharmacokinetics and in vitro ALDH1A inhibition kinetics. The time course of the effect of ALDH1A inhibition on tissue *at*RA concentrations was measured in liver, testis, and serum. The results show that ALDH1A inhibition decreases *at*RA concentrations in a tissue specific manner and may disrupt retinoid dependent processes throughout the body.

4.2 Methods

C*hemicals and reagents.*

all-trans retinoic acid (*at*RA), and *at*-retinal were purchased from Sigma-Aldrich (St. Louis, MO). Optima-grade water, Optima-grade acetonitrile, Optima-grade methanol, and mass spectrometry grade formic acid used for chemical analyses were purchased from Thermo Fisher Scientific (Waltham, MA). WIN 18,446 was obtained from Acros Organics (Geel, Belgium). *at*RA-d_5 was purchased from Santa Cruz Biotechnology (Santa Cruz, CA). Peptides labeled with [$^{13}C_6{}^{15}N_2$]-lysine or [$^{13}C_6{}^{15}N_2$]-arginine were purchased from Thermo Fisher Scientific (Waltham, MA).

Animal care and WIN 18,446 treatments

All animal experiments were approved by the Washington State University Animal Care and Use Committee and all animals were cared for in compliance with the principles for the care

and use of research animals of the National Institutions of Health. Male C57BL/6-129 mice between three and five months of age were housed in a temperature, humidity, and light controlled environment and were provided food and water *ad libitum*. These animals were euthanized via CO_2 asphyxiation followed by cervical dislocation. Adult animals were treated orally for one to eight days with WIN 18,446 or vehicle (1% gum tragacanth). The dosing protocols for WIN 18,446 were divided into two separate studies. In the first study, mice were given a single dose of 125 mg/kg of WIN 18,446 po, and three mice per time point were sacrificed at 0.5, 1, 2, 4, 8, 12, and 24 hours post dose. Three mice were administered vehicle and sacrificed immediately after vehicle administration. In the second study, mice were given 125 mg/kg WIN 18,446 or vehicle (control group) every 24 hours for 8 days. Three mice were sacrificed immediately before the 8^{th} dose was given and an additional three mice per time point were sacrificed immediately after dosing at 0.5, 1, 2, 4, 8, 12, and 24 hours post dose. For all groups, blood, testis and liver were collected upon sacrifice, plasma separated from blood by centrifugation and testes detunicated. All samples were collected in a light protected environment. The samples were snap frozen in liquid nitrogen and stored in -80°C until analysis.

Generation of subcellular fractions from mouse tissue

Mouse testis and liver S10 fractions containing microsomes and cytosol were separately generated from testes (17-45 mg) and livers (114-309 mg) of 14 individual mice. The tissue samples were from animals treated with a single dose of WIN 18,446 (n=3), 8 daily doses of WIN 18,446 (n=3) or from control animals (n=8) treated with vehicle (1% gum tragacanth). Briefly, samples were homogenized on ice using a drill powered 2 mL Potter-Elvehjem glass homogenizer (Kimbel Glass, Vineland, NJ) in 3x volume of tissue homogenization buffer (50 mM Potassium Phosphate, 250 mM sucrose with an EDTA free protease inhibitor cocktail

(Roche, San Francisco, CA)). The homogenizer was washed with 2x volume of tissue homogenization buffer and the wash volume combined with the homogenate. Large organelles and cell membranes were pelleted by centrifugation at 10,000 g for 25 minutes at 4°C and the supernatant was collected and aliquoted. The aliquots were flash frozen in liquid Nitrogen and stored at -80°C until use. The total protein concentration in each S10 fraction was measured using a BCA assay (Thermo Fisher, Waltham, MA). To isolate mouse liver microsomes and cytosol, the supernatant after the 10,000 g centrifugation was collected from the livers of four untreated mice and centrifuged at 93,000 g for 70 min. The supernatant contained cytosolic proteins while the pellet, containing microsomes, was resuspended in buffer (50 mM Potassium Phosphate and 250 mM sucrose pH 7.4). The protein concentration in the microsomes and cytosol was measured using a BCA assay (Thermo Fisher Scientific, Waltham, MA) and both were stored at -80°C.

Mass spectrometric quantification of ALDH1A enzymes

The expression of ALDH1A1 and ALDH1A2 was quantified in testis and liver S10 fractions as described previously using LC-MS/MS (Arnold et al., 2014) with a few modifications. Two signature peptides were chosen for each ALDH1A isoform one of which was used for quantification and the other to verify the identification of the protein. The signature peptides and their relevant [$^{13}C_6{}^{15}N_2$]-lysine or [$^{13}C_6{}^{15}N_2$]-arginine labeled internal standards are listed in Table 4.1 and were chosen based on their sensitivity, selectivity, and similarity to the corresponding peptide formed from the recombinant human protein. Recombinant human ALDH1A enzymes were used as calibrators for the quantification of tissue ALDH1A expression as described. An 11 point standard curve was generated with 0.018-14.4 pmol of ALDH1A1 and 0.005-2.7 pmol of ALDH1A2 and ALDH1A3. In order to account for the efficiency of the

trypsin digestion, a matching [$^{13}C_6{}^{15}N_2$]-lysine or [$^{13}C_6{}^{15}N_2$]-arginine labeled peptide extended past the trypsin cleavage site (Table 4.1) and required cleavage by trypsin to produce the target peptide was synthesized as an internal standard (Pierce, Rockford, IL) for the ALDH1A2 and ALDH1A3 quantification peptides. Each sample was prepared and digested in 96-well plates as previously described (Arnold et al., 2014) with a few modifications. Briefly, 20 µL of sample (recombinant ALDH1A standards or 4 mg/mL S10 fraction) were added to each well. Next, 2 µL of 700 nM ALDH1A2 lagging end peptide and 300 nM ALDH1A3 lagging end peptide were added together with 4 µL dithiothreitol (100 mM) and 10 µL of ammonium bicarbonate buffer (100 mM, pH 7.8). Next, 5 µL of 10% sodium deoxycholate were added to each well and the samples mixed before incubation at 95 °C for 5 minutes. After cooling to room temperature, 4 µL of iodoacetamide (200 mM) were added and the sample incubated at room temperature in the dark for 20 minutes. Trypsin was added at a 1:25 trypsin:protein ratio and the sample was digested for 24 hours at 37°C. The incubation was quenched by addition of 20 µL chilled acetonitrile with 8% trifluoroacetic acid containing the heavy labeled ALDH1A1 peptide internal standard. Samples were centrifuged at 3,000 g for 25 minutes at 4°C and were quantified by mass spectrometry using an AB Sciex 5500 qTrap Q-LIT mass spectrometer (AB Sciex, Foster City, CA) equipped with an Agilent 1290 UHPLC (Agilent, Santa Clara, CA). Peptides were separated using an Aeris Peptide XB-C18 column (50 X 2.1 mm) with 1.7 µm particle size at 40 °C and a SecurityGuard Ultra UHPLC C18-peptide cartridge (Phenomenex, Torrance, CA). The eluting solvents were A: H_2O + 0.1% formic acid and B: acetonitrile + 0.1% formic acid. For chromatographic separation the following 18 minute linear gradient with a 400 µL/minute flow rate was used: 0 → 3.5 minutes 3% B, then by 12.0 minutes increased to 40% B, 12.0 → 12.1 minutes 95% B and stayed 95% B until 15.0 minutes, then 15.0 → 15.1 minutes 3% B, 15.1 →

18 minutes 3% B. Each tissue sample was digested in triplicate and the resulting peak area for each quantitation peptide was normalized to its corresponding internal standard. The average value of the three digestions was used along with the standard curve for each protein to determine the pmol of enzyme in each sample. The amount of enzyme in each sample was normalized to the total S10 protein (0.08 mg) in each digestion. The stability of the peptides was validated by confirming there was no significant sample degradation (> 20%) after three freeze thaw cycles, 24 hours at 37°C, and 24 hours at room temperature. All data analysis was performed using Analyst (version 1.5.1) (AB Sciex, Foster City, CA). A signal to noise ratio of 9 was set as the minimum threshold for quantitation.

Mass spectrometric quantification of atRA, at-retinal, and WIN 18,446

The concentrations of *at*RA and *at*-retinal in incubations and tissue samples were measured using an AB Sciex 5500 qTrap Q-LIT mass spectrometer (Foster City, CA) equipped with an Agilent 1290 UHPLC (Santa Clara, CA) as previously described (Arnold et al., 2014) with several minor modifications. For in vitro incubation samples and to determine *at*-retinal fraction unbound, analytes were separated using a Kinetex C18 column (100 X 2.1 mm, 1.7 µm particle size) heated to 40°C with a SecurityGuard Ultra UHPLC C18 cartridge (Phenomenex, Torrance, CA) and a linear gradient with A: H_2O + 0.1% formic acid and B: Acetonitrile + 0.1% formic acid. The mobile phase flow was 600 µL/min with the following linear gradient: 0.0→ 0.25 minutes 40% B, then increased to 95% at 4.0 minutes, 4.0 → 5.0 minutes 95% B, 5.0 → 6 minutes 40% B. For detection, *at*RA was monitored using positive ion APCI and MS transitions of *m/z* 301→ 205 and *m/z* 301→ 123 with the 205 fragment used for quantification. For quantification, *at*RA peak areas were normalized to the *at*RA-d_5 internal standard peak area. *at*-retinal was measured only in fraction unbound experiments using positive ion APCI and the MS

transition *m/z* 285→161 with declustering potential of 66.0, collision energy of 13.0, and collision cell exit potential of 4.0. *at*-retinal-d_5 was used as an internal standard and was monitored using the 290→161 *m/z* transition. When tissue and serum *at*RA concentrations were measured, *at*RA was separated from endogenous interferences using a 150 mm x 2.1 mm Supelco Ascentis Express reverse phase amide column (Sigma, St. Louis, MO) with 2.7 µm particle size and an Ascentis Express reverse phase amide 2.7 µm guard cartridge. The solvents for the UHPLC analysis were A: H_2O + 0.1% formic acid and B: ACN/ MeOH (60/40) + 0.1% formic acid. The solvent flow was 500 µl/minute and the following linear gradient was used: 0.0 → 2.0 minutes 40% B, then increased to 95% B at 10.0 minutes, 10.0 → 15.0 minutes 95% B, 15.0 → 17.0 minutes 40% B. WIN 18,446 was quantified in serum samples extracted for *at*RA detection using an AB Sciex 4500 mass spectrometer (AB Sciex, Foster City, CA). The analytes were separated using an Agilent Zorbax C18 column (3.5 μm, 2.1 × 100 mm) coupled to a Shimadzu UFLC XR DGU-20A5 (Shimadzu Scientific Instruments, Columbia, MD). 10 µL of sample were injected and the solvent flow was 300 µL/minute. The solvents for the UHPLC analysis were A: H_2O + 0.1% formic acid and B: ACN + 0.1% formic acid. The following linear gradient was used: 0.0 → 0.5 minutes 3% B, then increased to 95% B at 8.0 minutes, 8.0→ 10.0 minutes 95% B, 10.0 → 13.0 minutes 3% B. The column was kept at a constant 40°C throughout the analysis. WIN 18,446 was detected using ESI^+ ionization with *m/z* transition of 367.0→69.0 for WIN 18,446 and 394.7→159.9 for N, N'-hexane-1,6-diylbis 2,2-dichloroacetamide (internal standard). For mass spectrometry parameters a declustering potential of 120, entrance potential of 10, curtain gas of 10, CAD gas of 9, ionspray voltage of 5500, temperature of 650°C, GS1 of 50, GS2 of 60, and collision cell exit potential of 6 were used. The collision energies were 47 (WIN 18,446) and 33 (internal standard). All data analysis was performed using Analyst (version

1.5.1) (AB Sciex, Foster City, CA). A signal:noise of 9 was set as the minimum threshold for quantitation. The tissue and serum *at*RA concentrations versus time data were used to determine the tissue $t_{1/2}$ following WIN 18,446 administration. The initial log-linear decline of the tissue *at*RA concentrations after WIN 18,446 administration concentration-time curves was fitted using Phoenix.

In vitro incubations

To determine *at*RA formation clearance (Cl_f) in tissue S10 protein from mice, the formation of *at*RA was measured in the liver and testis S10 fractions of three mice treated with vehicle control using previously described methods (Arnold et al., 2014). *at*-retinal at a nominal concentration of 100 nM was incubated with 5 μg S10 protein from each mouse in 100 μl of buffer consisting of 750 mM KCl, 50 mM Hepes, and 2 mM NAD^+ at pH 8.0. The incubations were performed in triplicate, initiated with substrate, and terminated after 10 minutes by transferring 75 μL of the incubation into an equal volume of chilled acetonitrile with 100 nM *at*RA-d_5 (internal standard) and analyzed by LC-MS/MS as described above. The measured concentration of *at*RA in each incubation was used to calculate the pmol of *at*RA formed per S10 protein (5 μg) in unit time (10 min) to determine the velocity of *at*RA formation. To determine the *at*RA Cl_f in tissue S10 protein for each mouse, the average *at*RA formation velocity from the three incubations was divided by the experimentally determined unbound substrate concentration in the activity assay. The average *at*RA Cl_f was calculated by combining the three *at*RA Cl_f values determined with the three mice. To further characterize the *at*RA formation in different subcellular fractions, mouse liver microsomes (5 μg) and cytosol (5 μg) were incubated with 1000 nM *at*-retinal in 100 μl of buffer consisting of 750 mM KCl, 50 mM Hepes, and 2 mM NAD^+ at a pH of 8.0. The incubations were performed in triplicate and terminated after 10

minutes by transferring 75 µL of the incubation into an equal volume of chilled acetonitrile with 100 nM *at*RA-d_5 and analyzed as described above.

The inhibition of *at*RA formation by WIN 18,446 was measured in vitro in pooled S10 fractions from testes and livers of vehicle treated mice in incubations conducted as described above. The inhibition assays used 100 nM of *at*-retinal as a substrate with eight increasing concentrations (0.001-5 µM) of WIN 18,446 in the testis and 12 increasing concentrations (0.001-20 µM) of WIN 18,446 in the liver. All activity assays for *at*RA formation from *at*-retinal with S10 fractions included 0.05 mg S10 protein (liver or testis) and 2 mM NAD^+, were initiated with substrate (10 µl of 1 µM *at*-retinal) and were terminated after 10 minutes by transferring 75 µL of the incubation into an equal volume of chilled acetonitrile with 100 nM *at*RA-d_5. The IC_{50} values of WIN 18,446 were determined by plotting the amount of activity remaining (%) against the corresponding log transformed WIN 18,446 concentrations and equation (1) was fitted to the data

$$\%\ \text{of control activity} = \text{Nonspecific Activity} + \frac{\text{Total Activity} - \text{Nonspecific Activity}}{1+10^{([I]-\log(IC_{50}))}} \quad (1)$$

in which the total activity is the % activity in the absence of inhibitor, the nonspecific activity is the % activity remaining when maximum inhibition has been achieved (activity contributed by non-inhibited enzymes), [I] is the concentration of WIN 18,446, and the IC_{50} is the concentration of inhibitor that causes 50% of the total measured inhibition.

To test whether WIN 18,446 is a time dependent inhibitor (TDI) of *at*RA formation in the liver and testis, 0.5 mg of S10 protein was incubated with and without 1 µM WIN 18,446 in the presence of 2 mM NAD^+ in a final volume of 25 µL of buffer (750 mM KCl and 50 mM Hepes at a pH of 8.0). At time points of 0.25, 15, and 30 minutes, 2 µL aliquots were diluted 50-fold into 100 µL of buffer (750 mM KCl and 50 mM Hepes at a pH of 8.0) containing NAD^+ (2 mM)

and a saturating concentration of *at*-retinal (1000 nM). *at*RA formation as measured as described in section 2.4. All incubations were performed in triplicate with a boiled enzyme control for the WIN 18,446 and *at*-retinal incubations.

The TDI kinetics of WIN 18,446 towards *at*RA formation was characterized in mouse testis S10 fractions. For testis S10 fractions with WIN 18,446, the S10 fractions were preincubated with WIN 18,446 for 0.25, 1, 2, and 3 minutes with seven concentrations of WIN 18,446 (0-3,000 nM) and diluted as described above for measuring *at*RA formation. The k_{inact} and K_I were determined by fitting equation (2) to the data in Graphpad Prism

$$\lambda = \frac{k_{inact}*[I]}{K_I+[I]} \quad (2)$$

where λ is the observed apparent first order inactivation rate (min^{-1}), k_{inact} is the maximum inactivation rate, and K_I is the concentration of inhibitor when the inactivation rate is half of the k_{inact} (Silverman, 1995).

To determine the contribution of AOX to *at*RA formation in mouse liver, the AOX inhibitor hydralazine was used. Based on the previously reported k_{inact} and K_I values of 3.8 ± 0.4 hr^{-1} and 83 ± 27 μM (Strelevitz et al., 2012), liver S10 protein (5 μg) was incubated with 1 mM hydralazine or vehicle control (water) in 90 μl of buffer consisting of 750 mM KCl, 50 mM Hepes, and 2 mM NAD^+ at a pH of 8.0 for 45 minutes to inactivate more than 95% of the AOX activity. After 45 minutes, vehicle control (ethanol), 1000 nM *at*-retinal or 1000 nM *at*-retinal together with 5000 nM WIN 18,446 was added into each of the incubations and the reactions were allowed to proceed for 10 minutes. The formation of *at*RA was measured by LC-MS/MS as described above and the formation of *at*RA was compared to vehicle control and percent inhibition determined.

Determination of unbound fractions

The protein binding of *at*-retinal in the activity assay was determined by ultracentrifugation as described before (Arnold et al., 2014; Thatcher et al., 2010). Liver and testis S10 protein were pooled from three individual vehicle treated mice and diluted to 0.05 mg/mL with 750 mM Potassium Chloride and 50 mM Hepes. *at*-retinal was added at a final concentration of 100 nM to 0.05 mg/mL pooled S10 protein. The samples were aliquoted into eight ultracentrifuge tubes (Beckman 343775) and four samples were centrifuged at 435,000 g at 37°C for 90 minutes using a Sorvall Discovery M150 SE ultracentrifuge with a Thermo Scientific S100-AT3 rotor (Waltham, MA) and 4 samples were incubated at 37°C for 90 minutes in a water bath to measure total concentrations. The incubated samples and supernatants from centrifuged samples were added to 100 µL ice cold acetonitrile containing 100 nM *at*-retinal-d_5. The samples were centrifuged at 3,000 g for 20 minutes at 4°C, transferred to a 96 well plate, and analyzed using LC-MS/MS as described. Before *at*-retinal was added into the liver S10 protein, hydralazine was added to a final concentration of 1 mM in the pooled liver S10 protein (0.5 mg/mL) and the samples were incubated at 37°C for 45 minutes to inactivate over 95% of AOX activity and minimize enzymatic depletion of *at*-retinal in the experiment.

The protein binding of WIN 18,446 in mouse serum was also determined by ultracentrifugation. WIN 18,446 was added to pooled mouse serum to a final concentration of 500 nM. Samples were aliquoted to eight ultracentrifuge tubes and four tubes were centrifuged at 435,000 g as described for *at*-retinal above and four tubes were incubated at 37°C to measure WIN 18,446 concentrations. After 90 minutes, the incubated samples or supernatants were added to 100 µl ice cold acetonitrile containing 500 nM N, N'-hexane-1,6-diylbis 2,2-dichloroacetamide (internal standard), centrifuged at 3,000 g for 20 minutes at 4°C, transferred to

a 96 well plate, and analyzed by LC-MS/MS. The fraction unbound was calculated as the ratio of *at*-retinal or WIN 18,446 with or without ultracentrifugation.

Predicting ALDH1A activity and relative contribution to atRA formation clearance

*at*RA Cl_f in liver and testis S10 fractions was predicted at a nominal *at*-retinal concentration of 100 nM using the ALDH1A expression levels quantified in three vehicle treated mice and previously determined kinetics of *at*RA formation by recombinant ALDH1A enzymes using equation (3)

$$Cl_f = \frac{v}{f_u[S]} = \frac{[ALDH1A1]*k_{cat}}{K_m+f_u[S]} + \frac{[ALDH1A2]*k_{cat}}{K_m+f_u[S]} \quad (3)$$

in which v is the predicted *at*RA formation velocity (pmol/min/mg S10 protein), [ALDH1A1] and [ALDH1A2] are the average measured expression levels of ALDH1A1 and ALDH1A2 enzyme in the liver and testis from each mouse (pmol/mg S10 protein), k_{cat} is the maximum product formation velocity measured for ALDH1A1 and ALDH1A2 (1.1 and 3.7 pmol/min/pmol enzymes), f_u is the experimentally determined fraction unbound in the S10 fractions (9 ± 2%), [S] is the total substrate concentration, and K_m is the Michaelis-Menten constant of *at*RA formation with ALDH1A (285 nM for ALDH1A1 and 55 nM for ALDH1A2) (Arnold et al., 2014). In the liver, [ALDH1A2] expression level was set at 0 as no ALDH1A2 was detected in this tissue. The *at*RA Cl_f in liver and testis S10 fractions was predicted for each mouse and these values were used to calculate the average predicted *at*RA Cl_f in each tissue. The predicted *at*RA Cl_f in the testis and liver S10 protein was compared to the measured formation clearances and the predicted contribution of each ALDH1A isoform to testicular *at*RA formation was predicted by dividing the predicted *at*RA Cl_f by each ALDH1A by the total predicted *at*RA Cl_f.

Predicting the effect of WIN 18,446 administration to atRA formation in mouse testes and liver

The effect of a single dose and multiple doses of WIN 18,446 on ALDH1A activity and

*at*RA formation in the testis and liver were predicted using the in vivo concentrations of WIN 18,446 and WIN 18,446 inhibition kinetics determined in vitro. The pharmacokinetic parameters for WIN 18,446 were determined using standard non-compartmental analysis with Phoenix (St. Louis, MO). The terminal $t_{1/2}$ was calculated from the linear terminal slope of the plasma concentration time curve. The area under the plasma concentration versus time curve from time 0 to infinity ($AUC_{0-\infty}$) for a single dose and 0 to 24 hrs (AUC_{0-24}) for multiple doses were calculated with Phoenix using linear trapezoidal method. The average inhibitor concentrations over the 24 hour dosing interval were determined by dividing the AUC_{0-24} by the dosing interval (24 hrs). Since the experimentally determined f_u for WIN 18,446 in mouse serum was > 0.99, total and unbound concentrations were assumed equal.

To simulate the concentrations of WIN 18,446 after a single dose, equation (4) analogous to a 2-compartment disposition with 1st order absorption was fitted to the measured plasma concentrations of WIN 18,446 using Graphpad Prism (La Jolla, CA).

$$[I](t) = A^{-\alpha t} + B^{-\beta t} + C^{-\gamma t} \quad (4)$$

To predict ALDH1A activity remaining after a single dose (pre steady state) of WIN 18,446, the time course of reversible inhibition of ALDH1A1 and inactivation of ALDH1A2 was simulated by Microsoft Excel (Redmond, WA). WIN 18,446 concentrations after a single dose were simulated using equation (5) at 0.5 hr intervals over a 24 hour time course post dose. The predicted percentage of ALDH1A1 activity remaining following WIN 18,446 administration as a function of time was predicted using equation (5)

$$\text{ALDH1A1 Activity Remaining (\%)} = 100 * \left(\frac{1}{1+\frac{[I](t)}{K_i}}\right) \quad (5)$$

in which [I](t) is the simulated concentration of WIN 18,446 at each time point and K_i is the previously reported reversible inhibition constant (102 nM) for WIN 18,446 with ALDH1A1

(Arnold et al., 2014; Rowland, 1973). The time dependent loss of active ALDH1A2 enzyme was calculated based on a differential equation previously described for CYP3A inactivation by diltiazem (Zhang et al., 2009). The loss of ALDH1A2 activity was calculated at 0.5 hr intervals with equation (6)

$$\frac{d[ALDH1A2]_{active}}{dt} = k_{syn} - ([ALDH1A2]_{active} * k_{deg}) - k_{inact} * \frac{[I]*[ALDH1A2]_{active}}{[I]+K_I} \quad (6)$$

where the k_{inact} and K_I are TDI inhibition kinetic parameters of ALDH1A2 inactivation by WIN 18,446 determined in mouse testis S10 protein, the k_{syn} is the zero order synthesis rate of ALDH1A2 protein, and the k_{deg} is the first order ALDH1A2 degradation rate constant. The ALDH1A2 activity remaining (%) at each time point was calculated by dividing the $[ALDH1A2]_{active}$ by the initial average ALDH1A2 concentration determined in the testis S10 protein of vehicle control treated mice (17.0 pmol/mg S10 protein) and multiplying the quotient by 100. Using the average ALDH1A2 concentration determined in the testis S10 protein of untreated mice (17.0 pmol/mg S10 protein) and the k_{deg} value of 0.0315 hr^{-1} previously reported for ALDH2 (Xiao et al., 1996), the synthesis rate (k_{syn}) of ALDH1A2 was determined to be 0.535 pmol/mg S10 protein/hr. The rate of change of ALDH1A2 was simulated at 0.5 hr intervals over the 24 hour dosing interval and used to calculate the amount of active ALDH1A2 as a function of time. The percent ALDH1A2 activity remaining was calculated as the quotient of the predicted ALDH1A2 concentration and baseline ALDH1A2 concentration (17.0 pmol/mg S10 protein). The effect of ALDH1A2 k_{deg} on the simulated activity was tested by sensitivity analysis using 10 values of k_{deg} spread equally between the physiologically plausible k_{deg} range of 0.0128 and 0.0693 hr^{-1}.

To characterize the inhibition of ALDH1A by WIN 18,446 after chronic dosing, static prediction models were used for both the reversible inhibition of ALDH1A1 and inactivation of ALDH1A2. The reversible inhibition of ALDH1A1 was predicted using equation (7)

$$\text{ALDH1A1 Activity Remaining (\%)} = 100 * \left(\frac{1}{1 + \frac{[I]_{avg}}{K_i}} \right) \quad (7)$$

where $[I]_{avg}$ is the average concentration of WIN 18,446 over a 24 hour period after the 8th dose of WIN 18,446. The irreversible inhibition of ALDH1A2 was predicted using equation (8) (Grimm et al., 2009)

$$\text{ALDH1A2 Activity Remaining (\%)} = 100 * \left(\frac{k_{deg}}{k_{deg} + \frac{k_{inact} * [I]_{avg}}{K_I + [I]_{avg}}} \right) \quad (8)$$

The net change in the intrinsic formation clearance of *at*RA in the testis (Cl_T) was predicted as a function of time following a single dose of WIN 18,446 using the formation clearances of *at*RA by ALDH1A1 and ALDH1A2 according to equation (9).

$$Cl_{T\ single} = \left(\left(\frac{[\text{Testis ALDH1A1}] * k_{cat}}{K_m} \right) * \left(\frac{1}{1 + \frac{[I](t)}{K_i}} \right) \right) + \left(\frac{[ALDH1A2]_{active} * k_{cat}}{K_m} \right) \quad (9)$$

where [Testis ALDH1A1] is the average ALDH1A1 protein expression determined from testis S10 protein generated from eight vehicle control treated mice, [I](t) and $[ALDH1A2]_{active}$ are the concentrations of inhibitor and active ALDH1A2 remaining at each time point as predicted above.

Since the inhibition studies suggested approximately 50% of *at*RA formation in the liver was by AOX, which is not inhibited by WIN 18,446, the effect of a single dose of WIN 18,446 on *at*RA formation clearance in the liver (Cl_L) was predicted after incorporating the formation of *at*RA by AOX (Cl_{AOX}) according to equation (10)

$$Cl_{L\ single} = \left(\left(\frac{[\text{Liver ALDH1A1}] * k_{cat}}{K_m} \right) * \left(\frac{1}{1 + \frac{[I](t)}{K_i}} \right) \right) + Cl_{AOX} \quad (10)$$

where [Liver ALDH1A1] is the average ALDH1A1 protein expression determined from liver S10 protein generated from eight vehicle control treated mice and Cl_{AOX} was assigned a value of 0.64 mL/min/mg S10 protein. The *at*RA Cl_f after eight daily doses of WIN 18,446 was predicted using static models of enzyme inhibition as shown in equation (11) for the testis and equation (12) for the liver.

$$Cl_{T\ multiple} = \left(\left(\frac{[\text{Testis ALDH1A1}] * k_{cat}}{K_m} \right) * \left(\frac{1}{1 + \frac{[I]_{avg}}{K_i}} \right) \right) + \left(\left(\frac{[\text{Testis ALDH1A2}] * k_{cat}}{K_m} \right) \left(\frac{k_{deg}}{k_{deg} + \frac{k_{inact} * [I]_{avg}}{K_I + [I]_{avg}}} \right) \right)$$

(11)

$$Cl_{L\ multiple} = \left(\left(\frac{[\text{Liver ALDH1A1}] * k_{cat}}{K_m} \right) * \left(\frac{1}{1 + \frac{[I]_{avg}}{K_i}} \right) \right) + Cl_{AOX} \quad (12)$$

The overall effect of WIN 18,446 inhibition on tissue *at*RA concentrations was predicted assuming *at*-retinal concentrations and *at*RA elimination clearance (Cl_{atRA}) were unaltered after WIN 18,446 administration and that *at*RA is solely formed in the target tissue using equation (15)

$$\frac{\text{Tissue } [atRA]_{avg\ inh}}{\text{Tissue } [atRA]_{avg}} = \frac{\frac{[at-\text{retinal}] * Cl_{f\ inh}}{Cl_{atRA}}}{\frac{[\text{at}-\text{retinal}] * Cl_f}{Cl_{atRA}}} \quad (15)$$

where $[atRA]_{avg}$ is the average concentration of *at*RA in vehicle treated mice, $[atRA]_{avg\ inh}$ is the tissue *at*RA concentration of mice treated for eight days, [*at*-retinal] is the tissue concentration of *at*-retinal, $Cl_{f\ inh}$ is the predicted *at*RA formation clearance in each tissue of mice treated with

WIN 18,446, Cl_f is the predicted *at*RA formation clearance in each tissue of vehicle treated mice, and Cl_{atRA} is the elimination clearance of *at*RA.

Quantification of atRA and WIN 18,446 in mouse tissues

To measure tissue concentrations of *at*RA, *at*RA was extracted from mouse livers (109-195 mg), testes (64-119 mg), and serum (50-150 μL) and analyzed using a previously described method with a few modifications (Arnold et al., 2014). Briefly, serum samples were transferred to 15 mL glass culture tubes followed by the addition of a 2:1 volume of acetonitrile with 1% formic acid. Liver and testis samples were homogenized with a 2 mL Potter-Elvehjem glass homogenizer (Kimbel Glass, Vineland, NJ) in a 1:1 volume of 0.9% NaCl and homogenates were transferred to a 15 mL glass culture tube followed by the addition of a 2:1 volume of acetonitrile with 1% formic acid. Next, 10 μL of 1 μM *at*RA-d_5 (internal standard) was spiked into each sample and *at*RA extracted with 10 mL of hexanes. The organic layer was transferred to a glass tube and dried under nitrogen at 37°C. The sample was reconstituted in 60:40 ACN/H_2O. Standard curves and quality control samples were generated using homogenized dog testicular tissue (a kind gift from Dr. Mary Zoulas of the Seattle Animal Shelter), rat livers, and rat serum depleted of endogenous *at*RA. Standard curves were prepared in homogenates that contained tissue at the average mass for the set of samples being quantified. Either 1 μL (serum), 2 μL (testis), or 4 μL (liver) of the stock solution was spiked into homogenate for each standard to make final concentrations in the standard curve of 0.5-15 pmol/g (serum), 1-30 pmol/g (testis), 2-60 pmol/gram (liver). The amount of *at*RA used in each standard curve spanned the range of observed *at*RA concentrations ensuring concentrations were within the linear detection range for each tissue.

To determine the concentrations of WIN 18,446 in mouse serum, WIN 18,446 was extracted from mouse serum samples together with *at*RA. Before extraction, 10 μL of an analog of WIN 18,446 (N, N'-hexane-1,6-diylbis 2,2-dichloroacetamide) was added into each serum sample at a concentration of 5 μM to serve as an internal standard. A standard curve for WIN 18,446 was prepared simultaneously in rat serum at concentrations of 0.001-10 μM.

Statistical Analysis

All data is reported as mean ± standard deviation. The average *at*RA concentration in each tissue following either single dose WIN 18,446 or multiple doses of WIN 18,446 was determined by combining all the *at*RA concentrations measured following a given dose of WIN 18,446 and these concentrations were compared to the tissue *at*RA concentrations measured in the vehicle treated mice using a student's t-test. To determine time dependent changes in tissue *at*RA concentrations ANOVA analysis was used with a student's t-test as a post hoc test. Changes in ALDH1A expression or *at*RA formation in vitro were tested with a student's t-test. For all statistical analysis, a p-value ≤ 0.05 was considered significant.

4.3 Results

Formation of atRA by ALDH1A in the mouse liver and testis

ALDH1A1 expression in the liver and testes was measured by LC-MS/MS and representative chromatograms are shown in Figure 4.1. ALDH1A1 was the predominant ALDH1A enzyme expressed in the mouse liver (average expression level 170 ± 50 pmol/mg S10 protein) and testes (average expression level 150 ± 30 pmol/mg S10 protein) (Figure 4.1). ALDH1A2 protein expression was not detected in the liver and it was only quantified in the testis (17.0 ± 4.8 pmol/mg S10 protein). Based on the lower limit of detection for the ALDH1A2 quantitation peptide (100 fmol injected) and the amount of S10 protein digested (80 μg), if ALDH1A2 is expressed in the liver, its concentration is less than 1.3 pmol/mg S10 protein.

ALDH1A3 was not detected in any of the testis or liver S10 samples. The lower limit of detection for the ALDH1A3 quantitation peptide was identical to that of ALDH1A2, so if ALDH1A3 is expressed in the liver or testis, its concentrations is also lower than 1.3 pmol/mg S10 protein.

Testicular and liver ALDH1A protein expression levels together with the *at*RA formation kinetics reported with recombinant ALDH1A enzymes were used to predict the *at*RA formation clearance (Cl_f) in three mouse livers and three testes of vehicle treated mice at a nominal *at*-retinal concentration of 100 nM (Table 4.2). The predicted *at*RA Cl_f in the liver (0.48 mL/min/mg S10 protein) was less than half of that in the testis (1.15 mL/min/mg S10 protein). However, when the *at*RA Cl_f was measured in both tissues, it was similar in the testis (1.9 ± 0.2 mL/min/mg S10 protein) and the liver (2.0 ± 0.3 mL/min/mg S10 protein) (Table 4.2). The observed *at*RA Cl_f in the testis was within 30% of the predicted *at*RA Cl_f. However, the *at*RA Cl_f in the liver was underpredicted by 70% suggesting a liver specific prediction error and potential contribution of other enzymes to *at*RA formation in the liver.

Inhibition of atRA formation by WIN 18,446 and hydralazine in mouse liver and testis in vitro

Based on the discrepancy in the prediction of liver *at*RA formation when compared to the testis, it was hypothesized that in the testis ALDH1A enzymes account for all *at*RA formation while in the liver other enzymes, such as AOX may contribute to *at*RA formation. To test this hypothesis WIN 18,446, which reversibly inhibits ALDH1A1 and ALDH1A3 and inactivates ALDH1A2 (Arnold et al., 2014), was used as a specific ALDH1A inhibitor in the liver and testis. In the testis S10 fractions, *at*RA formation was inhibited > 95% by WIN 18,446 with an IC_{50} value of 59 ± 1 nM (Figure 4.2A). The IC_{50} value for inhibition of *at*RA formation in liver S10 fractions by WIN 18,446 was 92 ± 2 nM (Figure 4.2B), but WIN 18,446 only inhibited a

maximum of 44 ± 2% of *at*RA formation in the liver S10 fractions suggesting ALDH1A is responsible for only half of the liver *at*RA formation. Since S10 fractions contain both microsomes and cytosol, it is possible that the remaining 56% of formation was due to microsomal *at*RA formation instead of cytosol. When mouse liver cytosol and microsomes were used separately to measure NAD^+ dependent *at*RA formation, no *at*RA was formed by the microsomal protein (Figure 4.2C), while significant *at*RA formation was observed in cytosol (Figure 4.2C). As it has been previously shown that AOX can form *at*RA from retinal (Huang et al., 1999), an irreversible inhibitor of AOX, hydralazine, was used to test whether AOX was responsible for forming *at*RA in the liver along with ALDH1A1. Hydralazine (1 mM) inhibited 45 ± 2 % of the *at*RA formation in the liver S10 fractions (Figure 4.2D). When hydralazine was used together with WIN 18,446, 95 ± 1% of *at*RA formation was inhibited (Figure 4.2D). Taken together, these data suggest that AOX is responsible for approximately 50% of the *at*RA formation in mouse liver S10 protein.

WIN 18,446 is a selective TDI of ALDH1A2 and therefore the time-dependent inhibition of *at*RA formation was used to determine the importance of ALDH1A2 to *at*RA formation in the mouse testes in comparison to the liver. WIN 18,446 was a TDI of *at*RA formation in the testis, but not in the liver (Figure 4.2E). Due to the TDI in the testis, the TDI kinetics of WIN 18,446 towards *at*RA formation in the testis was determined (Figure 4.2F). In mouse testes S10 fractions, WIN 18,446 had a K_I of 420 ± 190 nM and k_{inact} of 23.2 ± 3.5 hr^{-1} (Figure 4.2F).

Predicted effect of WIN 18,446 on in vivo ALDH1A activity and atRA formation

To evaluate the in vivo effect of ALDH1A inhibition on tissue *at*RA concentrations, WIN 18,446 was used as an in vivo inhibitor of ALDH1A enzymes. First the pharmacokinetics of WIN 18,446 were characterized using noncompartmental analysis. Following a single dose of

WIN 18,446, the $AUC_{0-\infty}$ was 2.5 hr*μmol /L and the $t_{1/2\beta}$ was 3.3 hrs. The maximum WIN 18,446 concentration (C_{max} of 1.3 μM) was reached rapidly by 30 minutes (Figure 4.3). The average concentration of WIN 18,446 over a 24 hour interval after a single dose was 0.1 μM. Following eight daily doses of WIN 18,446, the C_{max} was increased 7-fold to 8.5 μM and the AUC_{0-24} was 87.6 hr*μmol/L which was 35-fold greater than that predicted from the single dose data (Figure 4.3). The average concentration of WIN 18,446 on day 8 of dosing was 3.5 μM over the 24 hour dosing interval. When WIN 18,446 plasma concentration time curve after single dose was fitted to a two compartment model with first order absorption for simulation, the final parameters were A of -6.6 μM, B of 6.2 μM, C of 0.4 μM, α of $1.3*10^6$ hr^{-1}, β of 3.7 hr^{-1}, and γ of 0.2 hr^{-1}. The f_u of WIN 18,446 in plasma was > 99%.

The inhibition of ALDH1A1 and ALDH1A2 activity after administration of WIN 18,446 was predicted based on simulated WIN 18,446 plasma concentrations and in vitro ALDH1A inhibition kinetics. First, dynamic models of ALDH1A1 and ALDH1A2 inhibition by WIN 18,446 were used to predict the amount of ALDH1A activity remaining as a function of time following single oral dose of WIN 18,446. Figure 4.3 shows the time course of predicted reversible inhibition of ALDH1A1 following a single dose of WIN 18,446. A maximum of 98% inhibition of ALDH1A1 was predicted by 0.5 hours after WIN 18,446 dosing, and the activity was predicted to return to 97% of control by 24 hours. Due to the potent inactivation of ALDH1A2 by WIN 18,446, by 1 hour post dose less than 1% of the ALDH1A2 activity was predicted to remain and ALDH1A2 activity was not predicted to return to more than 8% of control by 24 hours (Figure 4.3). The sensitivity analysis of the range of k_{deg} values for ALDH1A2 all resulted in less than 10% active ALDH1A2 remaining 24 hours after WIN 18,446 dosing. After 8 daily doses of WIN 18,446, the activity of ALDH1A1 and ALDH1A2 were

predicted using static models. The activity of ALDH1A1 was predicted to be decreased to 3% of control after 8 daily doses of WIN 18,446 and ALDH1A2 activity was predicted to be decreased to < 1% of control on day 8 of dosing.

Since *at*RA formation depends on the activity of multiple enzymes in a tissue specific manner the net Cl_f of *at*RA was predicted in the liver after a single dose (Figure 4.4A) and after 8 daily doses (Figure 4.4B) of WIN 18,446. Due to the predicted 50% contribution of AOX to *at*RA formation in the liver and the lack of inhibition of AOX by WIN 18,446, the total CL_f in the liver was not predicted to decrease more than 50% after single or multiple doses of WIN 18,446 (Figure 4.4). The total *at*RA Cl_f in the liver was predicted to decrease approximately 50% by 0.5 hours and return to approximately 100% by 24 hours following a single dose of WIN 18,446 (Figure 4.4). For chronic dosing of WIN 18,446, the *at*RA Cl_f in the liver was predicted to decrease to approximately 50% of the control (Figure 4.4B). In the testes, the total *at*RA CL_f is a sum of the ALDH1A2 and ALDH1A1 contribution. ALDH1A2 was predicted to contribute to the majority of *at*RA formation (61%) in testicular S10 protein at a nominal *at*-retinal concentration of 100 nM. Hence the effect of WIN 18,446 on *at*RA Cl_f is a combination of the TDI of ALDH1A2 and reversible inhibition of ALDH1A1. Using the simulations, the net *at*RA Cl_f was predicted to remain decreased compared to control for the entire dosing interval following a single dose (Figure 4.4C). Following chronic dosing, the net Cl_f was predicted to be decreased more than 95% at the time of the 8^{th} dose and over the following 24 hours (Figure 4.4D). To determine if ALDH1A protein expression was altered by WIN 18,446 administration, ALDH1A1 and ALDH1A2 protein expression was quantified from the testes and livers of vehicle control and WIN 18,446 treated mice. After 8 days of treatment, the expression of ALDH1A1 or ALDH1A2 was not significantly changed in the liver or testis (Figure 4.4E).

However, likely due to the time dependent inhibition of ALDH1A2, *at*RA formation velocity was significantly decreased in the WIN 18,446 treated mice compared to control (Figure 4.4F). In the testes samples collected 24 hours after the single dose of WIN 18,446, *at*RA formation was decreased by 55 ± 2% ($p < 0.001$) while at the time of the 8th dose, *at*RA formation in the testes was decreased by 79 ± 5% ($p = 0.0001$) (Figure 4.4F).

In vivo tissue atRA concentrations measured after administration of WIN 18,446

To test whether the predicted tissue specific decrease in *at*RA CL_f in the testis and liver results in decreased *at*RA concentrations in the liver, testis or serum, *at*RA concentrations were measured as a function of time after WIN 18,446 administration. In the vehicle control mice of the single dose study, the average concentrations of *at*RA in the testis (7.3 ± 0.9 pmol/gram) and liver (10.8 ± 1.5 pmol/gram) were significantly greater (p-value < 0.05) than serum *at*RA (2.0 ± 0.7 pmol/gram). *at*RA concentrations were decreased in a tissue specific manner after a single dose of WIN 18,446 (Figure 4.5). The average *at*RA concentration over 24 hours was decreased to 8.0 ± 0.6 pmol/g ($p = 0.2$) in the liver (74% of control), to 2.4 ± 0.2 pmol/g ($p < 0.001$) in the testis (33% of control) and to 0.9 ± 0.1 pmol/g ($p < 0.01$) in serum (44% of control). Liver and testis *at*RA concentrations were significantly reduced ($p < 0.01$) already at 0.5 hours after the first dose of WIN 18,446, but serum *at*RA concentrations were not significantly decreased until 2 hours after WIN 18,446 dosing ($p < 0.05$). By 4 hours after dosing, liver *at*RA concentrations were decreased to 58% of control and returned to baseline concentrations after 12 hours (Figure 4.5A). In the testis, *at*RA concentration decreased to < 10% of control by 4 hours after single dose of WIN 18,446, and the concentration only returned to 23% of control at 24 hours after dosing (Figure 4.5B). Serum *at*RA decreased to < 20% of control by 4 hours and returned to baseline at 24 hours (Figure 4.5C). Since inhibition of ALDH1A by WIN 18,446 is nearly

instantaneous, the obtained tissue and serum *at*RA concentration versus time curves were used to determine the tissue half-life of *at*RA. The *at*RA tissue $t_{1/2}$ determined after single dose of WIN 18,446 was 1.3 ± 0.1 hrs in the testis and 0.5 ± 0.1 in the serum. In the liver, the $t_{1/2}$ of *at*RA was <30 min based on this analysis and hence could not be accurately determined.

When WIN 18,446 was dosed once a day for 8 days, the average liver *at*RA concentration of the treated mice (5.4 ± 1.9 pmol/g) was 32% lower ($p < 0.05$) than in the vehicle treated controls (8.0 ± 2.4 pmol/g) (Figure 4.5D). The average testicular concentration of *at*RA (1.5 ± 0.3 pmol/g) over the 24 hours dosing interval was significantly lower ($p < 0.01$) than the concentration in vehicle treated mice (5.5 ± 1.0 pmol/g). When compared to the vehicle treated controls, the testicular *at*RA concentrations were already decreased to 60% of control mice ($p=0.05$) at time 0 hr before the 8th dose of WIN 18,446 and remained decreased to 33% of control on average ($p < 0.001$) for the dosing interval (Figure 4.5E). The average serum concentration of *at*RA in mice treated for 8 days was 1.3 ± 0.7 pmol/g and was significantly lower ($p < 0.001$) than the vehicle treated mice (3.5 ± 0.9 pmol/g). Chronic dosing of WIN 18,446 decreased the average tissue to serum *at*RA ratio from 2 to 1 in the testis and increased it from 2 to 4 in the liver.

The predicted decrease in *at*RA Cl_f after chronic WIN 18,446 dosing was compared to the observed reduction in tissue *at*RA concentrations. In the liver, the *at*RA Cl_f was predicted to be decreased 48% and this was in good agreement with the average 32 ± 3% reduction in the liver *at*RA concentration of the treated mice. After 8 daily doses of WIN 18,446, the *at*RA Cl_f in the testis was predicted to be less than 1% of control. In vivo, the mice treated with WIN 18,446 for 8 days had testicular *at*RA concentrations that were decreased to 33 ± 5% of the vehicle treated controls.

4.4 Discussion

For the last decades, ALDH1A enzymes have been believed to be responsible for *at*RA formation, and it has been assumed that alterations in ALDH1A activity via enzyme inhibition, induction, or genetic changes is reflected in *at*RA concentrations in various tissues. Yet, a correlation between ALDH1A activity and *at*RA concentrations has never been shown, and the quantitative relationship between specific ALDH1A inhibition and tissue *at*RA concentrations has not been established. The work presented here demonstrates for the first time that *at*RA concentrations in retinoid target tissues can be decreased by pharmacological inhibition of *at*RA formation. In addition, the complement of enzymes responsible for *at*RA formation differs in each tissue, so inhibition of specific ALDH1A enzymes will cause a distinct reduction in *at*RA concentrations in individual tissues.

The results shown here demonstrate that ALDH1A1 and ALDH1A2 isoforms are responsible for more than 95% of the *at*RA formation in mouse testis which is in good agreement with our previous studies using human testicular tissue (Arnold et al., 2014). In both mouse and human testis, *at*RA formation is inhibited more than 95% by the ALDH1A inhibitor WIN 18,446 demonstrating the major role of ALDH1A in *at*RA formation in the testis. In addition, ALDH1A protein expression and in vitro *at*RA formation kinetics by recombinant ALDH1A accurately predicted *at*RA formation in the mouse and human testis. In agreement with previous studies detecting expression of ALDH1A1 and ALDH1A2 protein in the mouse testis (Vernet et al., 2006; Wang et al., 1996; Zhao et al., 1996), ALDH1A1 and ALDH1A2 were quantified in the mouse testis, and similar to human testes, ALDH1A1 was the predominant isoform detected. However, expression of ALDH1A1 in the mouse testis was approximately two-fold higher than in the human testis and the expression of ALDH1A2 was 10-fold higher in mice than humans

resulting in a higher *at*RA synthesis rate in mouse testis when compared to that observed in human (Arnold et al., 2014). At physiologically relevant *at*-retinal concentrations (Kane and Napoli, 2010), ALDH1A2 is predicted to contribute to the majority (61%) of *at*RA formation in mouse testicular S10 protein. This contribution was confirmed by the greater than 50% reduction in *at*RA formation when the testicular S10 protein was incubated with WIN 18,446 to inactivate ALDH1A2. Although ALDH1A2 is predicted to contribute to *at*RA formation in human and mouse testicular S10 protein at physiological relevant *at*-retinal concentrations (Arnold et al., 2014), the predicted 61% contribution of ALDH1A2 in the mouse testes is considerably greater than the approximate 15% contribution in the human testes. While ALDH1A enzymes are responsible for the overwhelming majority of testicular *at*RA biosynthesis in both species, the distinct difference in the roles of the individual ALDH1A isoforms suggests species-specific differences in how *at*RA synthesis is orchestrated within the testes.

WIN 18,446 was predicted to efficiently reduce testicular *at*RA formation in vivo primarily by inactivation of testicular ALDH1A2 activity but also due to the inhibition of ALDH1A1. Previously, when WIN 18,446 was administered to mice for 4 weeks (2mg/g of diet), increased liver and serum retinol concentrations were observed, and the intratesticular amount of *at*RA was reduced, suggesting WIN 18,446 inhibits ALDH1A in vivo (Paik et al., 2014a). Similarly in rabbits, WIN 18,446 treatment decreased intratesticular *at*RA concentrations (Amory et al., 2011a). However, WIN 18,446 exposure was not determined in these animals and the reduction in testicular *at*RA after a month of treatment was measured at a single time point preventing mechanistic analysis of the in vivo inhibition of ALDH1A enzymes. In this study, after a single oral dose of WIN 18,446, the C_{max} of 1.3 μM was reached by 0.5 hours and was over 10-fold greater than the K_i for inhibition of ALDH1A1 by WIN 18,446. However, due to

the rapid decline in WIN 18,446 concentrations, ALDH1A1 inhibition was removed by 24 hours. Based on the 3.5 hour $t_{1/2\beta}$ of WIN 18,446 after a single dose, accumulation of WIN 18,446 was not expected after chronic dosing every 24 hours. However, after 8 daily doses of WIN 18,446, accumulation of WIN 18,446 was observed and concentrations of the inhibitor were at least four-fold greater than the K_i for WIN 18,446 towards ALDH1A1 over the entire 24 hour dosing interval. The reason for the non-linearity is unclear, but WIN 18,446 inhibiting its own clearance and/or changes in oral bioavailability are likely causes for this effect. Based on the rapid elimination of WIN 18,446 from circulation after a single dose and the time dependent inhibition of ALDH1A2 by WIN 18,446, a dynamic time dependent model of ALDH1A inhibition was used to predict ALDH1A activity after a single dose of WIN 18,446. As a result, in the testis, although the reversible inhibition of ALDH1A1 was predicted to wane along with the rapid elimination of WIN 18,446 from circulation after a single dose, the potent inactivation of testicular ALDH1A2 by WIN 18,446 was predicted to prevent the testicular *at*RA Cl_f from returning to baseline. Since ALDH1A2 was predicted to play a predominant role in *at*RA formation in the testes, the inactivation of ALDH1A2 was predicted to result in a 92-99% decrease in *at*RA formation. As *at*RA $t_{1/2}$ was very short, approximately 1 hour or less in each tissue, the inhibition of ALDH1A mediated *at*RA formation by WIN 18,446 was predicted to result in rapid changes in testicular and liver *at*RA. In vivo, a testicular *at*RA concentration versus time profile similar to predicted *at*RA Cl_f versus time was observed demonstrating the good agreement between the predicted testicular *at*RA formation and the in vivo *at*RA concentrations. The importance of ALDH1A2 was further supported by the 55% reduction in the *at*RA formation capacity of the testicular S10 protein from the mice treated with a single dose of WIN 18,446 as this decrease in activity can only be attributed to inactivation of ALDH1A2. The

predominant role of ALDH1A2 in testicular *at*RA formation in mice may explain why spermatogenesis proceeds normally within the testes of *Aldh1a1*$^{-/-}$ mice (Molotkov and Duester, 2003).

Unlike the testis, ALDH1A1 was the only ALDH1A isoform detected in the mouse liver. Yet, in addition to ALDH1A1, *at*RA formation in the mouse liver was catalyzed by AOX. Previously, both mRNA and western blot studies have established that ALDH1A1 is the only ALDH1A isoform expressed in the mouse liver (Haselbeck et al., 1999; Kiefer et al., 2012; Nishimura and Naito, 2006). In addition, the requirement of NAD^+ for ALDH catalysis was used to demonstrate that at least 90% of *at*RA formation in mouse liver cytosol was by ALDH enzymes (Lee et al., 1991). Of the six ALDH enzymes purified from mouse liver cytosol, ALDH1A1 was identified to be responsible for more than 90% of the total *at*RA formation (Lee et al., 1991). However, when ALDH1A1 protein expression and in vitro *at*RA formation kinetics by ALDH1A1 were used to predict *at*RA formation in the mouse liver in this study, *at*RA formation was underpredicted suggesting that one or more additional enzymes contribute to *at*RA formation in the mouse liver. In support of an enzyme other than an ALDH1A, WIN 18,446 only inhibited approximately 50% of the *at*RA formation by liver S10 protein. Previous work has demonstrated that AOX forms *at*RA from *at*-retinal (Tomita et al., 1993) and contributes to approximately 50% of the *at*RA formation from *at*-retinal in the rabbit liver cytosol (Huang and Ichikawa, 1994). In agreement with this, the AOX inhibitor hydralazine inhibited approximately 50% of the mouse liver *at*RA formation suggesting a much greater importance of AOX in *at*RA formation in mice than previously suggested (Lee et al., 1991). For example, previously DBA/2 mice were used to determine the contribution of ALDH1A1 to liver *at*RA formation suggesting minimal AOX contribution (Lee et al., 1991). However, DBA/2 mice

have since been shown to lack AOX expression (Vila et al., 2004) explaining why significant AOX contribution to *at*RA formation was not observed in these mice. The expression of AOX may also explain the fertility and viability of the *Aldh1a1*$^{-/-}$ mice. The *Aldh1a1*$^{-/-}$ mouse model was generated with C57BL/6 mice (Molotkov and Duester, 2003) which have been shown to express AOX (Vila et al., 2004), suggesting that the formation of *at*RA by AOX along with ALDH1A2 and ALDH1A3 is enough to support the overall good health of *Aldh1a1*$^{-/-}$ mice. At this time, further studies are needed to determine the role of AOX in *at*RA biosynthesis in different species and tissues. The variation in AOX enzyme expression between species and between strains suggests that there is considerable variability in the role of specific enzymes in *at*RA formation and translation of pharmacological outcomes of specific enzyme inhibition need to be carefully quantitatively translated into humans.

The predicted decrease in liver *at*RA formation and ALDH1A activity after a single dose of WIN 18,446 was in good agreement with the observed decrease in liver *at*RA concentrations. Due to the approximate 50% contribution of ALDH1A to *at*RA formation in the liver, WIN 18,446 was not predicted to decrease the hepatic *at*RA Cl_f more than 50%. In addition, due to the reversible nature of ALDH1A1 inhibition by WIN 18,446, the inhibition of *at*RA formation was predicted to diminish as the inhibitor was cleared from circulation. In vivo, the hepatic *at*RA concentration decreased 42% after a single dose of WIN 18,446, but returned to 100% within 24 hours with a time course that was in good agreement with the simulated liver *at*RA Cl_f. The less than 50% decrease in liver *at*RA concentrations supports a substantial in vivo role for AOX in controlling *at*RA biosynthesis in the liver. The in vivo relevance of AOX in maintaining *at*RA concentrations in mice has also been previously described with an AOX Homolog 2 (AOH2) knockout mouse model (Terao et al., 2009). AOH2 expression is primarily localized to the

Harderian gland, but is detectable in the skin as well. In the Harderian glands and skin of *Aoh2*$^{-/-}$ mice, the *at*RA formation capacity was significantly reduced resulting in significantly decreased *at*RA concentrations in each tissue compared to wild-type mice.

In vivo, in C57BL/6-129 mice, ALDH1A enzymes are responsible for the majority of *at*RA formation in the testis but in the liver they only contribute to approximately 50% of *at*RA formation. The overall contribution of ALDH1A enzymes to tissue *at*RA was determined after eight daily doses of WIN 18,446 as *at*RA formation by ALDH1A was predicted to be inhibited more than 95% over the entire 24 hour dosing interval. The importance of intratesticular ALDH1A enzymes in forming *at*RA was previously demonstrated by generating Sertoli cell specific *Aldh1a*$^{-/-}$ mice (Raverdeau et al., 2012). The initiation of spermatogenesis is blocked within the testes of these mice suggesting circulating *at*RA does not significantly contribute to the testis *at*RA concentration although it is unclear how *Aldh1a* deletion in Sertoli cells alters testicular *at*RA concentrations. In this study, when ALDH1A activity was eliminated by chronic WIN 18,446 dosing, intratesticular *at*RA concentrations decreased 65% signifying the predominant role of ALDH1A enzymes in controlling intratesticular *at*RA concentrations. While the source of the remaining testicular *at*RA is not clear, multiple doses of WIN 18,446 decreased the testis to serum ratio of *at*RA to approximately 1 suggesting that the remainder of testicular *at*RA under ALDH1A inhibition might be coming from serum. In contrast to the testis, ALDH1A was not predicted to contribute to the majority of liver *at*RA formation. In good agreement with this prediction, the loss of ALDH1A activity did not reduce liver *at*RA concentrations more than 50%. While *at*RA concentrations were significantly reduced in liver and serum, the magnitude of the reduction in serum was approximately two-fold greater than liver, this resulted in the liver to serum *at*RA ratio increasing approximately two-fold after

multiple doses of WIN 18,446 suggesting other tissues except the liver may contribute to formation of circulating *at*RA. It has been previously reported that circulating concentrations of *at*RA do not correlate with tissue concentrations and this is believed to be due to the differential regulation of *at*RA biosynthesis in each retinoid dependent tissue (Obrochta et al., 2014). Therefore, it has been assumed that serum *at*RA concentrations can not be used to ascertain changes in tissue *at*RA. The reduction in tissue and serum *at*RA described in this study demonstrates that changes in serum *at*RA can be used as a surrogate marker of tissue *at*RA status following a pharmacological treatment, although establishing quantitative relationships for individual tissues will be challenging due to the time dependence and magnitude of *at*RA reduction. Further studies to determine the major sources of serum *at*RA and whole body *at*RA homeostasis are needed to better establish how serum *at*RA concentrations are regulated.

In addition to the ALDH1A enzymes regulating *at*RA synthesis, cellular retinol binding protein 1 (CRBP1) has been suggested to modify *at*RA synthesis rates and CRBP1 has been shown to interact with ALDH1A enzymes (Arnold et al., 2014; Posch et al., 1992). Hence it is possible that the contributions of ALDH1A enzymes to *at*RA synthesis in the liver and testis are affected by CRBP1 expression. In a previous study CRBP1 decreased *at*RA formation by ALDH1A1 by 50% and increased the activity of ALDH1A2 2.7-fold resulting in a greater predicted contribution of ALDH1A2 to intratesticular *at*RA formation than that predicted from recombinant enzyme activity alone (Arnold et al., 2014). CRBP1 may have a similar effect in the mouse testis. If CRBP1 is assumed to decrease ALDH1A1 activity by 50% and increase ALDH1A2 activity 2.7-fold the predicted contribution of ALDH1A2 to testicular *at*RA formation increases to 92%, and the predicted magnitude of inhibition of *at*RA Cl_f following single dose of WIN 18,446 increases to 87% at 24 hours after first WIN dose. This inhibition is

greater than the observed decrease in *at*RA concentrations (67% decrease) following WIN 18,446 dosing. However, because circulating *at*RA may also contribute to *at*RA concentrations in the testis in addition to the *at*RA formed in situ, the definitive role of CRBPs in the mouse testis cannot be determined from this data. Similarly, the effect of CRBP1 on AOX activity in the liver is not known but based on the excellent agreement between the in predicted and observed inhibition of *at*RA formation in the liver it is unlikely that CRBP1 in the liver alters the enzyme contributions to *at*RA formation. This may be due to the fact that CRBP1 in the liver is predominantly bound with retinol and hence retinal in the liver is unbound.

In conclusion, this study shows that decreased ALDH1A activity in adult animals results in decreased *at*RA concentrations in serum and tissues and that the magnitude of decrease in *at*RA concentrations in specific tissues can be quantitatively predicted based on understanding of the specific enzymes contributing to *at*RA formation in the tissues of interest, and the inhibition kinetics of the ALDH1A enzymes. This study also demonstrates that the enzymes important for *at*RA formation are tissue specific and therefore tissue specific decreases of *at*RA formation can be achieved by use of ALDH1A isoform specific inhibitors. The knowledge gained here is directly applicable to situations in which a xenobiotic inhibits ALDH1A activity and the side effect or beneficial effects of the compound are evaluated based on altered *at*RA concentrations, or in cases where ALDH1A genetic polymorphisms are identified and their effect to *at*RA disposition is rationalized.

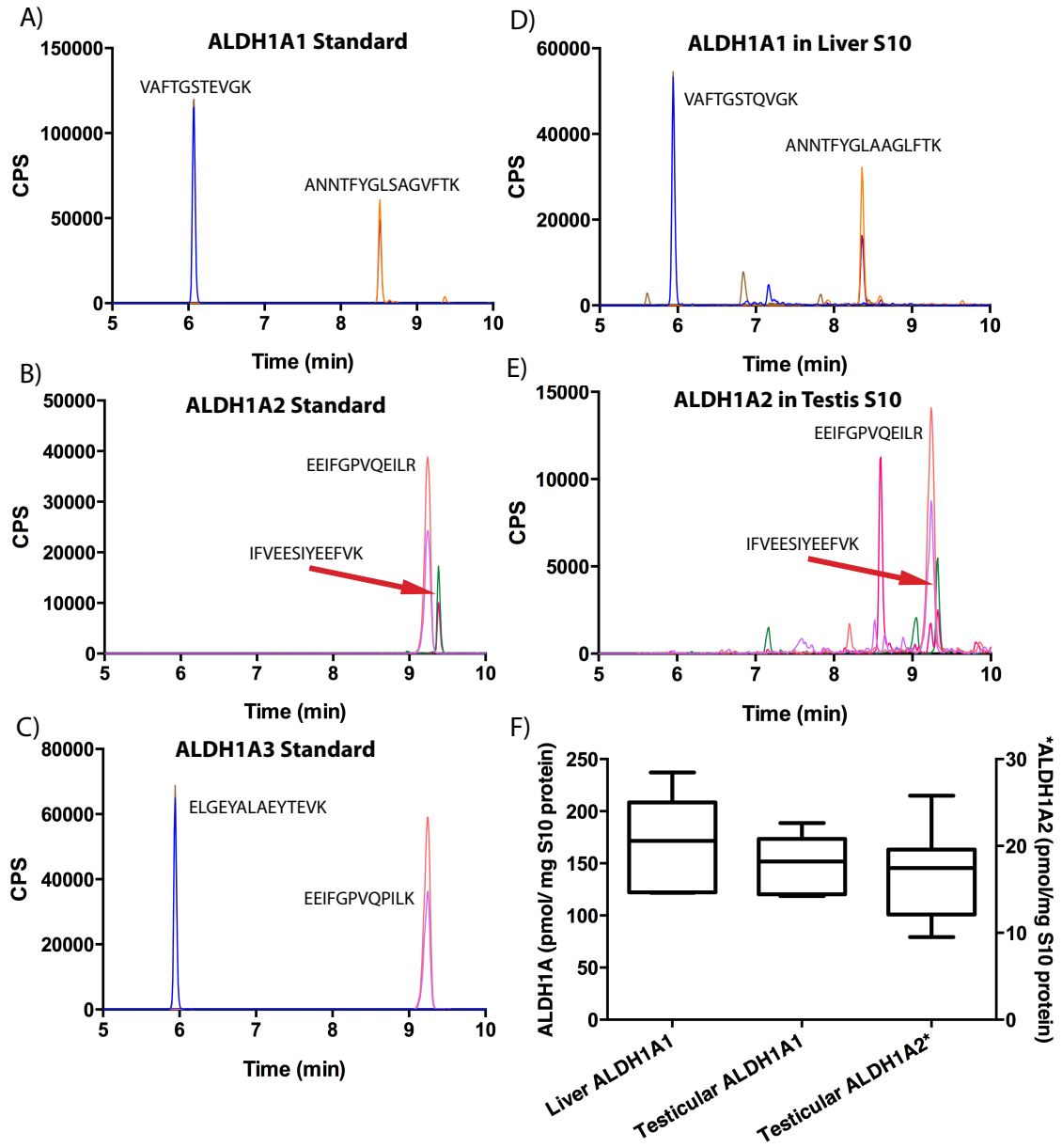

Figure 4.1: Quantification of ALDH1A expression in mouse liver and testis using LC-MS/MS peptide quantification. Recombinant human ALDH1A protein was digested with trypsin and two peptides generated from each protein were monitored using LC-MS/MS (A,B,C). Representative chromatograms of ALDH1A1 peptide detection in the liver (D) and ALDH1A2 in the testis (E) are shown. ALDH1A3 was not detected in the liver or the testis. Liver and testes from eight mice not treated with WIN 18,446 were used to determine the average ALDH1A isoform expression in each tissue and the measured concentrations are shown with a box and whiskers plot with Tukey distributions in Panel F. ALDH1A1 concentration in the liver was 170 ± 50 pmol/g and in the testis 150 ± 30 pmol/g and the average ALDH1A2 concentration in the testis was 17.0 ± 5.0 pmol/g.

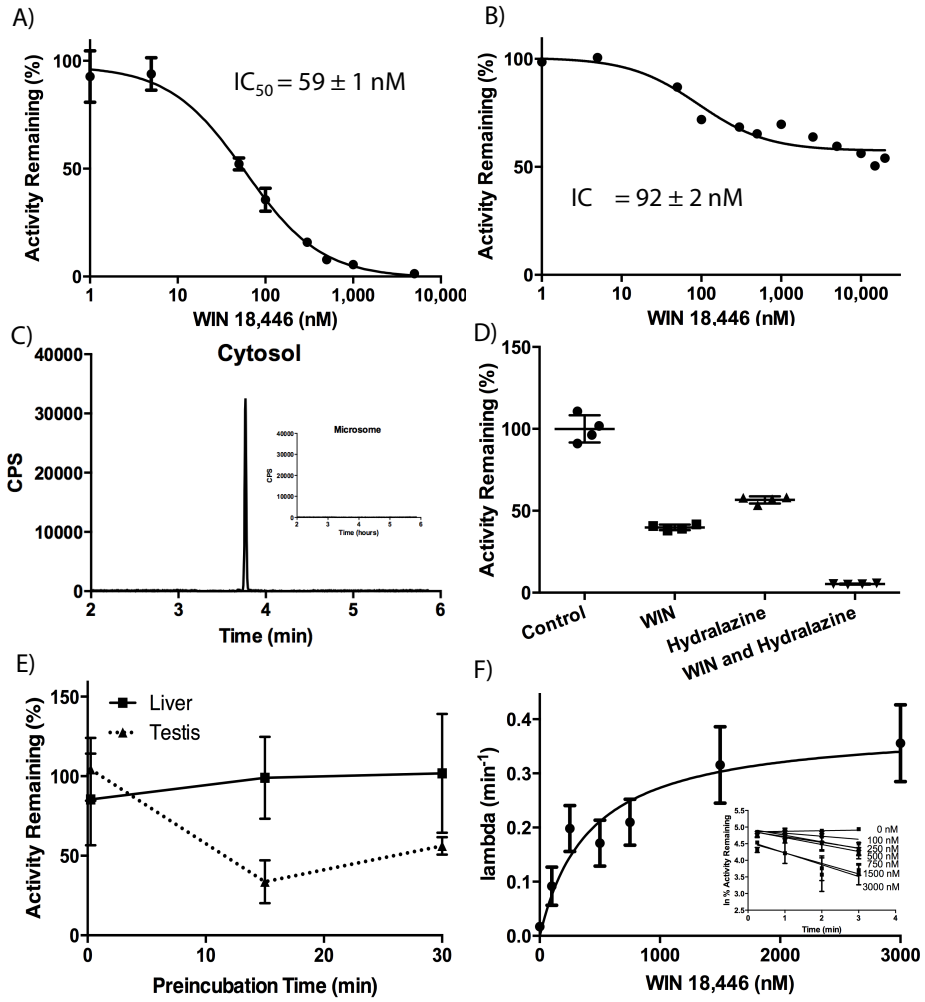

Figure 4.2: WIN 18,446 inhibits the formation of *at*RA in mouse liver and testis. The concentration dependent inhibition kinetics of *at*RA formation in mouse testis (A) and liver (B) S10 protein by WIN 18,446. The NAD^+ dependent *at*RA formation was detected in mouse liver cytosol (C) but not in mouse liver microsomes (Panel C inset). The aldehyde oxidase inhibitor hydralazine inhibited 45 ± 2% of the *at*RA formation while WIN 18,446 inhibited 60 ± 2% of *at*RA formation. Inhibition of *at*RA formation in mouse liver cytosol by WIN 18,446 and hydralazine is shown in panel (D). When hydralazine was combined with WIN 18,446, *at*RA formation was reduced by 95 ± 1% (D). Time dependent inhibition of *at*RA formation by WIN 18,446 was observed in pooled testis S10 protein, but not liver S10 protein (E). Since time dependent inhibition was observed in the testis S10 protein, the time dependent inhibition of *at*RA formation by WIN 18,446 was characterized. The rate of inactivation in testis S10 protein was determined with increasing concentrations of inhibitor (F inset) and plotted as a function of inhibitor concentration (F) to the determine the K_I of 420 ± 190 nM and k_{inact} of 23.2 ± 3.5 hr^{-1}. All experiments were conducted as described in materials and methods.

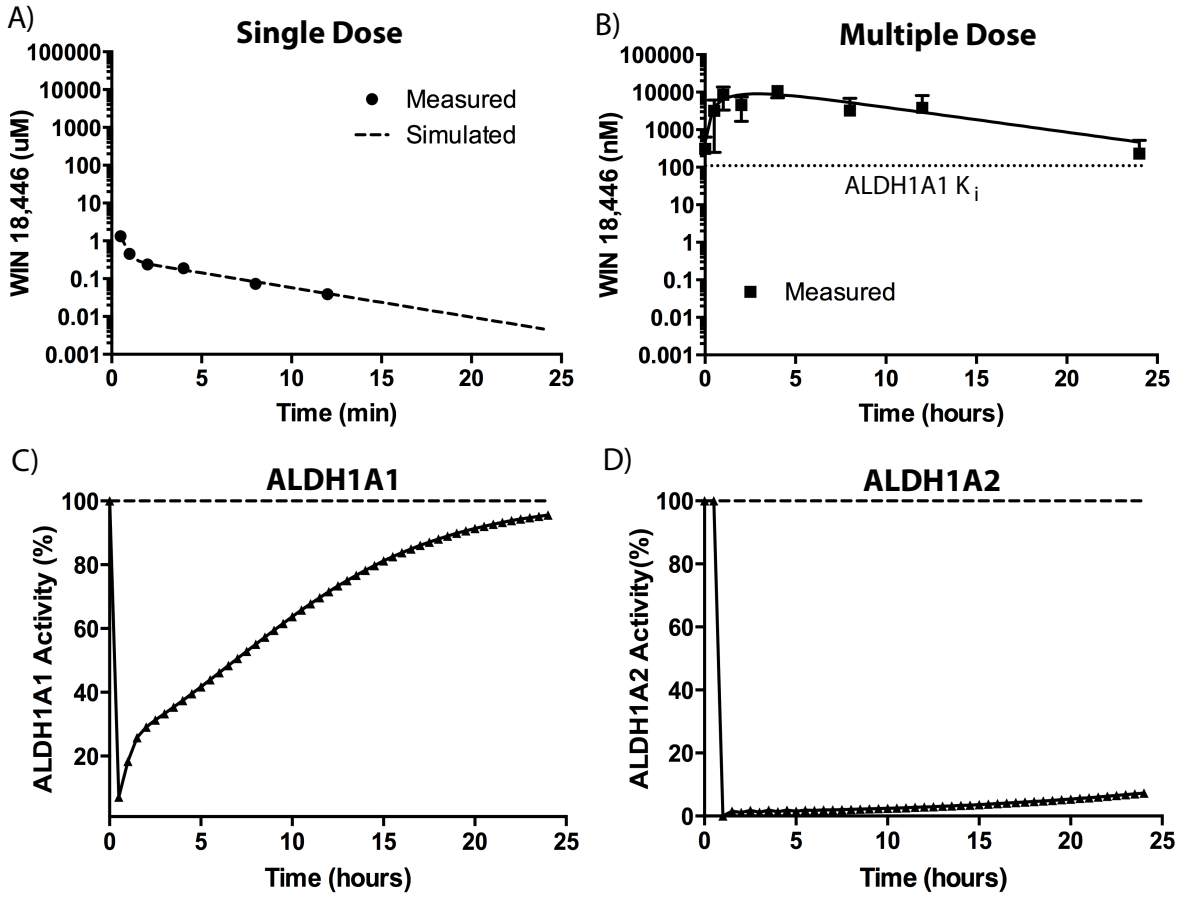

Figure 4.3: The disposition of WIN 18,446 in mice following single and multiple doses and predicted effects of WIN 18,446 on ALDH1A1 and ALDH1A2 activity. WIN 18,446 serum concentrations were measured after a single (A) or multiple (B) doses of 125 mg/kg WIN 18,446 given as an oral dose. The equation $[\text{WIN 18,446}](t)= A^{-\alpha t} + B^{-\beta t} + C^{-\gamma t}$ was fitted to the data (dashed line) for the single dose and was used to simulate WIN 18,446 concentrations. The simulated WIN 18,446 concentrations following a single dose of WIN 18,446 were used to predict the time course of ALDH1A1 (C) and ALDH1A2 (D) activity as described in materials and methods.

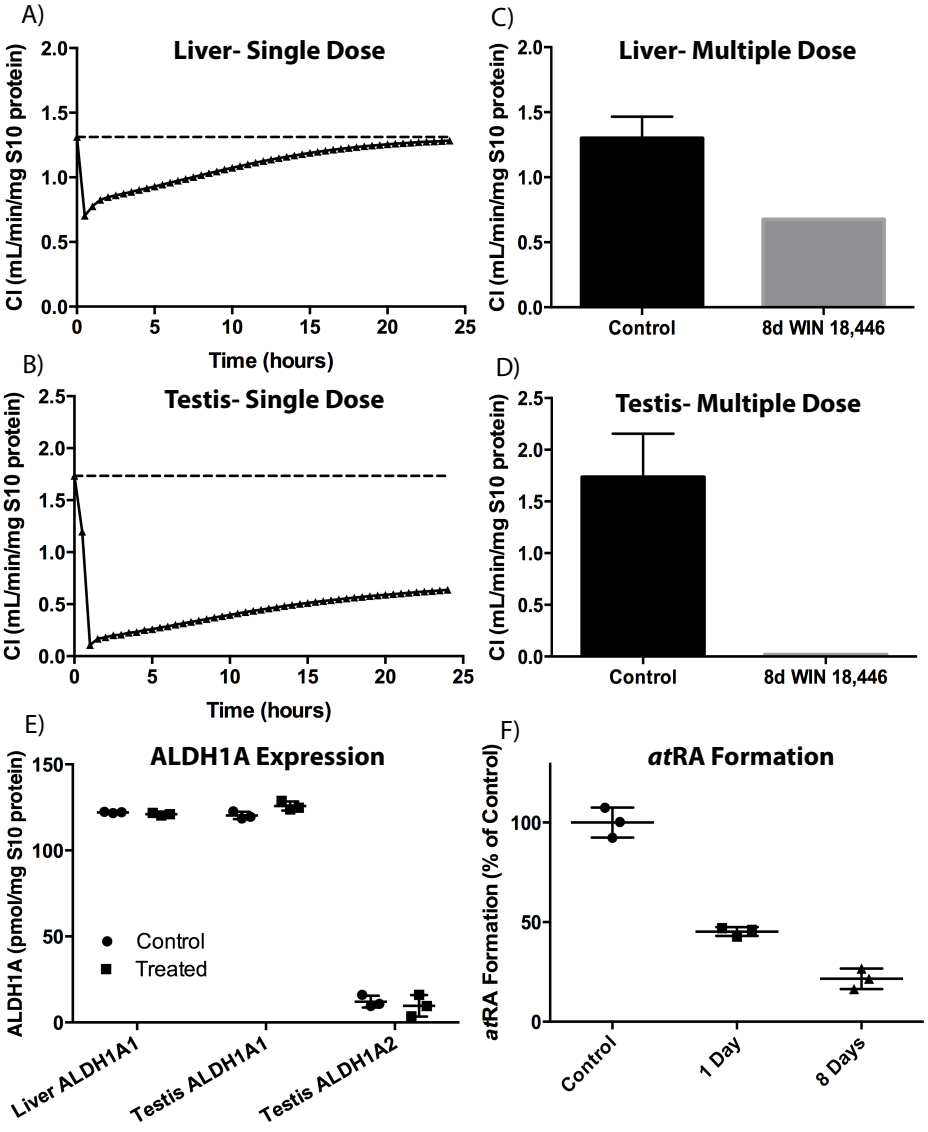

Figure 4.4: The predicted effect of WIN 18,446 administration on *at*RA Cl_f and ALDH1A expression in mouse liver and testis. The *at*RA Cl_f was predicted using measured WIN 18,446 disposition data, WIN 18,446 inhibition kinetics of recombinant ALDH1A, and *at*RA formation in mouse tissues as described in materials and methods. The total liver and testis *at*RA formation clearances were predicted with a dynamic model after a single dose of WIN 18,446 (A,B) or static model after multiple doses (C,D). The dashed line in A and B represents the total average predicted *at*RA Cl_f in the absence of WIN 18,446 administration. ALDH1A1 expression in the liver and testis and ALDH1A2 expression in the testes in control mice and in mice treated for 8 days with WIN 18,446 are shown (E). The expression levels were not significantly altered by WIN 18,446 treatment (E). The *at*RA formation velocities were measured in testes S10 fractions from control mice and mice sacrificed 24 hours after a single dose of WIN 18,446, or 24 hours after the 7th dose of WIN 18,446 (F). The decrease in activity represents the inactivation of ALDH1A activity by WIN 18,446.

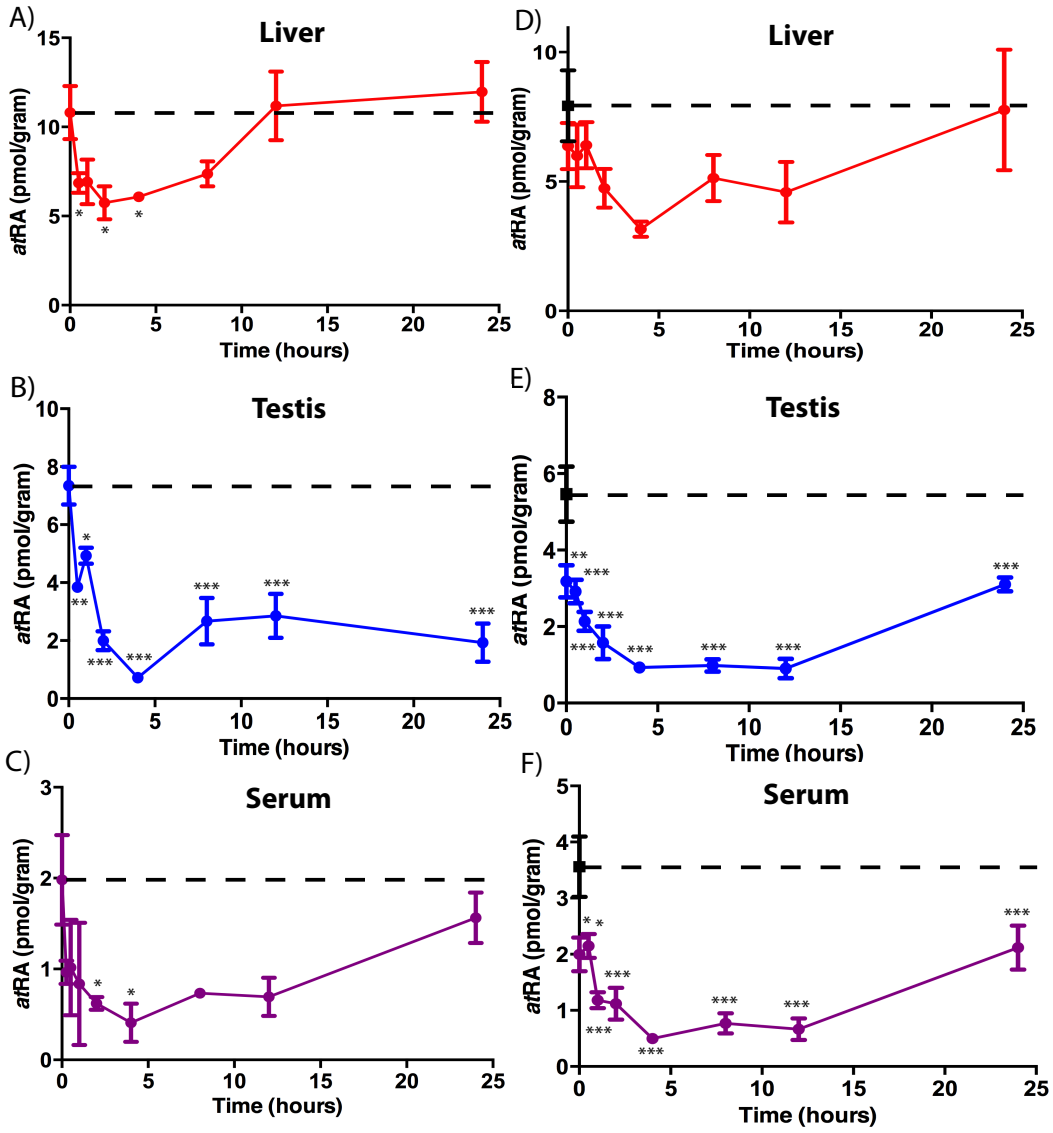

Figure 4.5: *at*RA concentrations are decreased in a tissue specific manner following single and multiple doses of WIN 18,446. Tissue and serum *at*RA concentrations were measured using LC-MS/MS over a 24 hour time course after single 125 mg/kg oral dose (A,B,C) and 8 daily doses (B,E,F) of 125 mg/kg WIN 18,446. The dashed lines represent the average concentration of *at*RA at time 0 of vehicle treated mice. Significant changes in *at*RA concentrations at any given time point in comparison to those measured at time 0 in the vehicle treated mice are indicated. (p- values: * < 0.05, ** <0.01, *** < 0.001)

Table 4.1: **Signature peptides and mass spectrometric conditions used for mouse ALDH1A quantitation.** Two signature peptides were chosen for quantification and confirmation of ALDH1A protein expression. For each quantitation peptide, a peptide with a [$^{13}C_6{}^{15}N_2$]-lysine or [$^{13}C_6{}^{15}N_2$]-arginine was synthesized and used as an internal standard. The internal standards for both ALDH1A2 and ALDH1A3 required trypsin cleavage to generate the target peptide (bolded). For each peptide, values of 10 and 13 were used for the entrance and collision exit potential.

Protein	Peptide (Amino Acid #)	Precursor Ion (*m/z*)	Fragments (*m/z*)	Declustering Potential	Collision Energy
ALDH1A1	ANNTFYGLAAGLFTK[A]* (420-434)	771.4	877.5 1040.6	120	20
	VAFTGSTQVGK[B] (232-251)	547.7	777.4 676.4	71	28
ALDH1A2	VTDDMRIAK**EEIFGPVQEILR*** (406-426)	715.4	911.5 854.5	83	35
	IFVEESIYEEFVK (325-337)	816.4	1014.5 927.5	91	38.2
ALDH1A3	EVTDNMRIAK**EEIFGPVQPILK*** (409-420)	685.4	851.5 794.5	81	34
	ELGEYALAEYTEVK (487-500)	807.9	839.4 921.5	83	35

* peptides used for quantification. [A]The corresponding sequence of the peptide generated from human ALDH1A1 is ANNTFYGLSAGVFTK. [B]The corresponding sequence of the peptide generated from human ALDH1A1 is VAFTGSTEVGK.

Table 4.2: **Predicted and observed *at*RA formation clearance (CL_f) in liver and testis S10 protein by the individual ALDH1A enzymes and by the net contribution of all enzymes.** The predicted contribution of ALDH1A2 to atRA formation in the testis was 61%.

	*at*RA CL_f (mL/min/mg S10 protein)			
Tissue	Predicted ALDH1A1	Predicted ALDH1A2	Predicted Total	Observed
Liver	0.48 ± 0.01	N/A	0.48 ± 0.01	1.8 ± 0.3
Testis	0.45 ± 0.01	0.70 ± 0.20	1.15 ± 0.17	1.6 ± 0.2

Chapter 5

General Conclusions

The studies reported in this thesis demonstrate the importance of ALDH1A enzymes in controlling RA formation in a tissue specific manner. To characterize the importance of ALDH1A enzymes in maintaining RA concentrations, ALDH1A protein concentrations were measured in multiple tissues. Selective, reproducible antibodies for the ALDH1A enzymes were not available; therefore, LC-MS/MS peptide quantification was explored as an alternative protein quantification method. LC-MS/MS peptide quantification affords a robust and specific method to quantify the expression of protein and was used to develop a validated method to quantify proteins responsible for maintaining RA homeostasis throughout the body. The development of the LC-MS/MS peptide quantification method demonstrated the critical importance of carefully selecting signature peptides to ensure accurate quantification of the target proteins. In addition, established IS methods were compared in the study and the validation criteria were only satisfied when a SIL-peptide was added in the quench of the protein digestion and used as an IS.

The protein quantification method was used in conjunction with novel methods to quantify RA formation to determine the contribution of ALDH1A isoforms to RA formation in the human testis. ALDH1A1 is the predominant ALDH1A enzyme expressed in the human testis and its expression is approximately 38-fold higher than ALDH1A2 and ALDH1A3. Yet, due to the efficient formation of *at*RA from *at*-retinal by ALDH1A2, ALDH1A2 was predicted to contribute to approximately 20% of testicular *at*RA formation at endogenous concentrations of *at*-retinal.

To test the predicted contribution of ALDH1A2 to human testicular *at*RA formation from *at*-retinal, WIN 18,446 was used to inactivate ALDH1A2 in human testicular S10 protein. When human testicular S10 protein was incubated with WIN 18,446, the decrease in *at*RA formation activity was in good agreement with the predicted contribution of ALDH1A2 thus demonstrating

the accuracy of the predicted ALDH1A isoform contributions to testicular *at*RA formation. In addition, the affect of cellular retinol binding protein (CRBP) 1 on *at*RA formation by the ALDH1A enzymes was determined for each of the ALDH1A isoforms. As a result, when *at*-retinal is bound to CRBP1, ALDH1A1 and ALDH1A2 are predicted to contribute equally to *at*RA formation in the testis and account for over 99% of the total testicular *at*RA formation.

To show that testicular RA was positively associated with ALDH1A activity in the human testis, testicular RA concentrations and RA formation was measured for each individual in the study. While intratesticular *at*RA was not associated with ALDH1A activity, an association was identified between intratesticular 13-*cis*RA and ALDH1A activity. The positive association between intratesticular 13-*cis*RA and ALDH1A activity is of interest, as ALDH1A1 is the only ALDH1A that catalyzes the formation of 13-*cis*RA from 13-*cis*-retinal. It is unclear why an association was not observed between intratesticular *at*RA and ALDH1A activity, but differential CYP26 activity between the individuals in the study may provide an explanation.

To demonstrate that the localization of the ALDH1A enzymes in the testis contribute to their unique roles in RA formation, the localization of ALDH1A was determined in the human testis. A distinct localization pattern was identified in the seminiferous tubule suggesting an *at*RA gradient is generated between the Sertoli cells and developing sperm. The necessity of ALDH1A for the generation of an *at*RA gradient during fetal development has been previously described and disruption of prenatal ALDH1A activity results in numerous congenital effects. The localization of ALDH1A enzymes in other human tissues has yet to be determined, but it is possible that *at*RA gradients are generated within additional tissues throughout adulthood to control *at*RA signaling in a spatiotemporal manner.

To test the hypothesis that ALDH1A enzymes control the formation of *at*RA in a tissue specific fashion, mouse liver and testicular ALDH1A expression levels and *at*RA formation kinetics by the ALDH1A enzymes were used to predict the formation of *at*RA. When ALDH1A expression was measured in each tissue, ALDH1A1 was quantified in the liver and testis, but ALDH1A2 was only detected and quantified in the testis. Together, the ALDH1A expression profiles and their respective *at*RA formation kinetics accurately predicted *at*RA formation in the mouse testis, but *at*RA formation was underpredicted in the liver suggesting the contribution of additional enzymes to liver *at*RA formation. Using an aldehyde oxidase specific inhibitor, aldehyde oxidase was determined to account for approximately 50% of the *at*RA formation in the liver.

To determine if altered ALDH1A activity directly influenced *at*RA concentrations in vivo, liver and testicular *at*RA concentrations were measured after administration of the ALDH1A inhibitor WIN 18,446. Based on the distinct ALDH1A localization pattern and the WIN 18,446 inhibition kinetics, administration of WIN 18,446 was predicted to generate a tissue specific reduction in *at*RA concentrations. As predicted, a single dose of WIN 18,446 decreased liver *at*RA concentrations approximately 50% and the concentration of *at*RA returned to baseline within 24 hours along with the elimination of WIN 18,446 from circulation. In contrast, testicular *at*RA concentrations were efficiently reduced more than 95% and did not recover within 24 hours. Taken together, these results demonstrate that *at*RA formation is controlled in a tissue specific manner and the methodology developed in this thesis will facilitate future studies on how *at*RA homeostasis is regulated throughout the body.

Bibliography

Abu-Abed, S., Dolle, P., Metzger, D., Beckett, B., Chambon, P., and Petkovich, M. (2001). The retinoic acid-metabolizing enzyme, CYP26A1, is essential for normal hindbrain patterning, vertebral identity, and development of posterior structures. Genes Dev *15*, 226-240.

Agger, S.A., Marney, L.C., and Hoofnagle, A.N. (2010). Simultaneous quantification of apolipoprotein A-I and apolipoprotein B by liquid-chromatography-multiple- reaction-monitoring mass spectrometry. Clinical chemistry *56*, 1804-1813.

Amengual, J., Petrov, P., Bonet, M.L., Ribot, J., and Palou, A. (2012). Induction of carnitine palmitoyl transferase 1 and fatty acid oxidation by retinoic acid in HepG2 cells. Int J Biochem Cell Biol *44*, 2019-2027.

Amengual, J., Ribot, J., Bonet, M.L., and Palou, A. (2010). Retinoic acid treatment enhances lipid oxidation and inhibits lipid biosynthesis capacities in the liver of mice. Cell Physiol Biochem *25*, 657-666.

Amory, J.K., Arnold, S., Lardone, M.C., Piottante, A., Ebensperger, M., Isoherranen, N., Muller, C.H., Walsh, T., and Castro, A. (2014). Levels of the retinoic acid synthesizing enzyme aldehyde dehydrogenase-1A2 are lower in testicular tissue from men with infertility. Fertil Steril *101*, 960-966.

Amory, J.K., Muller, C.H., Shimshoni, J.A., Isoherranen, N., Paik, J., Moreb, J.S., Amory, D.W., Sr., Evanoff, R., Goldstein, A.S., and Griswold, M.D. (2011a). Suppression of spermatogenesis by bisdichloroacetyldiamines is mediated by inhibition of testicular retinoic acid biosynthesis. J Androl *32*, 111-119.

Amory, J.K., Muller, C.H., Shimshoni, J.A., Isoherranen, N., Paik, J., Moreb, J.S., Amory, D.W., Sr., Evanoff, R., Goldstein, A.S., and Griswold, M.D. (2011b). Suppression of spermatogenesis by bisdichloroacetyldiamines is mediated by inhibition of testicular retinoic acid biosynthesis. J Androl *32*, 111-119.

An, B., Zhang, M., and Qu, J. (2014). Toward sensitive and accurate analysis of antibody biotherapeutics by liquid chromatography coupled with mass spectrometry. Drug metabolism and disposition: the biological fate of chemicals *42*, 1858-1866.

Arnold, S.L., Amory, J.K., Walsh, T.J., and Isoherranen, N. (2012). A sensitive and specific method for measurement of multiple retinoids in human serum with UHPLC-MS/MS. Journal of lipid research *53*, 587-598.

Arnold, S.L., Kent, T., Hogarth, C.A., Schlatt, S., Prasad, B., Haenisch, M., Walsh, T., Muller, C.H., Griswold, M.D., Amory, J.K*., et al.* (2014). Importance of ALDH1A enzymes in determining human testicular retinoic acid concentrations. Journal of lipid research.

Ashique, A.M., May, S.R., Kane, M.A., Folias, A.E., Phamluong, K., Choe, Y., Napoli, J.L., and Peterson, A.S. (2012). Morphological defects in a novel Rdh10 mutant that has reduced retinoic acid biosynthesis and signaling. Genesis *50*, 415-423.

Barnidge, D.R., Dratz, E.A., Martin, T., Bonilla, L.E., Moran, L.B., and Lindall, A. (2003). Absolute quantification of the G protein-coupled receptor rhodopsin by LC/MS/MS using proteolysis product peptides and synthetic peptide standards. Analytical chemistry *75*, 445-451.

Barnidge, D.R., Hall, G.D., Stocker, J.L., and Muddiman, D.C. (2004). Evaluation of a cleavable stable isotope labeled synthetic peptide for absolute protein quantification using LC-MS/MS. Journal of proteome research *3*, 658-661.

Berberian, D.A., Slighter RG, Surrey AR. (1961). In vitro and in vivo amebicidal activity of N, N'Bis(dichloroacetyl)diamines. Antibiot Chemother *11*, 245-255.

Berggren Soderlund, M., Fex, G., and Nilsson-Ehle, P. (2003). Decreasing serum concentrations of all-trans, 13-cis retinoic acids and retinol during fasting and caloric restriction. J Intern Med *253*, 375-380.

Berry, D.C., DeSantis, D., Soltanian, H., Croniger, C.M., and Noy, N. (2012). Retinoic acid upregulates preadipocyte genes to block adipogenesis and suppress diet-induced obesity. Diabetes *61*, 1112-1121.

Berry, D.C., and Noy, N. (2009). All-trans-retinoic acid represses obesity and insulin resistance by activating both peroxisome proliferation-activated receptor beta/delta and retinoic acid receptor. Molecular and cellular biology *29*, 3286-3296.

Bhat, P.V., and Samaha, H. (1999). Kinetic properties of the human liver cytosolic aldehyde dehydrogenase for retinal isomers. Biochem Pharmacol *57*, 195-197.

Blomhoff, R. (1987). Hepatic retinol metabolism: role of the various cell types. Nutr Rev *45*, 257-263.

Bonet, M.L., Ribot, J., and Palou, A. (2012). Lipid metabolism in mammalian tissues and its control by retinoic acid. Biochimica et biophysica acta *1821*, 177-189.

Brodeur, H., Chagnon, S., Parisotto, M., Mader, S., and Bhat, P.V. (2006). Kinetic properties of chimeric class I aldehyde dehydrogenases for retinal isomers. Biochem Cell Biol *84*, 799-804.

Bronsema, K.J., Bischoff, R., and van de Merbel, N.C. (2013). High-sensitivity LC-MS/MS quantification of peptides and proteins in complex biological samples: the impact of enzymatic digestion and internal standard selection on method performance. Analytical chemistry *85*, 9528-9535.

Brown, H.S., Ito, K., Galetin, A., and Houston, J.B. (2005). Prediction of in vivo drug-drug interactions from in vitro data: impact of incorporating parallel pathways of drug elimination and inhibitor absorption rate constant. Br J Clin Pharmacol *60*, 508-518.

Brun, V., Dupuis, A., Adrait, A., Marcellin, M., Thomas, D., Court, M., Vandenesch, F., and Garin, J. (2007). Isotope-labeled protein standards: toward absolute quantitative proteomics. Mol Cell Proteomics *6*, 2139-2149.

Bushue, N., and Wan, Y.J. (2010). Retinoid pathway and cancer therapeutics. Advanced drug delivery reviews *62*, 1285-1298.

Chapellier, B., Mark, M., Messaddeq, N., Calleja, C., Warot, X., Brocard, J., Gerard, C., Li, M., Metzger, D., Ghyselinck, N.B.*, et al.* (2002). Physiological and retinoid-induced proliferations of epidermis basal keratinocytes are differently controlled. EMBO J *21*, 3402-3413.

Chung, S.S., Wang, X., Roberts, S.S., Griffey, S.M., Reczek, P.R., and Wolgemuth, D.J. (2011). Oral administration of a retinoic Acid receptor antagonist reversibly inhibits spermatogenesis in mice. Endocrinology *152*, 2492-2502.

Chung, S.S., Wang, X., and Wolgemuth, D.J. (2009). Expression of retinoic acid receptor alpha in the germline is essential for proper cellular association and spermiogenesis during spermatogenesis. Development *136*, 2091-2100.

Chung, S.S., and Wolgemuth, D.J. (2004). Role of retinoid signaling in the regulation of spermatogenesis. Cytogenet Genome Res *105*, 189-202.

Clagett-Dame, M., and Knutson, D. (2011). Vitamin A in reproduction and development. Nutrients *3*, 385-428.

D'Ambrosio, D.N., Clugston, R.D., and Blaner, W.S. (2011). Vitamin A Metabolism: An Update. Nutrients *3*, 63-103.

Dockham, P.A., Lee, M.O., and Sladek, N.E. (1992). Identification of human liver aldehyde dehydrogenases that catalyze the oxidation of aldophosphamide and retinaldehyde. Biochem Pharmacol *43*, 2453-2469.

Duan, X., Abuqayyas, L., Dai, L., Balthasar, J.P., and Qu, J. (2012a). High-throughput method development for sensitive, accurate, and reproducible quantification of therapeutic monoclonal antibodies in tissues using orthogonal array optimization and nano liquid chromatography/selected reaction monitoring mass spectrometry. Anal Chem *84*, 4373-4382.

Duan, X., Dai, L., Chen, S.C., Balthasar, J.P., and Qu, J. (2012b). Nano-scale liquid chromatography/mass spectrometry and on-the-fly orthogonal array optimization for quantification of therapeutic monoclonal antibodies and the application in preclinical analysis. Journal of chromatography A *1251*, 63-73.

Dupe, V., Matt, N., Garnier, J.M., Chambon, P., Mark, M., and Ghyselinck, N.B. (2003). A newborn lethal defect due to inactivation of retinaldehyde dehydrogenase type 3 is prevented by maternal retinoic acid treatment. Proc Natl Acad Sci U S A *100*, 14036-14041.

Eckhoff, C., Bailey, J.R., Collins, M.D., Slikker, W., Jr., and Nau, H. (1991). Influence of dose and pharmaceutical formulation of vitamin A on plasma levels of retinyl esters and retinol and

metabolic generation of retinoic acid compounds and beta-glucuronides in the cynomolgus monkey. Toxicol Appl Pharmacol *111*, 116-127.

El Kares, R., Manolescu, D.C., Lakhal-Chaieb, L., Montpetit, A., Zhang, Z., Bhat, P.V., and Goodyer, P. (2010). A human ALDH1A2 gene variant is associated with increased newborn kidney size and serum retinoic acid. Kidney Int *78*, 96-102.

Elizondo, G., Corchero, J., Sterneck, E., and Gonzalez, F.J. (2000). Feedback inhibition of the retinaldehyde dehydrogenase gene ALDH1 by retinoic acid through retinoic acid receptor alpha and CCAAT/enhancer-binding protein beta. J Biol Chem *275*, 39747-39753.

Fan, X., Molotkov, A., Manabe, S., Donmoyer, C.M., Deltour, L., Foglio, M.H., Cuenca, A.E., Blaner, W.S., Lipton, S.A., and Duester, G. (2003). Targeted disruption of Aldh1a1 (Raldh1) provides evidence for a complex mechanism of retinoic acid synthesis in the developing retina. Molecular and cellular biology *23*, 4637-4648.

Fierce, Y., de Morais Vieira, M., Piantedosi, R., Wyss, A., Blaner, W.S., and Paik, J. (2008). In vitro and in vivo characterization of retinoid synthesis from beta-carotene. Archives of biochemistry and biophysics *472*, 126-138.

Fu, C., Di, L., Han, X., Soderstrom, C., Snyder, M., Troutman, M.D., Obach, R.S., and Zhang, H. (2013). Aldehyde oxidase 1 (AOX1) in human liver cytosols: quantitative characterization of AOX1 expression level and activity relationship. Drug metabolism and disposition: the biological fate of chemicals *41*, 1797-1804.

Gagnon, I., Duester, G., and Bhat, P.V. (2002). Kinetic analysis of mouse retinal dehydrogenase type-2 (RALDH2) for retinal substrates. Biochimica et biophysica acta *1596*, 156-162.

Gagnon, I., Duester, G., and Bhat, P.V. (2003). Enzymatic characterization of recombinant mouse retinal dehydrogenase type 1. Biochem Pharmacol *65*, 1685-1690.

Garattini, E., Fratelli, M., and Terao, M. (2008). Mammalian aldehyde oxidases: genetics, evolution and biochemistry. Cell Mol Life Sci *65*, 1019-1048.

Geoghegan, K.F., Hoth, L.R., Tan, D.H., Borzilleri, K.A., Withka, J.M., and Boyd, J.G. (2002). Cyclization of N-terminal S-carbamoylmethylcysteine causing loss of 17 Da from peptides and extra peaks in peptide maps. Journal of proteome research *1*, 181-187.

Gerber, S.A., Rush, J., Stemman, O., Kirschner, M.W., and Gygi, S.P. (2003). Absolute quantification of proteins and phosphoproteins from cell lysates by tandem MS. Proceedings of the National Academy of Sciences of the United States of America *100*, 6940-6945.

Goodman, D.W., Huang, H.S., and Shiratori, T. (1965). Tissue Distribution and Metabolism of Newly Absorbed Vitamin a in the Rat. Journal of lipid research *6*, 390-396.

Graham, C.E., Brocklehurst, K., Pickersgill, R.W., and Warren, M.J. (2006). Characterization of retinaldehyde dehydrogenase 3. Biochem J *394*, 67-75.

Grimm, S.W., Einolf, H.J., Hall, S.D., He, K., Lim, H.K., Ling, K.H., Lu, C., Nomeir, A.A., Seibert, E., Skordos, K.W., *et al.* (2009). The conduct of in vitro studies to address time-dependent inhibition of drug-metabolizing enzymes: a perspective of the pharmaceutical research and manufacturers of America. Drug metabolism and disposition: the biological fate of chemicals *37*, 1355-1370.

Gudas, L.J., and Wagner, J.A. (2011). Retinoids regulate stem cell differentiation. J Cell Physiol *226*, 322-330.

Haselbeck, R.J., Hoffmann, I., and Duester, G. (1999). Distinct functions for Aldh1 and Raldh2 in the control of ligand production for embryonic retinoid signaling pathways. Dev Genet *25*, 353-364.

Heikkinen, A.T., Friedlein, A., Lamerz, J., Jakob, P., Cutler, P., Fowler, S., Williamson, T., Tolando, R., Lave, T., and Parrott, N. (2012). Mass spectrometry-based quantification of CYP enzymes to establish in vitro/in vivo scaling factors for intestinal and hepatic metabolism in beagle dog. Pharm Res *29*, 1832-1842.

Hellemans, K., Verbuyst, P., Quartier, E., Schuit, F., Rombouts, K., Chandraratna, R.A., Schuppan, D., and Geerts, A. (2004). Differential modulation of rat hepatic stellate phenotype by natural and synthetic retinoids. Hepatology *39*, 97-108.

Heller, C.G., Moore, D.J., and Paulsen, C.A. (1961). Suppression of spermatogenesis and chronic toxicity in men by a new series of bis(dichloroacetyl) diamines. Toxicology and applied pharmacology *3*, 1-11.

Helvig, C., Taimi, M., Cameron, D., Jones, G., and Petkovich, M. (2011). Functional properties and substrate characterization of human CYP26A1, CYP26B1, and CYP26C1 expressed by recombinant baculovirus in insect cells. J Pharmacol Toxicol Methods *64*, 258-263.

Hildonen, S., Halvorsen, T.G., and Reubsaet, L. (2014). Why less is more when generating tryptic peptides in bottom-up proteomics. Proteomics *14*, 2031-2041.

Hogarth, C.A., and Griswold, M.D. (2010). The key role of vitamin A in spermatogenesis. J Clin Invest *120*, 956-962.

Hogarth, C.A., and Griswold, M.D. (2013). Immunohistochemical approaches for the study of spermatogenesis. Methods in molecular biology *927*, 309-320.

Hoting VE, S.B., Schirren C. (1992). Isotretinoin and acne conglobata: andrological evaluations (German). . Fortschur Med *23*, 427-430.

Huang, D.Y., Furukawa, A., and Ichikawa, Y. (1999). Molecular cloning of retinal oxidase/aldehyde oxidase cDNAs from rabbit and mouse livers and functional expression of recombinant mouse retinal oxidase cDNA in Escherichia coli. Arch Biochem Biophys *364*, 264-272.

Huang, D.Y., and Ichikawa, Y. (1994). Two different enzymes are primarily responsible for retinoic acid synthesis in rabbit liver cytosol. Biochem Biophys Res Commun *205*, 1278-1283.

Huq, M.D., Tsai, N.P., Gupta, P., and Wei, L.N. (2006). Regulation of retinal dehydrogenases and retinoic acid synthesis by cholesterol metabolites. EMBO J *25*, 3203-3213.

Idres, N., Marill, J., Flexor, M.A., and Chabot, G.G. (2002). Activation of retinoic acid receptor-dependent transcription by all-trans-retinoic acid metabolites and isomers. J Biol Chem *277*, 31491-31498.

Iwata, M., Hirakiyama, A., Eshima, Y., Kagechika, H., Kato, C., and Song, S.Y. (2004). Retinoic acid imprints gut-homing specificity on T cells. Immunity *21*, 527-538.

Jemal, M., Ouyang, Z., and Xia, Y.Q. (2010). Systematic LC-MS/MS bioanalytical method development that incorporates plasma phospholipids risk avoidance, usage of incurred sample and well thought-out chromatography. Biomedical chromatography : BMC *24*, 2-19.

Jenkins, R., Duggan, J.X., Aubry, A.F., Zeng, J., Lee, J.W., Cojocaru, L., Dufield, D., Garofolo, F., Kaur, S., Schultz, G.A.*, et al.* (2015). Recommendations for Validation of LC-MS/MS Bioanalytical Methods for Protein Biotherapeutics. The AAPS journal *17*, 1-16.

Kane, M.A., Folias, A.E., Pingitore, A., Perri, M., Obrochta, K.M., Krois, C.R., Cione, E., Ryu, J.Y., and Napoli, J.L. (2010). Identification of 9-cis-retinoic acid as a pancreas-specific autacoid that attenuates glucose-stimulated insulin secretion. Proc Natl Acad Sci U S A *107*, 21884-21889.

Kane, M.A., Folias, A.E., Wang, C., and Napoli, J.L. (2008). Quantitative profiling of endogenous retinoic acid in vivo and in vitro by tandem mass spectrometry. Anal Chem *80*, 1702-1708.

Kane, M.A., and Napoli, J.L. (2010). Quantification of endogenous retinoids. Methods in molecular biology *652*, 1-54.

Kastner, P., Mark, M., Leid, M., Gansmuller, A., Chin, W., Grondona, J.M., Decimo, D., Krezel, W., Dierich, A., and Chambon, P. (1996). Abnormal spermatogenesis in RXR beta mutant mice. Genes Dev *10*, 80-92.

Kasus-Jacobi, A., Ou, J., Bashmakov, Y.K., Shelton, J.M., Richardson, J.A., Goldstein, J.L., and Brown, M.S. (2003). Characterization of mouse short-chain aldehyde reductase (SCALD), an enzyme regulated by sterol regulatory element-binding proteins. The Journal of biological chemistry *278*, 32380-32389.

Kato, M., Blaner, W.S., Mertz, J.R., Das, K., Kato, K., and Goodman, D.S. (1985a). Influence of retinoid nutritional status on cellular retinol- and cellular retinoic acid-binding protein concentrations in various rat tissues. J Biol Chem *260*, 4832-4838.

Kato, M., Sung, W.K., Kato, K., and Goodman, D.S. (1985b). Immunohistochemical studies on the localization of cellular retinol-binding protein in rat testis and epididymis. Biology of reproduction *32*, 173-189.

Kavanagh, K.L., Jornvall, H., Persson, B., and Oppermann, U. (2008). Medium- and short-chain dehydrogenase/reductase gene and protein families : the SDR superfamily: functional and structural diversity within a family of metabolic and regulatory enzymes. Cell Mol Life Sci *65*, 3895-3906.

Kawakami, H., Ohtsuki, S., Kamiie, J., Suzuki, T., Abe, T., and Terasaki, T. (2011). Simultaneous absolute quantification of 11 cytochrome P450 isoforms in human liver microsomes by liquid chromatography tandem mass spectrometry with in silico target peptide selection. Journal of pharmaceutical sciences *100*, 341-352.

Kedishvili, N.Y. (2013). Enzymology of retinoic acid biosynthesis and degradation. Journal of lipid research *54*, 1744-1760.

Keil-Dlouha, V.V., Zylber, N., Imhoff, J., Tong, N., and Keil, B. (1971). Proteolytic activity of pseudotrypsin. FEBS letters *16*, 291-295.

Keshishian, H., Addona, T., Burgess, M., Kuhn, E., and Carr, S.A. (2007). Quantitative, multiplexed assays for low abundance proteins in plasma by targeted mass spectrometry and stable isotope dilution. Mol Cell Proteomics *6*, 2212-2229.

Kettenbach, A.N., Rush, J., and Gerber, S.A. (2011). Absolute quantification of protein and post-translational modification abundance with stable isotope-labeled synthetic peptides. Nature protocols *6*, 175-186.

Kiefer, F.W., Orasanu, G., Nallamshetty, S., Brown, J.D., Wang, H., Luger, P., Qi, N.R., Burant, C.F., Duester, G., and Plutzky, J. (2012). Retinaldehyde dehydrogenase 1 coordinates hepatic gluconeogenesis and lipid metabolism. Endocrinology *153*, 3089-3099.

Kim, H., Lapointe, J., Kaygusuz, G., Ong, D.E., Li, C., van de Rijn, M., Brooks, J.D., and Pollack, J.R. (2005a). The retinoic acid synthesis gene ALDH1a2 is a candidate tumor suppressor in prostate cancer. Cancer Res *65*, 8118-8124.

Kim, T.S., Maeda, A., Maeda, T., Heinlein, C., Kedishvili, N., Palczewski, K., and Nelson, P.S. (2005b). Delayed dark adaptation in 11-cis-retinol dehydrogenase-deficient mice: a role of RDH11 in visual processes in vivo. J Biol Chem *280*, 8694-8704.

Kito, K., and Ito, T. (2008). Mass spectrometry-based approaches toward absolute quantitative proteomics. Current genomics *9*, 263-274.

Koppaka, V., Thompson, D.C., Chen, Y., Ellermann, M., Nicolaou, K.C., Juvonen, R.O., Petersen, D., Deitrich, R.A., Hurley, T.D., and Vasiliou, V. (2012). Aldehyde dehydrogenase inhibitors: a comprehensive review of the pharmacology, mechanism of action, substrate specificity, and clinical application. Pharmacol Rev *64*, 520-539.

Krokhin, O.V., Antonovici, M., Ens, W., Wilkins, J.A., and Standing, K.G. (2006). Deamidation of -Asn-Gly- sequences during sample preparation for proteomics: Consequences for MALDI and HPLC-MALDI analysis. Analytical chemistry *78*, 6645-6650.

Kuhn, E., Wu, J., Karl, J., Liao, H., Zolg, W., and Guild, B. (2004). Quantification of C-reactive protein in the serum of patients with rheumatoid arthritis using multiple reaction monitoring mass spectrometry and 13C-labeled peptide standards. Proteomics *4*, 1175-1186.

Kumar, V., Barnidge, D.R., Chen, L.S., Twentyman, J.M., Cradic, K.W., Grebe, S.K., and Singh, R.J. (2010). Quantification of serum 1-84 parathyroid hormone in patients with hyperparathyroidism by immunocapture in situ digestion liquid chromatography-tandem mass spectrometry. Clinical chemistry *56*, 306-313.

Kunchala, S.R., Suzuki, T., and Murayama, A. (2000). Photoisomerization of retinoic acid and its influence on regulation of human keratinocyte growth and differentiation. Indian J Biochem Biophys *37*, 71-76.

Kurlandsky, S.B., Gamble, M.V., Ramakrishnan, R., and Blaner, W.S. (1995). Plasma delivery of retinoic acid to tissues in the rat. J Biol Chem *270*, 17850-17857.

Lanska, D.J. (2010). Chapter 29: historical aspects of the major neurological vitamin deficiency disorders: overview and fat-soluble vitamin A. Handbook of clinical neurology *95*, 435-444.

Lee, M.O., Manthey, C.L., and Sladek, N.E. (1991). Identification of mouse liver aldehyde dehydrogenases that catalyze the oxidation of retinaldehyde to retinoic acid. Biochem Pharmacol *42*, 1279-1285.

Lee, T. (1967). Historical notes on some vitamin-deficiency diseases in China. Diseases in Antiquity, 417-419.

Lesur, A., Varesio, E., and Hopfgartner, G. (2010). Accelerated tryptic digestion for the analysis of biopharmaceutical monoclonal antibodies in plasma by liquid chromatography with tandem mass spectrometric detection. Journal of chromatography A *1217*, 57-64.

Li, N., Nemirovskiy, O.V., Zhang, Y., Yuan, H., Mo, J., Ji, C., Zhang, B., Brayman, T.G., Lepsy, C., Heath, T.G.*, et al.* (2008). Absolute quantification of multidrug resistance-associated protein 2 (MRP2/ABCC2) using liquid chromatography tandem mass spectrometry. Anal Biochem *380*, 211-222.

Li, Y., Wong, K., Walsh, K., Gao, B., and Zang, M. (2013). Retinoic acid receptor beta stimulates hepatic induction of fibroblast growth factor 21 to promote fatty acid oxidation and control whole-body energy homeostasis in mice. J Biol Chem *288*, 10490-10504.

Lin, M., Zhang, M., Abraham, M., Smith, S.M., and Napoli, J.L. (2003). Mouse retinal dehydrogenase 4 (RALDH4), molecular cloning, cellular expression, and activity in 9-cis-retinoic acid biosynthesis in intact cells. J Biol Chem *278*, 9856-9861.

Lohnes, D., Kastner, P., Dierich, A., Mark, M., LeMeur, M., and Chambon, P. (1993). Function of retinoic acid receptor gamma in the mouse. Cell *73*, 643-658.

Luckow, V.A. (1993). Baculovirus systems for the expression of human gene products. Current opinion in biotechnology *4*, 564-572.

Lufkin, T., Lohnes, D., Mark, M., Dierich, A., Gorry, P., Gaub, M.P., LeMeur, M., and Chambon, P. (1993). High postnatal lethality and testis degeneration in retinoic acid receptor alpha mutant mice. Proc Natl Acad Sci U S A *90*, 7225-7229.

Luo, J., Pasceri, P., Conlon, R.A., Rossant, J., and Giguere, V. (1995). Mice lacking all isoforms of retinoic acid receptor beta develop normally and are susceptible to the teratogenic effects of retinoic acid. Mechanisms of development *53*, 61-71.

MacLean, B., Tomazela, D.M., Shulman, N., Chambers, M., Finney, G.L., Frewen, B., Kern, R., Tabb, D.L., Liebler, D.C., and MacCoss, M.J. (2010). Skyline: an open source document editor for creating and analyzing targeted proteomics experiments. Bioinformatics *26*, 966-968.

Mangelsdorf, D.J., and Evans, R.M. (1995). The RXR heterodimers and orphan receptors. Cell *83*, 841-850.

Mark, M., Ghyselinck, N.B., and Chambon, P. (2006). Function of retinoid nuclear receptors: lessons from genetic and pharmacological dissections of the retinoic acid signaling pathway during mouse embryogenesis. Annu Rev Pharmacol Toxicol *46*, 451-480.

Mitranond, V., Sobhon, P., Tosukhowong, P., and Chindaduangrat, W. (1979). Cytological changes in the testes of vitamin-A-deficient rats. I. Quantitation of germinal cells in the seminiferous tubules. Acta Anat (Basel) *103*, 159-168.

Molotkov, A., and Duester, G. (2003). Genetic evidence that retinaldehyde dehydrogenase Raldh1 (Aldh1a1) functions downstream of alcohol dehydrogenase Adh1 in metabolism of retinol to retinoic acid. The Journal of biological chemistry *278*, 36085-36090.

Mucida, D., Park, Y., Kim, G., Turovskaya, O., Scott, I., Kronenberg, M., and Cheroutre, H. (2007). Reciprocal TH17 and regulatory T cell differentiation mediated by retinoic acid. Science *317*, 256-260.

Munson, L., Chassy, L.M., and Asa, C. (2004). Efficacy, safety and reversibility of bisdiamine as a male contraceptive in cats. Theriogenology *62*, 81-92.

Napoli, J.L. (1996). Retinoic acid biosynthesis and metabolism. FASEB journal : official publication of the Federation of American Societies for Experimental Biology *10*, 993-1001.

Napoli, J.L. (2012). Physiological insights into all-trans-retinoic acid biosynthesis. Biochim Biophys Acta *1821*, 152-167.

Napoli, J.L., and Race, K.R. (1987). The biosynthesis of retinoic acid from retinol by rat tissues in vitro. Arch Biochem Biophys *255*, 95-101.

Napoli, J.L., and Race, K.R. (1990). Microsomes convert retinol and retinal into retinoic acid and interfere in the conversions catalyzed by cytosol. Biochimica et biophysica acta *1034*, 228-232.

Niederreither, K., Subbarayan, V., Dolle, P., and Chambon, P. (1999). Embryonic retinoic acid synthesis is essential for early mouse post-implantation development. Nature genetics *21*, 444-448.

Nishimura, M., and Naito, S. (2006). Tissue-specific mRNA expression profiles of human phase I metabolizing enzymes except for cytochrome P450 and phase II metabolizing enzymes. Drug Metab Pharmacokinet *21*, 357-374.

Nouri-Nigjeh, E., Zhang, M., Ji, T., Yu, H., An, B., Duan, X., Balthasar, J., Johnson, R.W., and Qu, J. (2014). Effects of calibration approaches on the accuracy for LC-MS targeted quantification of therapeutic protein. Anal Chem *86*, 3575-3584.

Noy, N. (2010a). Between death and survival: retinoic acid in regulation of apoptosis. Annu Rev Nutr *30*, 201-217.

Noy, N. (2010b). Between death and survival: retinoic acid in regulation of apoptosis. Annu Rev Nutr *30*, 201-217.

Nya-Ngatchou, J.J., Arnold, S. L. M., Walsh, T. J., Muller, C. H., Page, S. T., Isoherranen, N. and Amory, J. K (2012). Intratesticular 13-cis retinoic acid is lower in men with abnormal semen analyses: a pilot study. Andrology.

O'Shaughnessy, P.J., Abel, M., Charlton, H.M., Hu, B., Johnston, H., and Baker, P.J. (2007). Altered expression of genes involved in regulation of vitamin A metabolism, solute transportation, and cytoskeletal function in the androgen-insensitive tfm mouse testis. Endocrinology *148*, 2914-2924.

Obrochta, K.M., Kane, M.A., and Napoli, J.L. (2014). Effects of diet and strain on mouse serum and tissue retinoid concentrations. PLoS One *9*, e99435.

Ocana, M.F., and Neubert, H. (2010). An immunoaffinity liquid chromatography-tandem mass spectrometry assay for the quantitation of matrix metalloproteinase 9 in mouse serum. Analytical biochemistry *399*, 202-210.

Paik, J., Haenisch, M., Muller, C.H., Goldstein, A.S., Arnold, S., Isoherranen, N., Brabb, T., Treuting, P.M., and Amory, J.K. (2014a). Inhibition of Retinoic Acid Biosynthesis by the Bisdichloroacetyldiamine WIN 18,446 Markedly Suppresses Spermatogenesis and Alters Retinoid Metabolism in Mice. J Biol Chem *289*, 15104-15117.

Paik, J., Haenisch, M., Muller, C.H., Goldstein, A.S., Arnold, S., Isoherranen, N., Brabb, T., Treuting, P.M., and Amory, J.K. (2014b). Inhibition of Retinoic Acid Biosynthesis by WIN 18,446 Markedly Suppresses Spermatogenesis and Alters Retinoid Metabolism in Mice. J Biol Chem.

Pailleux, F., and Beaudry, F. (2012). Internal standard strategies for relative and absolute quantitation of peptides in biological matrices by liquid chromatography tandem mass spectrometry. Biomed Chromatogr *26*, 881-891.

Paine, M.F., Khalighi, M., Fisher, J.M., Shen, D.D., Kunze, K.L., Marsh, C.L., Perkins, J.D., and Thummel, K.E. (1997). Characterization of interintestinal and intraintestinal variations in human CYP3A-dependent metabolism. J Pharmacol Exp Ther *283*, 1552-1562.

Pan, S., Aebersold, R., Chen, R., Rush, J., Goodlett, D.R., McIntosh, M.W., Zhang, J., and Brentnall, T.A. (2009). Mass spectrometry based targeted protein quantification: methods and applications. J Proteome Res *8*, 787-797.

Petkovich, M., Brand, N.J., Krust, A., and Chambon, P. (1987). A human retinoic acid receptor which belongs to the family of nuclear receptors. Nature *330*, 444-450.

Piehowski, P.D., Petyuk, V.A., Orton, D.J., Xie, F., Moore, R.J., Ramirez-Restrepo, M., Engel, A., Lieberman, A.P., Albin, R.L., Camp, D.G.*, et al.* (2013). Sources of technical variability in quantitative LC-MS proteomics: human brain tissue sample analysis. Journal of proteome research *12*, 2128-2137.

Posch, K.C., Burns, R.D., and Napoli, J.L. (1992). Biosynthesis of all-trans-retinoic acid from retinal. Recognition of retinal bound to cellular retinol binding protein (type I) as substrate by a purified cytosolic dehydrogenase. J Biol Chem *267*, 19676-19682.

Prasad, B., and Unadkat, J.D. (2014). Comparison of Heavy Labeled (SIL) Peptide versus SILAC Protein Internal Standards for LC-MS/MS Quantification of Hepatic Drug Transporters. Int J Proteomics *2014*, 451510.

Pritchard, C., Quaglia, M., Ashcroft, A.E., and O'Connor, G. (2011). Considering the advantages and pitfalls of the use of isotopically labeled protein standards for accurate protein quantification. Bioanalysis *3*, 2797-2802.

Quadro, L., Blaner, W.S., Hamberger, L., Novikoff, P.M., Vogel, S., Piantedosi, R., Gottesman, M.E., and Colantuoni, V. (2004). The role of extrahepatic retinol binding protein in the mobilization of retinoid stores. Journal of lipid research *45*, 1975-1982.

Raner, G.M., Vaz, A.D., and Coon, M.J. (1996). Metabolism of all-trans, 9-cis, and 13-cis isomers of retinal by purified isozymes of microsomal cytochrome P450 and mechanism-based inhibition of retinoid oxidation by citral. Mol Pharmacol *49*, 515-522.

Raverdeau, M., Gely-Pernot, A., Feret, B., Dennefeld, C., Benoit, G., Davidson, I., Chambon, P., Mark, M., and Ghyselinck, N.B. (2012). Retinoic acid induces Sertoli cell paracrine signals for spermatogonia differentiation but cell autonomously drives spermatocyte meiosis. Proc Natl Acad Sci U S A *109*, 16582-16587.

Roberts, E.S., Vaz, A.D., and Coon, M.J. (1992). Role of isozymes of rabbit microsomal cytochrome P-450 in the metabolism of retinoic acid, retinol, and retinal. Mol Pharmacol *41*, 427-433.

Ross, A.C. (2007). Vitamin A supplementation and retinoic acid treatment in the regulation of antibody responses in vivo. Vitam Horm *75*, 197-222.

Ross, A.C., Cifelli, C.J., Zolfaghari, R., and Li, N.Q. (2011). Multiple cytochrome P-450 genes are concomitantly regulated by vitamin A under steady-state conditions and by retinoic acid during hepatic first-pass metabolism. Physiol Genomics *43*, 57-67.

Rowland, M., Matin, S.B. (1973). Kinetics of drug–drug interactions. J Pharmacokinet Biopharm.

Sakamoto, A., Matsumaru, T., Ishiguro, N., Schaefer, O., Ohtsuki, S., Inoue, T., Kawakami, H., and Terasaki, T. (2011). Reliability and robustness of simultaneous absolute quantification of drug transporters, cytochrome P450 enzymes, and Udp-glucuronosyltransferases in human liver tissue by multiplexed MRM/selected reaction monitoring mode tandem mass spectrometry with nano-liquid chromatography. J Pharm Sci *100*, 4037-4043.

Sandell, L.L., Sanderson, B.W., Moiseyev, G., Johnson, T., Mushegian, A., Young, K., Rey, J.P., Ma, J.X., Staehling-Hampton, K., and Trainor, P.A. (2007). RDH10 is essential for synthesis of embryonic retinoic acid and is required for limb, craniofacial, and organ development. Genes Dev *21*, 1113-1124.

Sato, Y., Miyashita, A., Iwatsubo, T., and Usui, T. (2012). Simultaneous absolute protein quantification of carboxylesterases 1 and 2 in human liver tissue fractions using liquid chromatography-tandem mass spectrometry. Drug metabolism and disposition: the biological fate of chemicals *40*, 1389-1396.

Schmitt-Hoffmann, A.H., Roos, B., Sauer, J., Schleimer, M., Kovacs, P., Stoeckel, K., and Maares, J. (2011). Influence of food on the pharmacokinetics of oral alitretinoin (9-cis retinoic acid). Clin Exp Dermatol *36 Suppl 2*, 18-23.

Schug, T.T., Berry, D.C., Shaw, N.S., Travis, S.N., and Noy, N. (2007). Opposing effects of retinoic acid on cell growth result from alternate activation of two different nuclear receptors. Cell *129*, 723-733.

Seegmiller, J.C., Barnidge, D.R., Burns, B.E., Larson, T.S., Lieske, J.C., and Kumar, R. (2009). Quantification of urinary albumin by using protein cleavage and LC-MS/MS. Clinical chemistry *55*, 1100-1107.

Seibert, C., Davidson, B.R., Fuller, B.J., Patterson, L.H., Griffiths, W.J., and Wang, Y. (2009). Multiple-approaches to the identification and quantification of cytochromes P450 in human liver tissue by mass spectrometry. J Proteome Res *8*, 1672-1681.

Shiota, G. (2005). Loss of function of retinoic acid in liver leads to steatohepatitis and liver tumor: A NASH animal model. Hepatol Res *33*, 155-160.

Siepen, J.A., Keevil, E.J., Knight, D., and Hubbard, S.J. (2007). Prediction of missed cleavage sites in tryptic peptides aids protein identification in proteomics. Journal of proteome research *6*, 399-408.

Silverman, R.B. (1995). Mechanism-based enzyme inactivators. Methods in enzymology *249*, 240-283.

Sima, A., Parisotto, M., Mader, S., and Bhat, P.V. (2009). Kinetic characterization of recombinant mouse retinal dehydrogenase types 3 and 4 for retinal substrates. Biochimica et biophysica acta *1790*, 1660-1664.

Singh, S.K., and Dominic, C.J. (1980). Effect of N,N'-bis(dichloroacetyl)-i,8-octamethylenediamine (WIN 18446) on the testis + epididymis of the musk shrew Suncus murinus L. Indian J Exp Biol *18*, 1217-1220.

Sladek, N.E., Kollander, R., Sreerama, L., and Kiang, D.T. (2002). Cellular levels of aldehyde dehydrogenases (ALDH1A1 and ALDH3A1) as predictors of therapeutic responses to cyclophosphamide-based chemotherapy of breast cancer: a retrospective study. Rational individualization of oxazaphosphorine-based cancer chemotherapeutic regimens. Cancer chemotherapy and pharmacology *49*, 309-321.

Strelevitz, T.J., Orozco, C.C., and Obach, R.S. (2012). Hydralazine as a selective probe inactivator of aldehyde oxidase in human hepatocytes: estimation of the contribution of aldehyde oxidase to metabolic clearance. Drug metabolism and disposition: the biological fate of chemicals *40*, 1441-1448.

Styrkarsdottir, U., Thorleifsson, G., Helgadottir, H.T., Bomer, N., Metrustry, S., Bierma-Zeinstra, S., Strijbosch, A.M., Evangelou, E., Hart, D., Beekman, M.*, et al.* (2014). Severe osteoarthritis of the hand associates with common variants within the ALDH1A2 gene and with rare variants at 1p31. Nat Genet *46*, 498-502.

Taibi, G., Paganini, A., Gueli, M.C., Ampola, F., and Nicotra, C.M. (2001). Xanthine oxidase catalyzes the synthesis of retinoic acid. J Enzyme Inhib *16*, 275-285.

Terao, M., Kurosaki, M., Barzago, M.M., Fratelli, M., Bagnati, R., Bastone, A., Giudice, C., Scanziani, E., Mancuso, A., Tiveron, C.*, et al.* (2009). Role of the molybdoflavoenzyme aldehyde oxidase homolog 2 in the biosynthesis of retinoic acid: generation and characterization of a knockout mouse. Molecular and cellular biology *29*, 357-377.

Thatcher, J.E., and Isoherranen, N. (2009). The role of CYP26 enzymes in retinoic acid clearance. Expert Opin Drug Metab Toxicol *5*, 875-886.

Thatcher, J.E., Zelter, A., and Isoherranen, N. (2010). The relative importance of CYP26A1 in hepatic clearance of all-trans retinoic acid. Biochem Pharmacol *80*, 903-912.

Tomita, S., Tsujita, M., and Ichikawa, Y. (1993). Retinal oxidase is identical to aldehyde oxidase. FEBS Lett *336*, 272-274.

Tong, M.H., Yang, Q.E., Davis, J.C., and Griswold, M.D. (2013). Retinol dehydrogenase 10 is indispensible for spermatogenesis in juvenile males. Proc Natl Acad Sci U S A *110*, 543-548.

Touma, S.E., Perner, S., Rubin, M.A., Nanus, D.M., and Gudas, L.J. (2009). Retinoid metabolism and ALDH1A2 (RALDH2) expression are altered in the transgenic adenocarcinoma mouse prostate model. Biochemical pharmacology *78*, 1127-1138.

Trasino, S.E., Harrison, E.H., and Wang, T.T. (2007). Androgen regulation of aldehyde dehydrogenase 1A3 (ALDH1A3) in the androgen-responsive human prostate cancer cell line LNCaP. Exp Biol Med (Maywood) *232*, 762-771.

Tsuchiya, H., Ikeda, Y., Ebata, Y., Kojima, C., Katsuma, R., Tsuruyama, T., Sakabe, T., Shomori, K., Komeda, N., Oshiro, S.*, et al.* (2012). Retinoids ameliorate insulin resistance in a leptin-dependent manner in mice. Hepatology *56*, 1319-1330.

Uehara, M., Yashiro, K., Mamiya, S., Nishino, J., Chambon, P., Dolle, P., and Sakai, Y. (2007). CYP26A1 and CYP26C1 cooperatively regulate anterior-posterior patterning of the developing brain and the production of migratory cranial neural crest cells in the mouse. Developmental biology *302*, 399-411.

Unni, E., Rao, M.R., and Ganguly, J. (1983). Histological & ultrastructural studies on the effect of vitamin A depletion & subsequent repletion with vitamin A on germ cells & Sertoli cells in rat testis. Indian J Exp Biol *21*, 180-192.

van Pelt, A.M., and de Rooij, D.G. (1990). Synchronization of the seminiferous epithelium after vitamin A replacement in vitamin A-deficient mice. Biol Reprod *43*, 363-367.

Vandermarliere, E., Mueller, M., and Martens, L. (2013). Getting intimate with trypsin, the leading protease in proteomics. Mass spectrometry reviews *32*, 453-465.

Veal, G.J., Cole, M., Errington, J., Pearson, A.D., Foot, A.B., Whyman, G., and Boddy, A.V. (2007). Pharmacokinetics and metabolism of 13-cis-retinoic acid (isotretinoin) in children with high-risk neuroblastoma - a study of the United Kingdom Children's Cancer Study Group. Br J Cancer *96*, 424-431.

Vernet, N., Dennefeld, C., Rochette-Egly, C., Oulad-Abdelghani, M., Chambon, P., Ghyselinck, N.B., and Mark, M. (2006). Retinoic acid metabolism and signaling pathways in the adult and developing mouse testis. Endocrinology *147*, 96-110.

Vila, R., Kurosaki, M., Barzago, M.M., Kolek, M., Bastone, A., Colombo, L., Salmona, M., Terao, M., and Garattini, E. (2004). Regulation and biochemistry of mouse molybdo-flavoenzymes. The DBA/2 mouse is selectively deficient in the expression of aldehyde oxidase homologues 1 and 2 and represents a unique source for the purification and characterization of aldehyde oxidase. J Biol Chem *279*, 8668-8683.

Wang, K., Chen, X., Zhan, Y., Jiang, W., Liu, X., Wang, X., and Wu, B. (2013). Increased expression of ALDH1A1 protein is associated with poor prognosis in clear cell renal cell carcinoma. Med Oncol *30*, 574.

Wang, X., Penzes, P., and Napoli, J.L. (1996). Cloning of a cDNA encoding an aldehyde dehydrogenase and its expression in Escherichia coli. Recognition of retinal as substrate. J Biol Chem *271*, 16288-16293.

Wang, X., Sperkova, Z., and Napoli, J.L. (2001). Analysis of mouse retinal dehydrogenase type 2 promoter and expression. Genomics *74*, 245-250.

Watanabe, K., Narimatsu, S., Yamamoto, I., and Yoshimura, H. (1991). Oxygenation mechanism in conversion of aldehyde to carboxylic acid catalyzed by a cytochrome P-450 isozyme. J Biol Chem *266*, 2709-2711.

Williamson, B.L., Purkayastha, S., Hunter, C.L., Nuwaysir, L., Hill, J., and Easterwood, L. (2011). Quantitative protein determination for CYP induction via LC-MS/MS. Proteomics *11*, 33-41.

Wolbach, S.B., and Howe, P.R. (1925). Tissue Changes Following Deprivation of Fat-Soluble a Vitamin. J Exp Med *42*, 753-777.

Wolf, G. (1996). A history of vitamin A and retinoids. FASEB journal : official publication of the Federation of American Societies for Experimental Biology *10*, 1102-1107.

Wolf, G. (2010). Retinoic acid activation of peroxisome proliferation-activated receptor delta represses obesity and insulin resistance. Nutr Rev *68*, 67-70.

Xi, J., and Yang, Z. (2008). Expression of RALDHs (ALDH1As) and CYP26s in human tissues and during the neural differentiation of P19 embryonal carcinoma stem cell. Gene expression patterns : GEP *8*, 438-442.

Xiao, Q., Weiner, H., and Crabb, D.W. (1996). The mutation in the mitochondrial aldehyde dehydrogenase (ALDH2) gene responsible for alcohol-induced flushing increases turnover of the enzyme tetramers in a dominant fashion. J Clin Invest *98*, 2027-2032.

Xing, Y., Luo, D.Y., Long, M.Y., Zeng, S.L., and Li, H.H. (2014). High ALDH1A1 expression correlates with poor survival in papillary thyroid carcinoma. World J Surg Oncol *12*, 29.

Xu, B., Gao, S., Wu, B., Yin, T., and Hu, M. (2014). Absolute quantification of UGT1A1 in various tissues and cell lines using isotope label-free UPLC-MS/MS method determines its turnover number and correlates with its glucuronidation activities. Journal of pharmaceutical and biomedical analysis *88*, 180-190.

Yang, L., Ren, Y., Yu, X., Qian, F., Bian, B.S., Xiao, H.L., Wang, W.G., Xu, S.L., Yang, J., Cui, W.*, et al.* (2014). ALDH1A1 defines invasive cancer stem-like cells and predicts poor prognosis in patients with esophageal squamous cell carcinoma. Mod Pathol *27*, 775-783.

Yashiro, K., Zhao, X., Uehara, M., Yamashita, K., Nishijima, M., Nishino, J., Saijoh, Y., Sakai, Y., and Hamada, H. (2004). Regulation of retinoic acid distribution is required for proximodistal patterning and outgrowth of the developing mouse limb. Dev Cell *6*, 411-422.

Yoshida, A., Hsu, L.C., and Dave, V. (1992). Retinal oxidation activity and biological role of human cytosolic aldehyde dehydrogenase. Enzyme *46*, 239-244.

Yoshida, A., Rzhetsky, A., Hsu, L.C., and Chang, C. (1998). Human aldehyde dehydrogenase gene family. Eur J Biochem *251*, 549-557.

Zhai, Y., Sperkova, Z., and Napoli, J.L. (2001). Cellular expression of retinal dehydrogenase types 1 and 2: effects of vitamin A status on testis mRNA. J Cell Physiol *186*, 220-232.

Zhang, M., Hu, P., Krois, C.R., Kane, M.A., and Napoli, J.L. (2007). Altered vitamin A homeostasis and increased size and adiposity in the rdh1-null mouse. FASEB journal : official publication of the Federation of American Societies for Experimental Biology *21*, 2886-2896.

Zhang, X., Quinney, S.K., Gorski, J.C., Jones, D.R., and Hall, S.D. (2009). Semiphysiologically based pharmacokinetic models for the inhibition of midazolam clearance by diltiazem and its major metabolite. Drug metabolism and disposition: the biological fate of chemicals *37*, 1587-1597.

Zhao, D., McCaffery, P., Ivins, K.J., Neve, R.L., Hogan, P., Chin, W.W., and Drager, U.C. (1996). Molecular identification of a major retinoic-acid-synthesizing enzyme, a retinaldehyde-specific dehydrogenase. Eur J Biochem *240*, 15-22.

Zhu, W., Smith, J.W., and Huang, C.M. (2010). Mass spectrometry-based label-free quantitative proteomics. Journal of biomedicine & biotechnology *2010*, 840518.

Ziouzenkova, O., Orasanu, G., Sharlach, M., Akiyama, T.E., Berger, J.P., Viereck, J., Hamilton, J.A., Tang, G., Dolnikowski, G.G., Vogel, S.*, et al.* (2007). Retinaldehyde represses adipogenesis and diet-induced obesity. Nature medicine *13*, 695-702.

Vita

Samuel La Montagne Arnold was born in Decatur, Georgia. In 2009, he earned a Bachelor of Science in Biochemistry and a minor in Chemistry from the University of Colorado.